Coherent anti-Stokes Raman scattering microscopy for pharmaceutics

A shift in the right direction

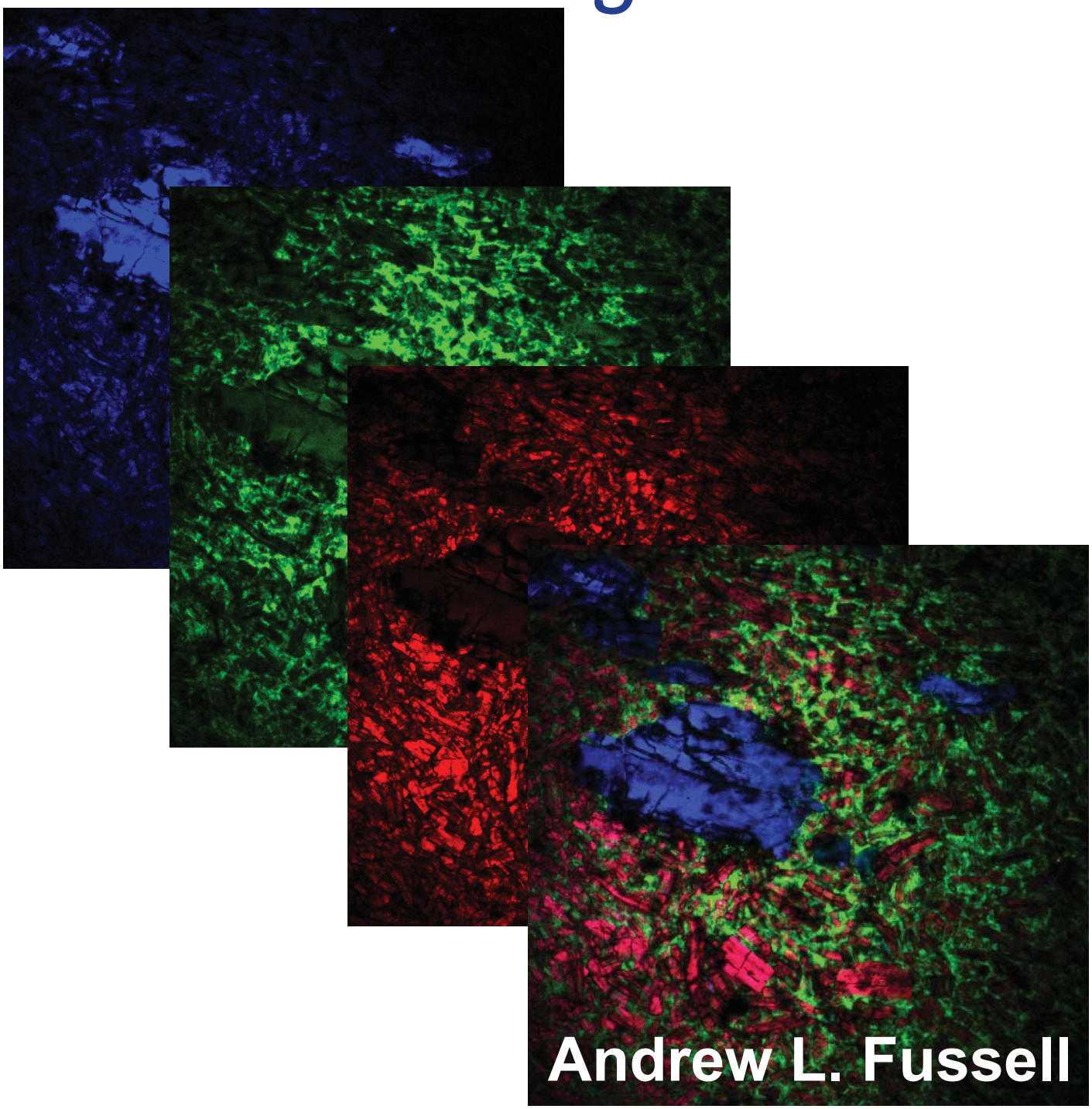

Andrew L. Fussell

Coherent anti-Stokes Raman scattering microscopy for pharmaceutics

A shift in the right direction

Composition of the graduation committee:

Prof. dr. H. Hilgenkamp	University of Twente, Enschede, the Netherlands
Prof. dr. J.L. Herek	University of Twente, Enschede, the Netherlands
Dr. ir. H.L. Offerhaus	University of Twente, Enschede, the Netherlands
Dr. C.J. Strachan	University of Helsinki, Helsinki, Finland
Dr. J.A. Zeitler	University of Cambridge, Cambridge, England
Prof. dr. K.J. Boller	University of Twente, Enschede, the Netherlands
Prof. dr. M.M.A.E. Claessens	University of Twente, Enschede, the Netherlands
Prof. dr. P. Kleinebudde	Heinrich-Heine University, Düsseldorf, Germany
Prof. dr. A.G.J.M. van Leeuwen	Academisch Medisch Centrum Amsterdam

This research is supported by the Dutch Technology Foundation STW, which is part of the Netherlands Organisation for Scientific Research (NWO) and partly funded by the Ministry of Economic Affairs (project number OTP11114).

This work was carried out primarily at:

Optical Sciences group, MESA+ Institute for Nanotechnology, Faculty of Science and Technology (TNW), University of Twente, the Netherlands.

Cover design: Multispectral CARS image of a three component tablet. Tablet prepared by Sinan Güres and imaged by Andrew L. Fussell.

Photo: Kamilla Koichumanova

ISBN: 978-90-365-3671-4

Author email: andrewlfussell@gmail.com

COHERENT ANTI-STOKES RAMAN SCATTERING MICROSCOPY FOR PHARMACEUTICS

A SHIFT IN THE RIGHT DIRECTION

DISSERTATION

to obtain

the degree of doctor at the University of Twente,

on the authority of the rector magnificus,

prof. dr. H. Brinksma,

on account of the decision of the graduation committee,

to be publicly defended

on Friday 4th of July 2014 at 16.45

by

Andrew Luke Fussell

Born on 21st of January 1987

in Auckland, New Zealand

This dissertation is approved by:

Prof. dr. J.L Herek (Promoter)

Dr. ir. H.L. Offerhaus (Assistant promoter)

Dr. C.J. Strachan (Assistant promoter)

Contents

Introduction

Chapter one

A pharmaceutical scientist is dedicated to developing promising drug compounds into lifesaving medicines. The development process is a time consuming process typically taking a number of years between chemical discovery and release on the market. A large number of analytical techniques are employed by pharmaceutical scientists during the development process, with each technique providing insight into different physical and chemical properties of the compound under development. This dissertation demonstrates coherent anti-Stokes Raman scattering (CARS) microscopy as a tool for solid state pharmaceutical development suitable for early stage analysis of pure powders and late stage analysis of complex dosage forms. Variants of CARS microscopy are used to identify changes in solid state form both in dry oral dosage forms and in situ during dissolution testing. Additionally, CARS microscopy is applied to provide chemically selective imaging for formulation strategies in the area of inhalation medicines and poorly water soluble medicines.

1.1 Pharmaceutical solid state

Pharmaceutical science is the area focused on converting pharmacologically active molecules into marketable medicines. Formulation development is an integral part of this process. Formulation development is loosely divided into two areas: solid state formulations and liquid state formulations depending on whether the final dosage form is a tablet, capsule, syrup, suspension, or injection. Liquid state formulations will not be covered in this work. Instead the focus is on solid state formulations: primarily tablets but also particles.

A solid state form is generally thought to refer to a crystalline structure where molecules are arranged in a three dimensional (3D) repeating unit in a crystal lattice. However, common usage of the term solid state also includes multi-component crystals and non-crystalline amorphous structures. Polymorphism refers to different crystal structures where under different environment conditions (i.e. kinetic, temperature and pressure) molecules can arrange themselves in a different 3D repeating unit resulting in different crystalline lattices. Figure 1 shows schematic illustrations of these different solid state forms. Active pharmaceutical ingredients (APIs) are known to exist in various solid state forms that can change during processing, production and storage, creating challenges for formulation scientists.

An example of a multi-component crystal is that of a solvate. A solvate is a crystalline material that has incorporated molecules of a solvent into the crystal lattice. A commonly encountered solvate in pharmaceutical development is a hydrate in which water molecules are incorporated into the crystal lattice of APIs. Hydrate formation can occur during processing when the sample is exposed to moisture in the air or potentially during dissolution testing when oral dosage forms are exposed to liquid water. Further details about hydrate formation during dissolution can be found in Chapter three.

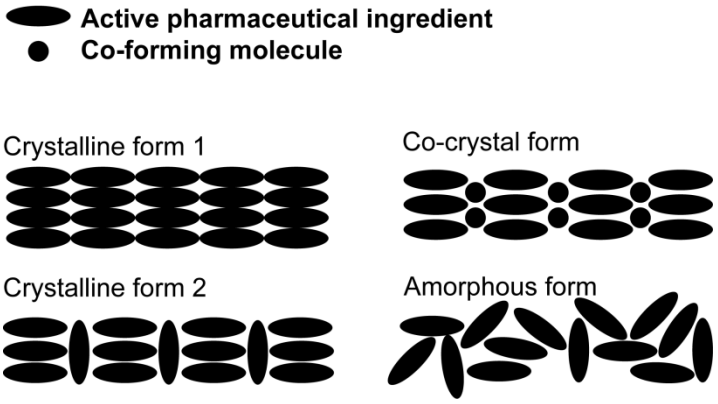

Figure 1. Schematic illustrating solid state forms of an active pharmaceutical ingredient.

The majority of drugs currently under development have issues with poor water solubility [1]. Solubility is of particular importance for solid formulations because the drug molecules must first dissolve before being absorbed for a therapeutic effect. This issue of solubility makes the amorphous form an interesting option during formulation development.

The amorphous form has no long range order without a crystalline lattice and is often considered to be a quench cooled liquid [2]. Due to the increased structural disorder the amorphous form has a higher thermodynamic activity which leads to an increased reactivity in many cases, a higher apparent solubility and increased dissolution rate [2]. However, the higher thermodynamic activity also provides instability, giving the amorphous form a tendency to crystallize during storage [3] and in some cases during dissolution testing [4].

Overcoming issues of amorphous instability is the subject of a large area of pharmaceutical research with numerous formulation strategies under investigation. Examples of these strategies include solid dispersions [5, 6], co-amorphous mixtures [7, 8], and drug loaded porous silica/ silicon microparticles [9, 10]. Figure 2 outlines schematically these formulation strategies; it is apparent that the basis of these stabilization strategies is physical separation with the API molecules separated from

each other, thereby preventing crystallization. In some cases it has been shown that there is also a chemical interaction between the API and the excipients involved in the formulation [11].

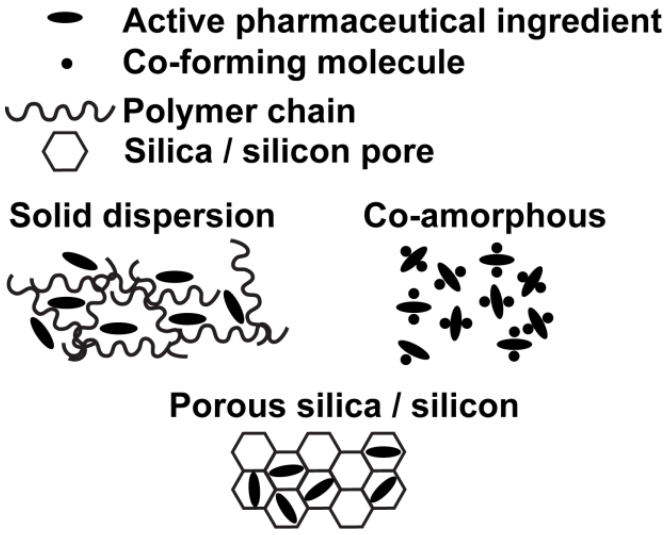

Figure 2. Schematic illustrating amorphous stabilization formulation techniques.

Solid-dispersions were first introduced as a potential formulation strategy for poorly water soluble drugs by Sekiguchi and Obi [12] in 1961 where they dispersed sulfathiazole in urea and found that the dispersed sulfathiazole had a higher absorption into the blood. A solid-dispersion has been defined as “a dispersion of one or more active ingredients in an inert carrier or matrix at solid state prepared by the melting, solvent, or melting-solvent method” [6]. These methods allow supersaturation of the drug in the mixture and quench cooling to form an amorphous solid sample [5]. The inert carrier in the solid-dispersion needs to be freely water soluble, non-toxic, thermally stable (melting methods) and chemically stable (solvent procedures). Some examples of commonly used carriers include polymers (e.g. polyvinylpyrrolidone and polyethylene glycol), sugars, and urea [5, 13].

There are similarities between co-amorphous mixtures and solid-dispersions, in that both strategies involve formulating poorly soluble drugs with co-forming chemicals

designed to stabilize the amorphous form of the drug [14]. However, a solid-dispersion carrier is typically a large molecule such as a polymer or bile salt while a co-amorphous co-former is typically a small molecule such as citric acid [8], amino acids [15], and other drug molecules [7, 11, 16]. Methods used to prepare the co-amorphous mixtures also vary with mechanical activation by cryo-milling the most common method used followed by quench cooling of the melt [14].

Mesoporous silica and silicon is another formulation strategy for poorly water soluble drugs. Mesoporous materials contain nanosized pores between 2–50 nm [17-19], allowing the loading of drug molecules inside the pores. The materials are synthesized either using a top-down method [20, 21] where a non-porous sample is etched to create pores or a bottom-up method [22] where the material is grown by template synthesis. Porous silicon is most commonly fabricated top-down using electrochemical anodization of monocrystalline silicon wafers while porous silica is usually fabricated using the bottom-up approach by reacting tetraethyl orthosilicate with a template made of micellar rods [10] resulting in an ordered layout of pores with a controlled size.

Incorporation of drug into the pores can be performed using solvent deposition methods [23-25], mechanical activation methods [26, 27] or vapor-phase mediated mass transfer [19]. The solvent deposition method is based on dissolving the drug into an organic solvent at a high concentration and mixing the solvent with the mesoporous silica allowing the drug to migrate through diffusion into the pores of the mesoporous silica particles. This process is followed by a solvent removal step where the excess solvent is removed, leaving the remaining drug loaded in the mesoporous silica.

Formulation development for medication delivery to the airways provides different challenges to overcome. For instance, the airways provide a large surface area with a good blood supply usually making drug absorption not an issue for drug delivery. However, API powder particle size is very important for deep penetration into the

airways. Research has shown that there is an optimal particle size of between 1-5 μm, with particles smaller than 1 μm being exhaled and particles larger than 5 μm typically being swallowed instead of reaching the airways [28, 29].

One of the issues that arise when trying to prepare particles within this size range is cohesion due to electrostatic interactions. In other words, small particles preferentially clump together essentially losing the advantage of small particle size. To overcome this issue attempts have been made to stabilize the small particle size by combining finely powdered API with coarsely powdered carrier particles creating mixtures where the API is coated on the surface of the carrier particles. These mixtures are known as adhesive mixtures for inhalation and further details can be found about this formulation strategy in Chapter four.

1.2 Pharmaceutical analytical techniques

Pharmaceutical analytical techniques play a fundamental role in solid dosage form development. Different analytical techniques are applied at different stages of the development process depending on the physical or chemical property of the material of interest. Traditional analytical techniques include x-ray powder diffraction (XRPD), differential scanning calorimetry (DSC), thermogravimetric analysis (TGA), scanning electron microscopy (SEM), infrared (IR) and spontaneous Raman spectroscopy.

X-ray powder diffraction is based on the fact that when x-rays are incident on crystalline solids they are scattered over a large area. Some of this scattered radiation destructively interferes while some of it constructively interferes, leading to strong intensity scattering peaks which can be detected using a diffractometer [30]. Bragg's law describes the angles where constructive interference occurs for crystalline materials:

$$n\lambda = 2d \sin\theta \tag{1.1}$$

where λ is the wavelength of the incident x-ray, *d* is the distance between the planes in the crystal lattice and *θ* is the angle between the incident x-ray and the scattered radiation.

X-ray powder diffraction is often considered a gold standard in the analysis of pharmaceutical materials and is used to both to investigate polymorphism [31] of APIs and to investigate onset of crystallization for amorphous samples [32]. XRPD is capable of identifying different polymorphs due to differences in their x-ray diffractograms, but it provides no information about the relative stability of the polymorphs; for this other techniques are required.

Thermal analysis includes techniques such as differential scanning calorimetry (DSC) and thermogravimetric analysis (TGA). These techniques are capable of determining the relative stability of polymorphs by investigating the energies involved in phase changes between various polymorphs [33]. Thermal analysis is based on the principle that a physical change in a material is associated with a release or absorption of heat. Thermogravimetric analysis (TGA) is a commonly used thermal analytical technique. A typical TGA instrument consists of a precision analytical balance combined with a furnace that is programmed for a linear rise of temperature with time [34]. In the area of pharmaceutical analysis TGA is commonly used to study dehydration [35, 36] as well as for determining the loading of drug loaded silica/silicon [37, 38].

Thermal methods are useful in early stage development where they can provide a large amount of information about the API under development. However, the thermal methods are destructive techniques that are unsuitable for analyzing complex dosage forms containing excipients such as tablets or capsules. When analyzing complex dosage forms imaging methods are especially useful.

Scanning electron microscopy (SEM) is a widely employed imaging technique in pharmaceutical development providing extremely high resolution (~1 nm) morphological information for a wide range of solid samples [39-41]. Such high resolution can be achieved by using a highly focused electron beam which is scanned over the surface of the sample with scattered secondary electrons collected by a type of scintillator-photomultiplier detector known as the Everhart-Thornley detector [42, 43]. SEM is an extremely high spatial resolution technique providing morphological information for complex dosage forms. However, in many cases SEM is incapable of distinguishing between API and excipients and in these cases it is necessary to employ a chemically specific technique.

In 1928 Raman and Krishnan [44] reported what they called “a new type of secondary radiation” where they observed molecules in dust-free liquids or gases exhibiting modified scattered radiation of degraded frequency. This scattering has become known as spontaneous Raman scattering and is a form of inelastic scattering of light where light is scattered at either a higher (anti-Stokes shifted) or lower (Stokes shifted) frequency than the incident light. The frequency shift of the scattered light is due to an interaction between the incident light and the vibrating chemical bonds of the molecule, making Raman scattering a chemically specific technique. If the electrons are in the ground state during the interaction they are excited to a virtual state which then relaxes to a vibrational level while emitting lower frequency photons (Stokes shifted). If however, the electrons are already in a higher vibrational level, the excited electrons relax emitting higher frequency photons (anti-Stokes shifted). These processes are illustrated in Figure 3. In environmental conditions the electrons are mostly in the ground state making Stokes shifted scattering the predominant effect [45].

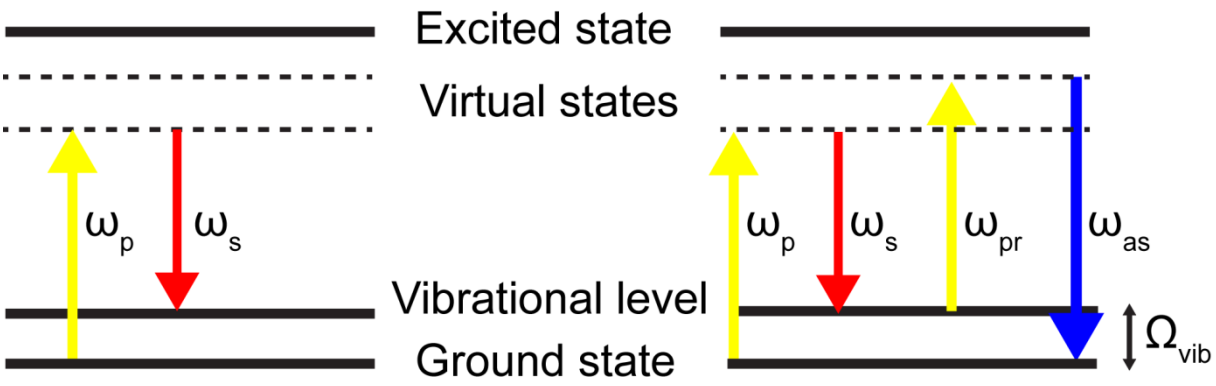

Figure 3. Jablonski energy level diagrams illustrating stokes Raman scattering (left) and coherent anti-Stokes Raman scattering (right).

Raman scattering techniques can be loosely divided into spectroscopic or imaging techniques. A typical spontaneous Raman spectroscopy system consists of a continuous wave laser with a charge coupled device (CCD) spectrometer used to collect the scattered photons and is capable of recording a full spectrum (400-4000 cm^{-1}) in a matter of seconds [46, 47]. Raman imaging is a spatially resolved technique that collects Raman spectra from various spatial areas on the surface of a sample which are then combined into a surface map [48].

Pharmaceutical applications of spontaneous Raman are numerous, including studies on polymorphism [49-51], process induced changes [47, 52], drug loading of mesoporous silica [53] and during dissolution testing [54, 55].

As mentioned earlier, oral solid dosage forms require the drug to dissolve before it can be absorbed for a therapeutic effect. Dissolution testing involves immersing the drug either in a powdered form or as a dosage form such as a tablet or capsule into a liquid medium such as water and measuring how long it takes for the drug to dissolve into the medium [56].

Dissolution testing is useful during both early stage development when it can help decide which API molecule is worth advancing for further development and in late development as part of quality control when it can be used to compare different batches of dosage forms to ensure the production process is reproducible.

In 1897 Arthur Amos Noyes and Willis Rodney Whitney proposed an equation to calculate in quantitative terms the rate at which a solid dissolves in a solvent using what is now known as the Noyes-Whitney equation:

$$\frac{\delta M}{\delta t} = \frac{DS}{h}(C_s - C) \tag{1.2}$$

where $\frac{\delta M}{\delta t}$ is the change in mass per unit time, *D* is the diffusion coefficient of the solute in the solvent, *S* is the surface area of the exposed solid, *h* is the thickness of the diffusion layer, C_s is the saturation solubility of the solid and *C* is the concentration of the solute in bulk solution at time *t* [56].

Dissolution testing usually involves removing aliquots of the dissolution medium over a series of time points to determine the concentration of dissolved drug. This method provides indirect information about the dissolution process but it gives no direct information about potential changes in solid state form that may be occurring on the surface of the dissolving dosage form. This lack of direct information has led to attempts to combine *in situ* analytical techniques such as spontaneous Raman scattering [4, 55], IR imaging [57], UV spectroscopy [58] and imaging [59, 60] and now coherent anti-Stokes Raman scattering microscopy (see Chapter 3) with dissolution testing.

1.3 Coherent anti-Stokes Raman scattering (CARS) microscopy

Coherent anti-Stokes Raman scattering is a nonlinear optical technique that can probe the same molecular vibrations as spontaneous Raman. Nonlinear optics describes the behavior of intense light usually from a laser light source in the presence of nonlinear materials [61]. A nonlinear material is a material which responds to the strength of the applied optical field in a nonlinear manner. In other words, if the material generates light at a different frequency than of the input light it is said to be a nonlinear effect. One of the first demonstrations of nonlinear optics was second harmonic generation by Franken et al. [62] in 1961, in which 694.3 nm light incident on crystalline quartz produced light at 347.15 nm.

Another way to look at an optical nonlinearity is to consider the polarization $\tilde{P}$(t), of the material which depends on the strength $\tilde{E}$(t) of an applied optical field. In linear optics the induced polarization depends linearly on the strength of the electric field: [61]

$$\tilde{P}(t) = \epsilon_0 \chi^{(1)} \tilde{E}(t) \tag{1.3}$$

where $\chi^{(1)}$ is the linear susceptibility and ϵ_0 is the permittivity of free space. Nonlinear optical responses can be written showing the polarization $\tilde{P}$(t) as a power series in the field strength $\tilde{E}$(t):

$$\tilde{P}(t) = \epsilon_0 \left[\chi^{(1)} \tilde{E}(t) + \chi^{(2)} \tilde{E}(t) + \chi^{(3)} \tilde{E}(t) + \cdots\right] \tag{1.4}$$

where $\chi^{(2)}$ and $\chi^{(3)}$ are second and third-order nonlinear optical susceptibilities respectively [61].

Coherent Raman scattering is a term that covers the techniques CARS and stimulated Raman scattering (SRS) and variants of these techniques. CARS is a third-order nonlinear optical technique that was first reported by Maker and Terhune

in 1965 [63] but was originally known as a three wave mixing experiment. The term coherent anti-Stokes Raman scattering was coined in 1974 when Begley et al. [64] published their article about CARS spectroscopy.

Further development in the area lead Duncan et al.[65] to introduce a scanning CARS microscope in 1982. They used two synchronously pumped continuous wave dye lasers to produce the pump and stokes beams which were scanned with a scanning mirror across a sample of onion skin cells [65]. Zumbusch et al.[66] utilized a high numerical aperture in their CARS microscope with co-linear beam alignment making implementation of the CARS technique easier to standard optical microscopes. In addition to easy implementation of the technique they showed that, due to the nonlinear effect, the excitation was limited to the small volume of the laser foci resulting in reduced background signal, reduced photodamage and the ability to perform three-dimensional microscopy [66].

There are a number of ways to realize a coherent Raman system microscope system, with each setup having its own capabilities and limitations. Coherent Raman techniques are loosely divided into narrowband and broadband techniques, where the division is based on the excitation lasers used, with narrowband systems typically employing two picosecond pulsed lasers while a broadband system employs a femtosecond laser combined with a picosecond laser. The distinction between CARS and SRS is based on differences in detection methods with CARS measuring a wavelength separated signal while SRS detection relies on detecting a gain or a loss due to modulation of one of the excitation beams. Narrowband CARS systems have been more commonly used in the analysis of pharmaceutical samples and are the focus of this dissertation so they will be discussed first and in most detail.

A typical narrowband CARS microscope consists of two picosecond pulsed laser sources overlapped in space (spatially) and time (temporally) which are focused on the sample with a high NA microscope objective and scanned across the surface using a pair of XY scanning mirrors. The generated CARS signal is scattered in both

the forward direction (propagation direction of the lasers) and the backward direction (known as epi-CARS) and is first filtered from the excitation light before being detected typically using photomultiplier tubes (PMT) [67]. Practically, the picosecond pulsed laser source is usually a Nd:YVO_4 or Nd:YAG laser which pumps an optical parametric oscillator (OPO) which produces two lasers known as signal and idler that are tunable in wavelength. Usually the fundamental laser source is combined with the signal beam by free space optics and the overlapped beams are directed into a beam scanning microscope.

A typical broadband CARS microscope setup consists of two laser sources one of which provides femtosecond pulses while the other provides picosecond pulses. The femtosecond pulses are commonly provided by a Ti:Sapphire laser source which produces 60-70 fs pulses with a 80 MHz repetition around 800 nm [68, 69]. The narrowband picosecond pulse source can be an electronically locked Nd:YVO_4 laser [68], or it is possible to use a beam splitter to divert a portion of the femtosecond light source into a dispersion-less filter to prepare a narrowband pulse source [69]. As with the narrowband CARS systems the broadband setups also have pulses spatially and temporally overlapped before focused on the sample using a high NA microscope objective. In contrast to the narrowband CARS systems the broadband setups typically use a CCD spectrometer to collect the scattered CARS signal.

Stimulated Raman scattering (SRS) is a more recent addition to the tools of coherent Raman scattering but is now implemented in both broadband [70] and narrowband configurations [71]. A typical SRS system is very similar to that of a CARS system with overlapped focused pulsed lasers, but instead of detecting the anti-Stokes scattered light using a PMT or CCD spectrometer, the modulation on one of laser sources is detected using a photodiode with a lock-in [71]. The modulation that is detected during SRS is usually generated by placing an acoustic optic modulator or an electro optic modulator in the beam path of one of the excitation lasers prior to beam combination. This modulation results in either a gain or loss to the stimulated Raman signal depending whether the pump (gain) or Stokes (loss) beam is

modulated which can be detected using the lock-in with a photodiode. Figure 4. shows a schematic illustrating the pump and Stokes pulse trains in SRS.

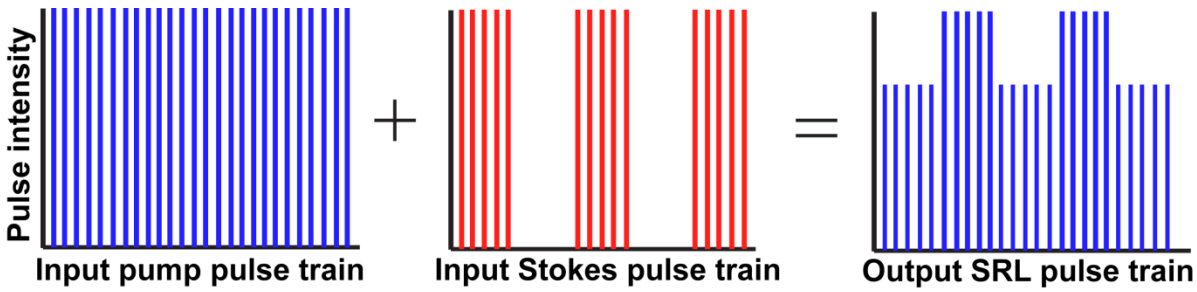

Figure 4. Schematic illustration of the pump (blue) and Stokes (red) pulse trains in stimulated Raman scattering adapted from Freudiger et al. [71].

Coherent Raman techniques are well established in biomedical imaging where narrowband CARS is particularly suitable for investigating lipid content in biological cells [67]. Up until recently, pharmaceutical research has been primarily focused on spontaneous Raman spectroscopy and mapping but it is slowly gaining interest in coherent Raman techniques. Most of the work done in this area was performed using narrowband CARS with some of the earliest work performed analyzing the composition of dodecane emulsions [72]. Still in the area of emulsions Day et al.[73] used narrowband CARS to discriminate between undigested oil and lipolytic breakdown products without labeling.

In the area of solid dosage forms Kang et al. [74-76] investigated drug loaded polymer films initially imaging the drug distribution in the film. This was followed by imaging the drug release using a static medium. The authors found that CARS microscopy provided visual evidence for an accelerated burst release of drug which was followed by a slower sustained release of drug. Windbergs et al.[77] and Jurna et al.[78] went a step further and imaged drug dissolution from lipid based extrudates and tablets using a dynamic medium. They reported that the drug theophylline crystallized into theophylline monohydrate during dissolution when prepared from pure powdered samples while this was not the case for tablets produced from lipid extrudates.

There has also been work done in the area of pharmaceutical analysis using other variants of coherent Raman techniques namely SRS and broadband CARS microscopy. Slipchenko et al.[79] employed SRS to investigate drug and excipient distributions in commercial available tablets. They found that by using SRS it was possible to distinguish between amlodipine tablets provided by six different manufacturers. Wang et al. [80] used SRS to investigate the drug distribution of drug loaded polymer films as part of their work done on developing the SRS technique. Broadband CARS microscopy was the technique employed by Hartshorn et al.[81] to image the API and excipient distribution in tablets containing the model drug indomethacin. Additionally they investigated the ability of broadband CARS to distinguish between the α and γ forms of indomethacin.

1.4 Dissertation overview

CARS microscopy is a nonlinear optical imaging technique that provides rapid chemically selective imaging without the requirement of labels and is free from single photon fluorescence. CARS microscopy is capable of three dimensional optional sectioning resulting high resolution diffraction limited images. The previous work mentioned earlier investigated the potential for CARS microscopy as a tool for pharmaceutical analysis. This dissertation expands upon the previous work and demonstrates coherent anti-Stokes Raman scattering (CARS) microscopy as a tool in pharmaceutical solid state development. CARS microscopy is suitable for early stage development, analyzing pure API powders as well as late stage analysis of more complex dosage forms. The strengths and weaknesses of CARS microscopy are explored in the context of pharmaceutical analysis over a wide range of samples covering a number of commonly used pharmaceutical formulation strategies.

Chapter two introduces and discusses hyperspectral CARS microscopy as a tool for determining pharmaceutical solid state form capable of distinguishing between

hydrous and anhydrous polymorphic forms as well as between crystalline and amorphous forms.

Chapter three presents CARS and hyperspectral CARS as a tool for dissolution analysis capable of correlating visualized changes on the surface of a dosage form with changes observed in the dissolution rate. Chapter 3 begins with details about the design and building of the dissolution setup and is followed by results obtained from a number of theophylline containing oral dosage forms.

Chapter four introduces the area of inhalation medicine and looks at the capabilities of CARS microscopy to provide useful information about the formulation strategy known as adhesive mixtures. The chapter begins with analyzing drug distribution followed by particle size calculations and ends with correlative imaging combining CARS with scanning electron microscopy (SEM).

Chapter five looks at a drug loaded mesoporous silica particles, which is a formulation strategy aimed at stabilizing the amorphous form of poorly water soluble drugs. CARS and hyperspectral CARS were utilized to firstly identify the three dimensional drug distribution of the loaded silica particles and secondly to confirm the amorphous nature of the loaded drug. Finally more correlative CARS and SEM imaging was performed to confirm that the loaded drug was contained within the pores of the silica.

1.5 References

1. Ku, M., *Use of the Biopharmaceutical Classification System in Early Drug Development.* The AAPS Journal, 2008. **10**(1): p. 208-212.
2. Zhang, G.G.Z., et al., *Phase transformation considerations during process development and manufacture of solid oral dosage forms.* Advanced Drug Delivery Reviews, 2004. **56**(3): p. 371-390.
3. Yoshioka, M., B.C. Hancock, and G. Zografi, *Crystallization of indomethacin from the amorphous state below and above its glass transition temperature.* Journal of Pharmaceutical Sciences, 1994. **83**(12): p. 1700-1705.
4. Savolainen, M., et al., *Better understanding of dissolution behaviour of amorphous drugs by in situ solid-state analysis using Raman spectroscopy.* European Journal of Pharmaceutics and Biopharmaceutics, 2009. **71**(1): p. 71-79.
5. Ford, J.L., *The Current Status of Solid Dispersions.* Pharmaceutica Acta Helvetiae, 1986. **61**(3): p. 69-88.
6. Chiou, W.L. and S. Riegelman, *Pharmaceutical applications of solid dispersion systems.* Journal of Pharmaceutical Sciences, 1971. **60**(9): p. 1281-1302.
7. Alleso, M., et al., *Enhanced dissolution rate and synchronized release of drugs in binary systems through formulation: Amorphous naproxen-cimetidine mixtures prepared by mechanical activation.* Journal of Controlled Release, 2009. **136**(1): p. 45-53.
8. Lu, Q. and G. Zografi, *Phase behavior of binary and ternary amorphous mixtures containing indomethacin, citric acid, and PVP.* Pharmaceutical Research, 1998. **15**(8): p. 1202-1206.
9. Wang, S., *Ordered mesoporous materials for drug delivery.* Microporous and Mesoporous Materials, 2009. **117**(1–2): p. 1-9.
10. Santos, H.A., et al., *Mesoporous materials as controlled drug delivery formulations.* Journal of Drug Delivery Science and Technology, 2011. **21**(2): p. 139-155.
11. Chieng, N., et al., *Physical characterization and stability of amorphous indomethacin and ranitidine hydrochloride binary systems prepared by*

mechanical activation. European Journal of Pharmaceutics and Biopharmaceutics, 2009. **71**(1): p. 47-54.

12. Sekiguchi, K. and N. Obi, *Studies on Absorption of Eutectic Mixture. I. A Comparison of the Behavior of Eutectic Mixture of Sulfathiazole and that of Ordinary Sulfathiazole in Man.* CHEMICAL & PHARMACEUTICAL BULLETIN, 1961. **9**(11): p. 866-872.
13. Leuner, C. and J. Dressman, *Improving drug solubility for oral delivery using solid dispersions.* European Journal of Pharmaceutics and Biopharmaceutics, 2000. **50**(1): p. 47-60.
14. Laitinen, R., et al., *Emerging trends in the stabilization of amorphous drugs.* International Journal of Pharmaceutics, 2013. **453**(1): p. 65-79.
15. Löbmann, K., et al., *Amino acids as co-amorphous stabilizers for poorly water soluble drugs – Part 1: Preparation, stability and dissolution enhancement.* European Journal of Pharmaceutics and Biopharmaceutics, 2013. **85**(3, Part B): p. 873-881.
16. Lobmann, K., et al., *Co-amorphous simvastatin and glipizide combinations show improved physical stability without evidence of intermolecular interactions.* European Journal of Pharmaceutics and Biopharmaceutics, 2012. **81**(1): p. 159-169.
17. Yiu, H.H.P. and P.A. Wright, *Enzymes supported on ordered mesoporous solids: a special case of an inorganic-organic hybrid.* Journal of Materials Chemistry, 2005. **15**(35-36): p. 3690-3700.
18. Selvam, P., S.K. Bhatia, and C.G. Sonwane, *Recent Advances in Processing and Characterization of Periodic Mesoporous MCM-41 Silicate Molecular Sieves.* Industrial & Engineering Chemistry Research, 2001. **40**(15): p. 3237-3261.
19. Qian, K.K. and R.H. Bogner, *Application of mesoporous silicon dioxide and silicate in oral amorphous drug delivery systems.* Journal of Pharmaceutical Sciences, 2012. **101**(2): p. 444-463.
20. Uhlir, A., *Electrolytic Shaping of Germanium and Silicon.* Bell System Technical Journal, 1956. **35**(2): p. 333-347.
21. Turner, D.R., *Electropolishing Silicon in Hydrofluoric Acid Solutions.* Journal of the Electrochemical Society, 1958. **105**(7): p. 402-408.

22. Kresge, C.T., et al., *Ordered mesoporous molecular sieves synthesized by a liquid-crystal template mechanism.* Nature, 1992. **359**(6397): p. 710-712.
23. Kinnari, P., et al., *Comparison of mesoporous silicon and non-ordered mesoporous silica materials as drug carriers for itraconazole.* International Journal of Pharmaceutics, 2011. **414**(1–2): p. 148-156.
24. Ambrogi, V., et al., *Improvement of dissolution rate of piroxicam by inclusion into MCM-41 mesoporous silicate.* European Journal of Pharmaceutical Sciences, 2007. **32**(3): p. 216-222.
25. Prestidge, C.A., et al., *Mesoporous silicon: a platform for the delivery of therapeutics.* Expert Opinion on Drug Delivery, 2007. **4**(2): p. 101-110.
26. Watanabe, T., et al., *Solid state radical recombination and charge transfer across the boundary between indomethacin and silica under mechanical stress.* Journal of Solid State Chemistry, 2002. **164**(1): p. 27-33.
27. Hailu, S.A. and R.H. Bogner, *Complex effects of drug/silicate ratio, solid-state equivalent pH, and moisture on chemical stability of amorphous quinapril hydrochloride coground with silicates.* Journal of Pharmaceutical Sciences, 2011. **100**(4): p. 1503-1515.
28. Patton, J.S. and P.R. Byron, *Inhaling medicines: delivering drugs to the body through the lungs.* Nature Reviews Drug Discovery, 2007. **6**(1): p. 67-74.
29. Byron, P.R., *Prediction of drug residence times in regions of the human respiratory tract following aerosol inhalation.* Journal of Pharmaceutical Sciences, 1986. **75**(5): p. 433-438.
30. Brittain, H.G., ed. *Physical Characterization of Pharmaceutical Solids*. 1995, Marcel Dekker Inc.: New York. 424.
31. Threlfall, T.L., *Analysis of Organic Polymorphs - a Review.* Analyst, 1995. **120**(10): p. 2435-2460.
32. Graeser, K.A., et al., *Physicochemical properties and stability of two differently prepared amorphous forms of simvastatin.* Crystal Growth & Design, 2008. **8**(1): p. 128-135.
33. Bernstein, J., *Polymorphism in Molecular Crystals*2002, Oxford: Oxford university press. 410.
34. Coats, A.W. and J.P. Redfern, *Thermogravimetric analysis. A review.* Analyst, 1963. **88**(1053): p. 906-924.

35. Nunes, C., A. Mahendrasingam, and R. Suryanarayanan, *Investigation of the multi-step dehydration reaction of theophylline monohydrate using 2-dimensional powder X-ray diffractometry.* Pharmaceutical Research, 2006. **23**(10): p. 2393-2404.
36. Takata, N., et al., *A Spironolactone-Saccharin 1:1 Cocrystal Hemihydrate.* Crystal Growth & Design, 2010. **10**(5): p. 2116-2122.
37. Salonen, J., et al., *Mesoporous silicon microparticles for oral drug delivery: Loading and release of five model drugs.* Journal of Controlled Release, 2005. **108**(2–3): p. 362-374.
38. Limnell, T., et al., *Delivery Formulations of Ordered and Nonordered Mesoporous Silica: Comparison of Three Drug Loading Methods.* Journal of Pharmaceutical Sciences, 2011. **100**(8): p. 3294-3306.
39. Shur, J. and R. Price, *Advanced microscopy techniques to assess solid-state properties of inhalation medicines.* Advanced Drug Delivery Reviews, 2012. **64**(4): p. 369-382.
40. Tian, F., et al., *Influence of polymorphic form, morphology, and excipient interactions on the dissolution of carbamazepine compacts.* Journal of Pharmaceutical Sciences, 2007. **96**(3): p. 584-594.
41. Sprunk, A., S. Page, and P. Kleinebudde, *Influence of process parameters and equipment on dry foam formulation properties using indomethacin as model drug.* International Journal of Pharmaceutics, 2013. **455**(1–2): p. 189-196.
42. Everhart, T.E. and R.F.M. Thornley, *Wide-band detector for micro-microampere low-energy electron currents.* Journal of Scientific Instruments, 1960. **37**(7): p. 246.
43. Mcmullan, D., *Scanning Electron-Microscopy 1928-1965.* Scanning, 1995. **17**(3): p. 175-185.
44. Raman, C.V. and K.S. Krishnan, *A New Type of Secondary Radiation.* Nature, 1928. **121**(3048): p. 501.
45. Smith, E. and G. Dent, *Modern Raman Spectroscopy*2005: John Wiley and Sons. 210.
46. Strachan, C.J., et al., *Quantitative analysis of polymorphic mixtures of carbamazepine by Raman spectroscopy and principal components analysis.* Journal of Raman Spectroscopy, 2004. **35**(5): p. 347-352.

47. Wikström, H., P.J. Marsac, and L.S. Taylor, *In-line monitoring of hydrate formation during wet granulation using Raman spectroscopy.* Journal of Pharmaceutical Sciences, 2005. **94**(1): p. 209-219.
48. Sasic, S., *Raman mapping of low-content API pharmaceutical formulations. I. Mapping of alprazolam in Alprazolam/Xanax tablets.* Pharmaceutical Research, 2007. **24**(1): p. 58-65.
49. Taylor, L.S. and G. Zografi, *The Quantitative Analysis of Crystallinity Using FT-Raman Spectroscopy.* Pharmaceutical Research, 1998. **15**(5): p. 755-761.
50. Czernicki, W. and M. Baranska, *Carbamazepine polymorphs: Theoretical and experimental vibrational spectroscopy studies.* Vibrational Spectroscopy, 2013. **65**(0): p. 12-23.
51. Aaltonen, J., et al., *Hyphenated spectroscopy as a polymorph screening tool.* Journal of Pharmaceutical and Biomedical Analysis, 2007. **44**(2): p. 477-483.
52. Savolainen, M., et al., *Determination of amorphous content in the pharmaceutical process environment.* Journal of Pharmacy and Pharmacology, 2007. **59**(2): p. 161-170.
53. Vanea, E. and V. Simon, *XPS and Raman study of zinc containing silica microparticles loaded with insulin.* Applied Surface Science, 2013. **280**(0): p. 144-150.
54. Haaser, M., et al., *Analysis of Matrix Dosage Forms During Dissolution Testing Using Raman Microscopy.* Journal of Pharmaceutical Sciences, 2011. **100**(10): p. 4452-4459.
55. Aaltonen, J., et al., *In situ measurement of solvent-mediated phase transformations during dissolution testing.* Journal of Pharmaceutical Sciences, 2006. **95**(12): p. 2730-2737.
56. Sinko, P.J., ed. *Martin's Physical Pharmacy and Pharmaceutical Sciences*. 5th ed. 2006, Lippincott Williams and Wilkins: Baltimore. 795.
57. van der Weerd, J., K.L. Andrew Chan, and S.G. Kazarian, *An innovative design of compaction cell for in situ FT-IR imaging of tablet dissolution.* Vibrational Spectroscopy, 2004. **35**(1–2): p. 9-13.
58. Florence, A.J. and A. Johnston, *Applications of ATR UV/vis spectroscopy in physical form characterisation of pharmaceuticals*, in *Spectroscopy Europe*2004, John Wiley & Sons Ltd. p. 4.

59. Ostergaard, J., et al., *Monitoring Lidocaine Single-Crystal Dissolution by Ultraviolet Imaging.* Journal of Pharmaceutical Sciences, 2011. **100**(8): p. 3405-3410.
60. Hulse, W.L., J. Gray, and R.T. Forbes, *A discriminatory intrinsic dissolution study using UV area imaging analysis to gain additional insights into the dissolution behaviour of active pharmaceutical ingredients.* International Journal of Pharmaceutics, 2012. **434**(1–2): p. 133-139.
61. Boyd, R.W., *Nonlinear Optics*. third edition ed2008, Burlington: Academic Press.
62. Franken, P.A., et al., *Generation of Optical Harmonics.* Physical Review Letters, 1961. **7**(4): p. 118-&.
63. Maker, P.D. and R.W. Terhune, *Study of Optical Effects Due to an Induced Polarization Third Order in Electric Field Strength.* Physical Review, 1965. **137**(3A): p. A801-&.
64. Begley, R.F., A.B. Harvey, and R.L. Byer, *Coherent Anti-Stokes Raman-Spectroscopy.* Applied Physics Letters, 1974. **25**(7): p. 387-390.
65. Duncan, M.D., J. Reintjes, and T.J. Manuccia, *Scanning coherent anti-Stokes Raman microscope.* Opt. Lett., 1982. **7**(8): p. 350-352.
66. Zumbusch, A., G.R. Holtom, and X.S. Xie, *Three-Dimensional Vibrational Imaging by Coherent Anti-Stokes Raman Scattering.* Physical Review Letters, 1999. **82**(20): p. 4142.
67. Evans, C.L. and X.S. Xie, *Coherent anti-stokes Raman scattering microscopy: chemical imaging for biology and medicine.* Annu Rev Anal Chem (Palo Alto Calif), 2008. **1**: p. 883-909.
68. Postma, S., et al., *Application of spectral phase shaping to high resolution CARS spectroscopy.* Optics Express, 2008. **16**(11): p. 7985-7996.
69. Parekh, S.H., et al., *Label-Free Cellular Imaging by Broadband Coherent Anti-Stokes Raman Scattering Microscopy.* Biophysical Journal, 2010. **99**(8): p. 2695-2704.
70. Ploetz, E., et al., *Femtosecond stimulated Raman microscopy.* Applied Physics B-Lasers and Optics, 2007. **87**(3): p. 389-393.
71. Freudiger, C.W., et al., *Label-Free Biomedical Imaging with High Sensitivity by Stimulated Raman Scattering Microscopy.* Science, 2008. **322**(5909): p. 1857-1861.

72. Pautot, S., et al., *Spontaneous formation of lipid structures at oil/water lipid interfaces.* Langmuir, 2003. **19**(24): p. 10281-10287.
73. Day, J.P.R., et al., *Label-Free Imaging of Lipophilic Bioactive Molecules during Lipid Digestion by Multiplex Coherent Anti-Stokes Raman Scattering Microspectroscopy.* Journal of the American Chemical Society, 2010. **132**(24): p. 8433-8439.
74. Kang, E., et al., *In Situ Visualization of Paclitaxel Distribution and Release by Coherent Anti-Stokes Raman Scattering Microscopy.* Analytical Chemistry, 2006. **78**(23): p. 8036-8043.
75. Kang, E., et al., *Paclitaxel distribution in poly(ethylene glycol)/poly(lactide-co-glycolic acid) blends and its release visualized by coherent anti-Stokes Raman scattering microscopy.* Journal of Controlled Release, 2007. **122**(3): p. 261-268.
76. Kang, E., et al., *Application of coherent anti-stokes Raman scattering microscopy to image the changes in a paclitaxel–poly(styrene-b-isobutylene-b-styrene) matrix pre- and post-drug elution.* Journal of Biomedical Materials Research Part A, 2008. **87A**(4): p. 913-920.
77. Windbergs, M., et al., *Chemical Imaging of Oral Solid Dosage Forms and Changes upon Dissolution Using Coherent Anti-Stokes Raman Scattering Microscopy.* Analytical Chemistry, 2009. **81**(6): p. 2085-2091.
78. Jurna, M., et al., *Coherent anti-Stokes Raman scattering microscopy to monitor drug dissolution in different oral pharmaceutical tablets.* Journal of Innovative Optical Health Sciences, 2009. **2**(1): p. 37-43.
79. Slipchenko, M.N., et al., *Vibrational imaging of tablets by epi-detected stimulated Raman scattering microscopy.* Analyst, 2010. **135**(10): p. 2613-2619.
80. Wang, P., et al., *Mechanisms of Epi-Detected Stimulated Raman Scattering Microscopy.* Ieee Journal of Selected Topics in Quantum Electronics, 2012. **18**(1): p. 384-388.
81. Hartshorn, C.M., et al., *Multicomponent Chemical Imaging of Pharmaceutical Solid Dosage Forms with Broadband CARS Microscopy.* Analytical Chemistry, 2013. **85**(17): p. 8102-8111.

Hyperspectral CARS microscopy for solid state form determination

Chapter two

Hyperspectral CARS is a recent development expanding the capabilities of CARS microscopy from single frequency imaging to hyperspectral imaging where images are recorded rapidly for a large number of vibrational frequencies. This chapter explores the ability of hyperspectral CARS to determine the solid state form of drugs. Systems were investigated involving changes in crystalline polymorphs including conversions from anhydrous to hydrous forms as well as differences between amorphous and crystalline forms. Aspects of this work have been published in Garbacik et al. [1], Fussell et al. [2], and presented at conferences including SPIE Photonics west and the PBP world meeting.

2.1 Introduction

Active pharmaceutical ingredients (API)s can exist in a number of solid state forms including various crystalline polymorphs, the amorphous form and multi-component crystals including co-crystals and salt forms [3]. In the pharmaceutical industry there is a particular interest in identifying solid state forms and their physicochemical properties during the drug development process. Properties such as apparent solubility, physical and chemical stability, and dissolution rate can vary between different solid state forms and have a great influence on the developability of the API [4, 5]. There are reports of ever increasing issues of poor water solubility of drugs in the development pipeline with estimates suggesting around 60% of all molecules in development having solubility issues [6]. One of the strategies employed to overcome issues of poor water solubility is using the amorphous form of the API under development.

The amorphous form refers to a form where long range molecular order has been broken down [7]. This breakdown in order results in a high energy disordered state which has been found in many cases to have improved solubility and dissolution rate [8] compared to crystalline forms. Karmwar et al. [9] reported a 9-fold increase in dissolved concentration after 60 minutes of dissolution for amorphous indomethacin prepared by cryo-milling for 240 minutes when compared to both alpha and gamma crystalline indomethacin. The amorphous form is a thermodynamically high energy state and has a tendency to crystallize which is a drawback for the drug development process. There is a large area of research in the field of amorphous form stabilization including solid dispersions [10, 11], co-amorphous mixtures [12, 13] and drug loaded silica [14, 15] and silicon particles [16, 17].

Traditional solid state analytical techniques such as differential scanning calorimetry (DSC), thermogravimetric analysis (TGA), x-ray powder diffraction (XRPD), Fourier transform infrared spectroscopy (FTIR) and Fourier transform spontaneous Raman

spectroscopy (FT Raman) are well established in studying the different solid state forms of APIs. For example, Grzesiak et al. [18] published work where they used XRPD, DSC, hot stage microscopy and FTIR to study the four anhydrous polymorphs of carbamazepine. They reported that all used techniques were capable of distinguishing between the different polymorphs but the most reliable way to determine the polymorphic form was with XRPD as each form provided a number of high intensity distinguishing peaks. Taylor and Langkilde [19] investigated the potential of FT Raman to identify the solid state form of a number of APIs including ranitidine, theophylline, prednisolone, enalapril and warfarin contained in tablets and capsules. For most of the APIs they reported that FT Raman is capable of identifying the solid state form of the drug in commercially available dosage forms even though in some samples the API was present in a low concentration.

CARS microscopy is a third order non-linear optical imaging technique that probes the same molecular vibrational frequencies as spontaneous Raman scattering. Coherent Raman techniques such as CARS and stimulated Raman scattering allow rapid chemically selective imaging up to video rate [20]. CARS microscopy can be roughly divided into two groups, namely narrowband and broadband CARS. Narrowband CARS is performed using lasers with picosecond pulse duration, whereas broadband CARS uses a femtosecond pulse for either the pump or Stokes beam and a picosecond pulse for the other beam.

A narrowband CARS microscope generally consists of two picosecond pulsed lasers one of which is tunable in wavelength. In practice this is normally achieved by using a frequency doubled Nd:YAG or Nd:YVO_4 laser source which pumps an optical parametric oscillator (OPO) producing a further two output beams known as signal and idler. Imaging is usually performed by spatially and temporally overlapping the fundamental laser (called Stokes) with the signal beam (called pump) from the OPO and directing the beams into an inverted microscope where they are focused on the sample using a microscope objective. If the frequency difference between the two incident lasers matches a Raman vibrational resonance, an anti-Stokes (blue shifted with respect to the pump beam) CARS signal is generated. The CARS signal can be

collected in either the forwards direction or in the backwards direction where it is collected using a photomultiplier tube (PMT). For this work the CARS signal was detected in the backwards direction. CARS signal is diffraction limited and only generated within the focal volume, making it an inherently confocal, imaging technique.

Narrowband CARS microscopy is images a single Raman vibrational mode which can make it difficult or even impossible to distinguish between different solid state forms of the same API. This difficulty occurs because usually there are only minor differences between vibrational spectra for various solid state forms. Broadband CARS is a potential solution to this issue as it is capable of probing a wider spectral range (around 600-3200 cm^{-1}) but with a reduced spectral resolution of about 10 cm^{-1} and a slower imaging speed (about 50 ms/pixel) when compared to narrowband CARS systems [21, 22]. Hyperspectral narrowband CARS microscopy is a recently developed technique capable of rapidly imaging over a wide spectral range overcoming the drawback of single vibrational mode imaging [23, 24]. Hyperspectral CARS has been used to rapidly identify various amino acids in physical mixtures [23] as well as investigating polymorphism in a number of pharmaceutically relevant chemicals [1].

In this chapter hyperspectral CARS microscopy is introduced and the application of this recently developed technique to rapidly and visually identify various solid state forms of the model drugs carbamazepine, theophylline, griseofulvin and itraconazole is investigated. The focus is initially on polymorphic conversions from anhydrous to hydrous forms for carbamazepine and theophylline. This is followed by analyzing differences between crystalline and amorphous forms for griseofulvin and itraconazole. Finally, issues and drawbacks with the hyperspectral method are discussed.

2.2 Materials and Methods

2.2.1 Materials

United states pharmacopeial (USP) grade carbamazepine (CBZ) form III (Sigma-Aldrich, USA) was purchased and used to prepare CBZ form I, and CBZ dihydrate. USP grade Theophylline anhydrate (TPa) and theophylline monohydrate (TPm) were gifted from BASF (Ludwigshafen, Germany). Crystalline itraconazole (ITRA) (Orion Pharma, Finland) was used to prepare amorphous ITRA, while crystalline griseofulvin (GRIS) (Sigma-Aldrich, USA) was used to prepare amorphous GRIS.

2.2.2 Methods

Hydrate formation

CBZ dihydrate and TPm were prepared through recrystallization from CBZ form III and TPa respectively. Samples of the anhydrous APIs were placed on a microscope slide and distilled water was added dropwise until all of the material was covered the sample was then left to allow the excess water to evaporate.

Amorphous formation

Amorphous ITRA and GRIS were prepared through quench cooling of melted crystalline ITRA and GRIS.

Carbamazepine form I formation

CBZ form I was prepared through recrystallization of CBZ form III. CBZ form III was heated in an oven for three hours at 150 °C. The sample was then allowed to cool over silica gel and stored in the fridge before analysis.

Pellet preparation

Pellets (75 mg, Ø 8 mm) were compressed using a manual pellet press with a pressure of about 0.1 ton applied for about 30 s. The pure chemical CARS spectra were compared before and after pellet preparation to ensure changes did not occur during compression.

CARS microscope setup

The CARS microscopy system is illustrated in Figure 1 and is described in more detail elsewhere [23]. A Nd:YVO_4 picosecond pulsed laser (Coherent Inc., USA) operated at a fundamental wavelength of 1064 nm was frequency doubled to pump an optical parametric oscillator (OPO) (APE Berlin GmbH, Germany) which produced two dependently tunable laser beams. The fundamental laser beam was combined with the signal beam from the OPO and directed into an inverted laser-scanning microscope (Olympus IX71/FV300, Japan) where they were focused onto the sample using a 20X/0.5 NA objective. The backscattered CARS signal was collected by the focusing objective, spectrally filtered to remove the excitation wavelengths, and detected with a photomultiplier tube (Hamamatsu R3896, Japan). The CARS microscope system using a 20X/0.5 NA objective had an axial spatial resolution of about 10 µm and a lateral spatial resolution of about 1 µm.

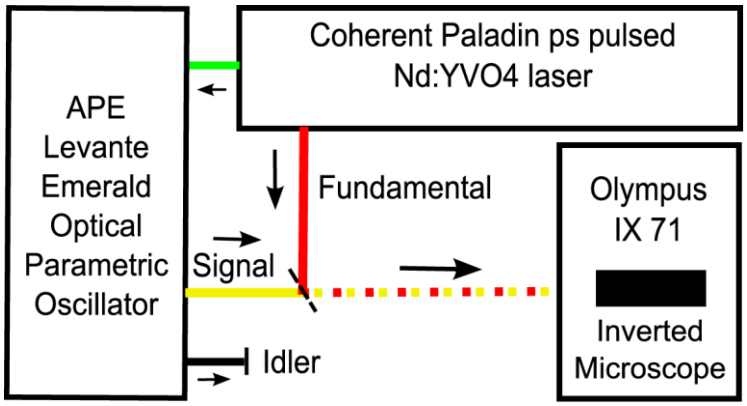

Figure 1. Schematic illustration of the custom built CARS microscope system

Hyperspectral imaging

The method to record and project hyperspectral CARS images has been published in great detail in Garbacik et al. [23]. Briefly, CARS images are recorded rapidly while the wavelength of the OPO produced signal beam is swept using stepwise changes in the Lyot filter position resulting in a large number of frames (around 50) with each frame corresponding to a different vibrational frequency. After image collection every pixel in the hyperspectral data is normalized in intensity and then projected using an arbitrary color look-up table wherein each frame of the hyperspectral data is colored using a different color and the brightness of each pixel is scaled by its intensity. The projection of the hyperspectral data is performed using additive mixing with a maximum intensity projection creating an output image that contains maximum pixel values over all images in the data stack. The resulting hyperspectral image is a two dimensional projection of the hyperspectral data with each color representing a different chemical compound or solid state form. Figure 2 is a schematic illustrating the hyperspectral process.

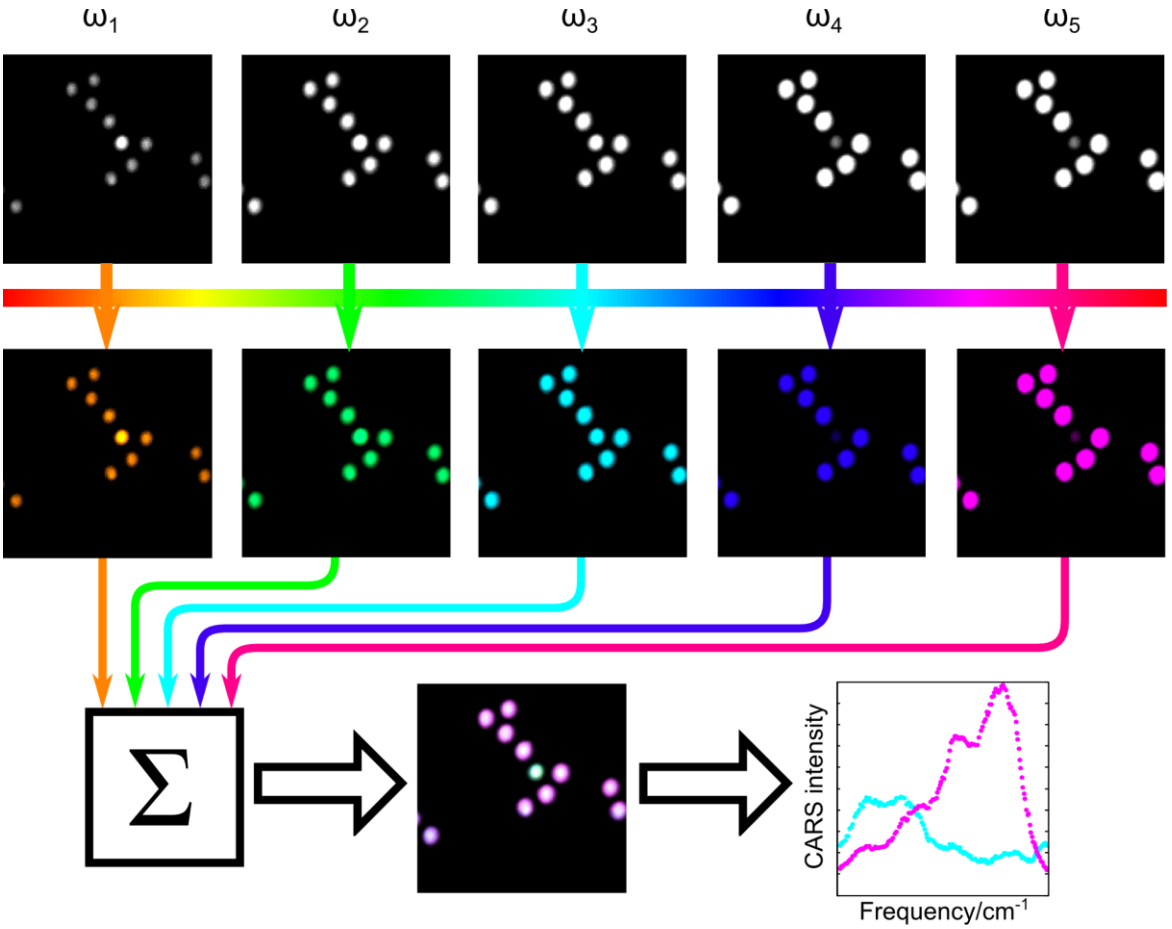

Figure 2. Schematic illustrating hyperspectral imaging process using plastic beads as a model sample. Reproduced from Garbacik et al.[23]

2.3 Results and Discussion

Crystalline polymorphic form discrimination

The first solid state conversion to be investigated using hyperspectral CARS microscopy was the conversion from anhydrous to hydrous for both theophylline and carbamazepine. Theophylline is known to convert from anhydrate to monohydrate in the presence of water or moisture [25, 26]. Mixtures of TPa and TPm were compressed into pellets and analyzed using hyperspectral CARS. Figure 3 shows a hyperspectral CARS image (Figure 3A) and the extracted CARS spectra (Figure 3B) for TPa and TPm covering the range of 3050 cm^{-1} to 3150 cm^{-1}. Looking at the hyperspectral image (Figure 3A) TPa can be seen as a yellow color (for the color table displayed on top of Figure 3B) while TPm appears as a pink-red color. The color change in the hyperspectral image can be explained due to a peak shift which is seen in the CARS spectra (Figure 3B). TPa has a peak maximum around 3118 cm^{-1} while for TPm this peak has shifted to around 3105 cm^{-1}. This peak has been assigned to the imidazole ring C-H stretching ($\nu C_{(8)}$-H) and the red-shift is due to $C_{(8)}$-H···O intermolecular hydrogen bonding in the TPm form [27, 28].

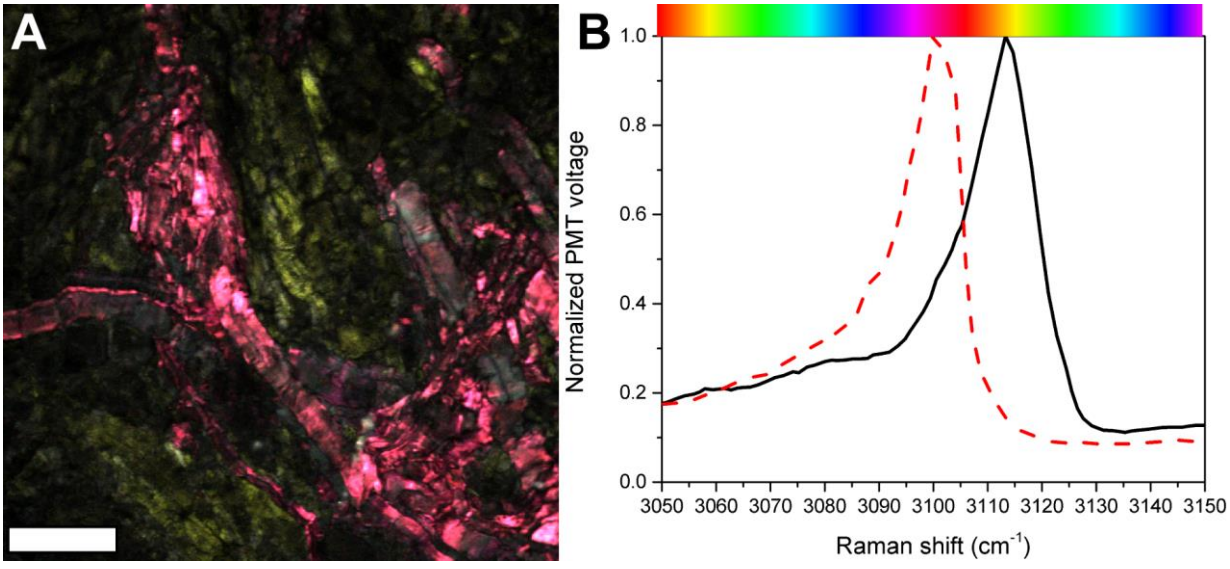

Figure 3. Hyperspectral image (A) and extracted CARS spectra (B) for a pellet prepared containing TPa and TPm. In the hyperspectral image TPa can be seen as yellow while the pink-red color represents TPm. Hyperspectral image covers the C-H stretch range from 3050-3150 cm^{-1}. The scale bar represents 100 µm.

The conversion of CBZ form III to CBZ dihydrate was studied using a similar method with pellets compressed using physical mixtures of both solid state forms. Figure 4 shows a hyperspectral image (Figure 4A) and extracted CARS spectra (Figure 4B) for a pellet containing both CBZ III and CBZ dihydrate covering the range from 2980 cm^{-1} to 3080 cm^{-1}. In the hyperspectral image CBZ III appears as a blue-green color while CBZ dihydrate appears as a reddish color (for the color table above Figure 4B). There is also a small area (indicated by red dashed circle) of sample damage due to laser heating which is seen as a dark yellow color. Unlike TP the color differences for CBZ are not due to a shift in a peak but rather a change in relative intensities for three peaks observed in this spectral region. These peaks have been assigned to represent C-H stretching [29].

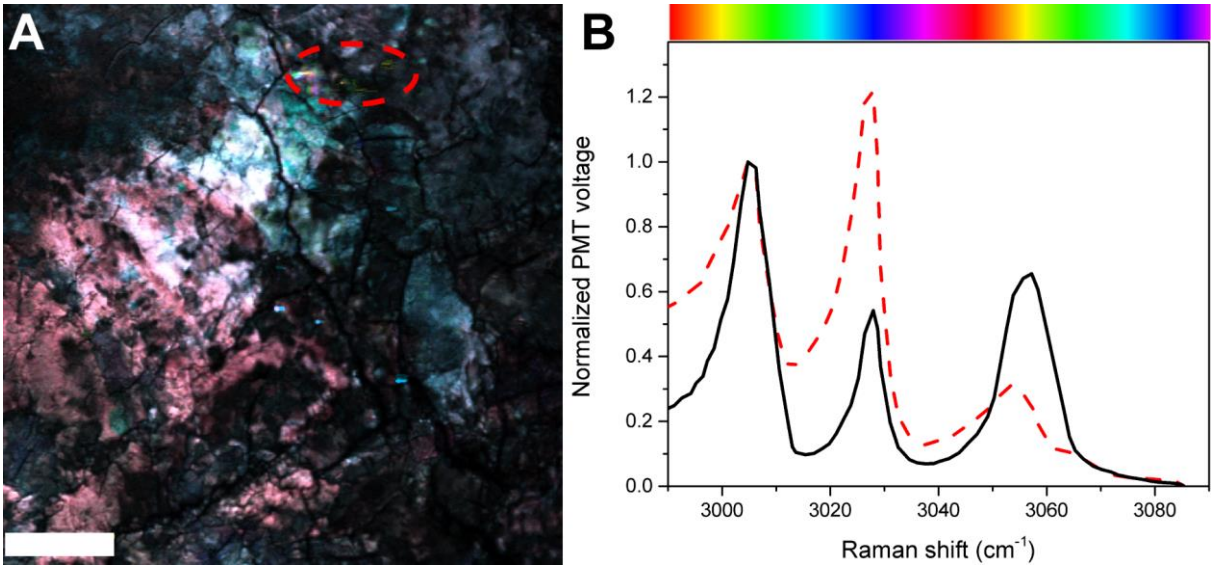

Figure 4. Hyperspectral image (A) and extracted CARS spectra (B) for a pellet prepared containing CBZ form III and CBZ dihydrate. CBZ form III can be seen as blue-green while the red color represents CBZ dihydrate. Hyperspectral image covers the C-H stretch range from 2990-3080 cm^{-1}. The scale bar represents 100 µm.

After analyzing the differences between anhydrous and hydrous solid state forms it was decided to attempt to visualize the difference between two anhydrous solid state forms. For this it was chosen to prepare mixtures containing both CBZ form III and CBZ form I. CBZ form III is a *P*-monoclinic crystal structure and the stable form of

CBZ while CBZ form I is a triclinic crystal structure and is metastable [18]. Figure 5 shows a hyperspectral image (Figure 5A) for CBZ III with CBZ I and extracted CARS spectra (Figure 5B) covering the range from 2970 cm^{-1} to 3075 cm^{-1}. Looking at the hyperspectral image CBZ III appears as a pink-purple color while CBZ I is colored blue-purple (for the color table above Figure 5B). The similarity between the two colors can be partly explained to be due to both forms of CBZ having a peak around 3010 cm^{-1} which is the most intense peak for both forms while the other peaks (around 3030 cm^{-1} and 3060 cm^{-1}) have a considerably lower intensity, meaning they have weaker contribution toward the final color of the image.

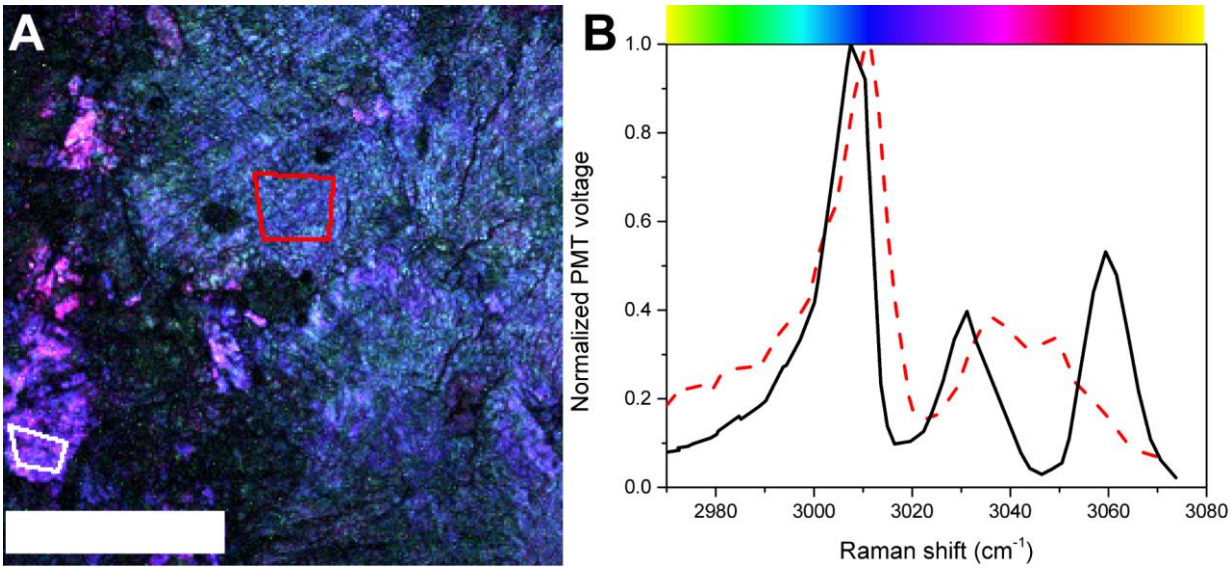

Figure 5. Hyperspectral image and extracted CARS spectra for a pellet prepared containing CBZ form III and CBZ form I. CBZ form III can be seen as pink-purple while the blue-purple color represents CBZ form I. Hyperspectral image covers the C-H stretch range from 2970-3075 cm^{-1}. Regions of interest showing where the CARS spectra were extracted from have been outlined for CBZ form III (white) and CBZ form I (red). Scale bar represents 100 µm.

Crystalline and amorphous discrimination

As part of the work performed investigating drug loaded mesoporous silica (covered in Chapter 5) it was decided to investigate spectral differences between crystalline and amorphous forms of GRIS and ITRA. Figure 6 shows hyperspectral images for crystalline GRIS (Figure 6A) and quench cooled amorphous GRIS (Figure 6B) along

with their extracted CARS spectra (Figure 6C) covering the range from 2860 cm^{-1} to 2960 cm^{-1}. The hyperspectral image for crystalline GRIS appears to show two colors with some of the sample appearing pink and some of the sample appearing cyan (for the color table shown above Figure 6C). This two color hyperspectral image can probably be explained to be due to crystal lattice orientation with respect to the laser polarization as it is known that CARS is sensitive to polarization [1]. The CARS spectra from the crystalline GRIS sample have been plotted along with the spectrum from the amorphous GRIS. Comparing the extracted CARS spectra it is obvious there are differences between the crystalline and amorphous solid state forms because none of the sharp peaks observed for crystalline GRIS can be seen in the amorphous spectrum. Instead the amorphous spectrum is halo-like with a broad peak observed around 2940 cm^{-1}. This broad peak has been assigned to be representing C-H_3 stretching [30].

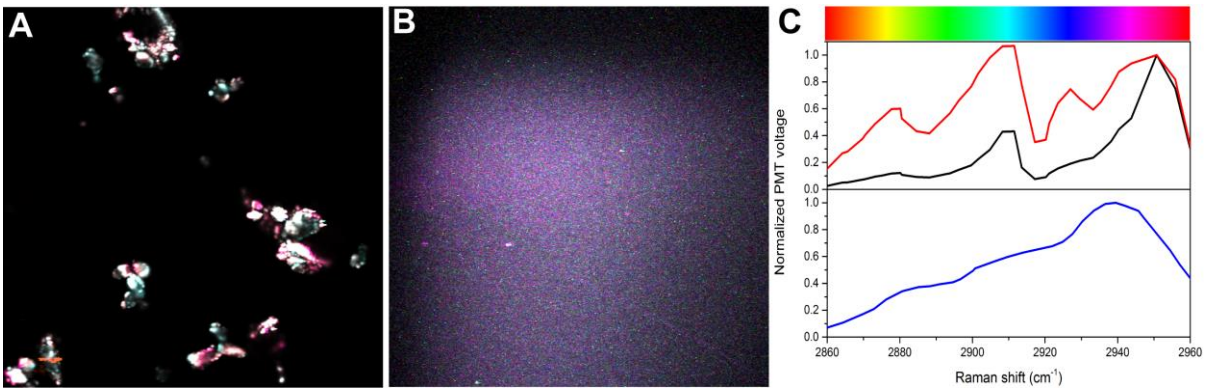

Figure 6. Hyperspectral images for crystalline GRIS (A) and amorphous GRIS (B) and extracted CARS spectra (C) showing crystalline (black and red lines) and amorphous (blue line) covering the range of 2860-2960 cm^{-1}.

A similar result was obtained for the ITRA sample with two colors observed in the hyperspectral image for crystalline ITRA. Figure 7 shows hyperspectral images for crystalline ITRA and amorphous ITRA along with the extracted CARS spectra. In the hyperspectral image for crystalline ITRA it can be seen that the sample appears as both cyan and pink colored. As with the GRIS sample (Figure 6) it is most likely that the second color is due to crystal lattice orientation with respect to the laser polarization. The hyperspectral image for the amorphous sample also has more than

one color in this case it is most likely that the colors are due to sample damage due to heating with the color of the damage depending on at which stage during the scan the damage occurs. Comparing the spectra obtained it is clear that there are differences between the crystalline and amorphous forms with the sharp peaks observed in the crystalline form replaced with a broad halo-like spectrum similar to that seen for amorphous GRIS (Figure 6). However, instead of having a peak maximum around 2940 cm^{-1} as seen for amorphous GRIS, the amorphous ITRA has a peak maximum around 2930 cm^{-1}. This broad peak has been assigned to represent C-H_3 stretching [30].

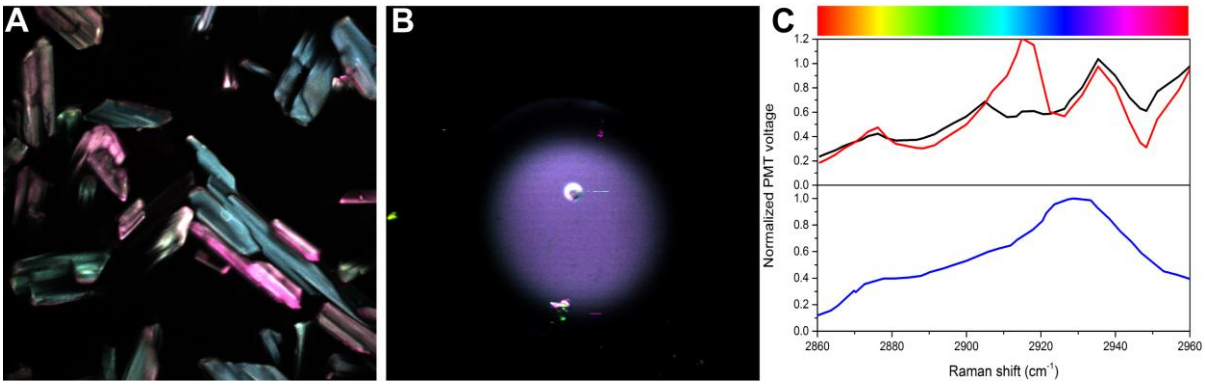

Figure 7. Hyperspectral images for crystalline ITRA (A) and amorphous ITRA (B) and extracted CARS spectra (C) showing crystalline (black and red lines) and amorphous (blue line) covering the range of 2860-2960 cm^{-1}.

Hyperspectral imaging considerations

Hyperspectral CARS imaging has been shown to be capable of discriminating between differences in solid state form. It is a rapid visual method giving chemical contrast to otherwise white powdered samples and also provides a simple way to extract CARS spectra from the sample. However, there are a number of limitations and drawbacks to the technique. Firstly, the sensitivity to crystal lattice orientation causing the sample to appear as two colors when only one is expected makes working with the technique more difficult. This extra difficulty is because sometimes the unexpected second color could be due to a contamination in the sample or due to an unexpected polymorphic conversion. Secondly, the hyperspectral technique is limited to static environments because any sample movement during the image

collection will result in a change in intensity and a change in the final color for the hyperspectral image. Thirdly, there are issues with differences in signal intensity between the solid state forms due to differences in scattering cross-section. This was particularly a problem for the amorphous form as it produced less intense scattering than the crystalline forms making it almost impossible to image both forms together in one image. Due to this mismatch in imaging intensity it led to images where either the crystalline form was saturated or the amorphous form was not visible. Although, this issue hampers single frequency CARS imaging it is particularly problematic in hyperspectral imaging where the extracted CARS spectra can vary significantly due to saturation. Finally, another issue with the projection of hyperspectral images is the issue of primary colors and secondary colors discussed in Garbacik et al. [1] where a compound with one peak can appear the same (or very similar) color to that of another compound that has two peaks in different positions. To overcome this issue sometimes it is necessary to present the same image projected using a more than one color look up table.

2.4 Conclusions and Outlook

Hyperspectral CARS imaging has been shown to be a powerful imaging technique for rapid visual discrimination between different solid state forms of APIs based on slight differences in their Raman vibrational spectra. This work demonstrated discrimination between anhydrous and hydrous polymorphic forms, as well as between two anhydrous forms of CBZ in pellets prepared from physical mixtures. Additionally, discrimination between crystalline and amorphous forms of GRIS and ITRA has been shown. Future research in this area could investigate more complex dosage forms containing excipients and lower proportions of APIs.

2.5 References

1. Garbacik, E.T., et al., *Hyperspectral coherent anti-Stokes Raman scattering microscopy for in situ analysis of solid-state crystal polymorphs.* Multiphoton Microscopy in the Biomedical Sciences Xiii, 2013. **8588**.
2. Fussell, A.L., et al., *Coherent anti-Stokes Raman scattering (CARS) microscopy driving the future of drug loaded ordered mesoporous silica imaging.* Analytical Chemistry, Submitted.
3. Brittain, H.G., ed. *Polymorphism in Pharmaceutical Solids*. 1999, Informa Healthcare: New York. 448.
4. Haleblia.J and W. Mccrone, *Pharmaceutical Applications of Polymorphism.* Journal of Pharmaceutical Sciences, 1969. **58**(8): p. 911-&.
5. Hilfiker, R., ed. *Polymorphism in the Pharmaceutical Industry*. 2006, WILEY-VCH Verlag GmbH: Weinheim. 414.
6. Ku, M., *Use of the Biopharmaceutical Classification System in Early Drug Development.* The AAPS Journal, 2008. **10**(1): p. 208-212.
7. Threlfall, T.L., *Analysis of Organic Polymorphs - a Review.* Analyst, 1995. **120**(10): p. 2435-2460.
8. Simonelli, A.P., S.C. Mehta, and W.I. Higuchi, *Dissolution rates of high energy sulfathiazole-povidone coprecipitates II: Characterization of form of drug controlling its dissolution rate via solubility studies.* Journal of Pharmaceutical Sciences, 1976. **65**(3): p. 355-361.
9. Karmwar, P., et al., *Effect of different preparation methods on the dissolution behaviour of amorphous indomethacin.* European Journal of Pharmaceutics and Biopharmaceutics, 2012. **80**(2): p. 459-464.
10. Ford, J.L., *The Current Status of Solid Dispersions.* Pharmaceutica Acta Helvetiae, 1986. **61**(3): p. 69-88.
11. Leuner, C. and J. Dressman, *Improving drug solubility for oral delivery using solid dispersions.* European Journal of Pharmaceutics and Biopharmaceutics, 2000. **50**(1): p. 47-60.
12. Lu, Q. and G. Zografi, *Phase behavior of binary and ternary amorphous mixtures containing indomethacin, citric acid, and PVP.* Pharmaceutical Research, 1998. **15**(8): p. 1202-1206.

13. Alleso, M., et al., *Enhanced dissolution rate and synchronized release of drugs in binary systems through formulation: Amorphous naproxen-cimetidine mixtures prepared by mechanical activation.* Journal of Controlled Release, 2009. **136**(1): p. 45-53.
14. Kinnari, P., et al., *Comparison of mesoporous silicon and non-ordered mesoporous silica materials as drug carriers for itraconazole.* International Journal of Pharmaceutics, 2011. **414**(1–2): p. 148-156.
15. Wang, S., *Ordered mesoporous materials for drug delivery.* Microporous and Mesoporous Materials, 2009. **117**(1–2): p. 1-9.
16. Sarparanta, M., et al., *18F-Labeled Modified Porous Silicon Particles for Investigation of Drug Delivery Carrier Distribution in Vivo with Positron Emission Tomography.* Molecular Pharmaceutics, 2011. **8**(5): p. 1799-1806.
17. Prestidge, C.A., et al., *Mesoporous silicon: a platform for the delivery of therapeutics.* Expert Opinion on Drug Delivery, 2007. **4**(2): p. 101-110.
18. Grzesiak, A.L., et al., *Comparison of the four anhydrous polymorphs of carbamazepine and the crystal structure of form I.* Journal of Pharmaceutical Sciences, 2003. **92**(11): p. 2260-2271.
19. Taylor, L.S. and F.W. Langkilde, *Evaluation of solid-state forms present in tablets by Raman spectroscopy.* Journal of Pharmaceutical Sciences, 2000. **89**(10): p. 1342-1353.
20. Saar, B.G., et al., *Video-Rate Molecular Imaging in Vivo with Stimulated Raman Scattering.* Science, 2010. **330**(6009): p. 1368-1370.
21. Parekh, S.H., et al., *Label-Free Cellular Imaging by Broadband Coherent Anti-Stokes Raman Scattering Microscopy.* Biophysical Journal, 2010. **99**(8): p. 2695-2704.
22. Hartshorn, C.M., et al., *Multicomponent Chemical Imaging of Pharmaceutical Solid Dosage Forms with Broadband CARS Microscopy.* Analytical Chemistry, 2013. **85**(17): p. 8102-8111.
23. Garbacik, E.T., et al., *Rapid identification of heterogeneous mixture components with hyperspectral coherent anti-Stokes Raman scattering imaging.* Journal of Raman Spectroscopy, 2012. **43**(5): p. 651-655.
24. Bégin, S., et al., *Coherent anti-Stokes Raman scattering hyperspectral tissue imaging with a wavelength-swept system.* Biomed. Opt. Express, 2011. **2**(5): p. 1296-1306.

25. Matsuo, K. and M. Matsuoka, *Solid-state polymorphic transition of theophylline anhydrate and humidity effect.* Crystal Growth & Design, 2007. **7**(2): p. 411-415.
26. Matsuo, K. and M. Matsuoka, *Kinetics of humidity driven solid-state polymorphic transition of theophylline anhydrates.* Journal of Chemical Engineering of Japan, 2007. **40**(7): p. 541-549.
27. Nolasco, M.M., A.M. Amado, and P.J.A. Ribeiro-Claro, *Computationally-assisted approach to the vibrational spectra of molecular crystals: Study of hydrogen-bonding and pseudo-polymorphism.* ChemPhysChem, 2006. **7**(10): p. 2150-2161.
28. Ribeiro-Claro, P.J.A. and P.D. Vaz, *Towards the understanding of the spectroscopic behaviour of the C-H oscillator in C-H center dot center dot center dot O hydrogen bonds: the effect of solvent polarity.* Chemical Physics Letters, 2004. **390**(4-6): p. 358-361.
29. Czernicki, W. and M. Baranska, *Carbamazepine polymorphs: Theoretical and experimental vibrational spectroscopy studies.* Vibrational Spectroscopy, 2013. **65**(0): p. 12-23.
30. Smith, E. and G. Dent, *Modern Raman Spectroscopy*2005: John Wiley and Sons. 210.

In situ dissolution analysis using CARS microscopy

Chapter three

Dissolution testing is an important aspect of pharmaceutical oral product development as oral formulations need to dissolve and be absorbed for therapeutic efficacy. In situ dissolution analysis has the potential to provide a greater understanding of the dissolution process. This chapter encompasses the work done to incorporate dissolution testing into the CARS microscopy setup to allow in situ analysis. This work starts from system building and finishes with results from a number of pharmaceutically relevant samples. The methods and results from this work have been published in Fussell et al.[1, 2].

3.1 Introduction

Dissolution testing is an important part of pharmaceutical oral dosage form development because active pharmaceutical ingredients (APIs) are required to be dissolved and then absorbed for a therapeutic effect. APIs are known to exist in various solid state forms, including crystalline and amorphous forms. These can change during storage and during dissolution affecting the dissolution rate of the drug product. More details about solid state polymorphism can be found in chapter two.

Solid state changes that occur during dissolution are known as solvent-mediated phase transformations and they occur when a metastable form (higher solubility) converts to a stable form (lower solubility) through precipitation from a supersaturated solution [3]. Solvent-mediated phase transformation kinetics are determined by the relative rates of growth and dissolution [3, 4]. In the literature there are many reported cases of solvent mediated phase transformations. Savolainen *et al*. [5] performed dissolution testing on α, γ and amorphous forms of indomethacin (IMC). They found that the initial dissolution rate for amorphous IMC was faster than the crystalline forms but the dissolution rate decreased as the sample began to crystallize to α-IMC during dissolution testing. Additionally, the solvent mediated phase transformations of theophylline (TP) anhydrate (TPa) to theophylline monohydrate (TPm) [6, 7] and the conversion of nitrofurantoin anhydrate (form β) to monohydrate (form II) [6] during dissolution testing have been published.

As these solid state conversions during dissolution reduce the dissolution rate there is a need to investigate methods of inhibiting or delaying them. Most of the work in this area focusses on the conversion from anhydrous to hydrous form conversions. Katzhendler *et al*. [8] investigated the polymer hydroxypropylmethylcellulose (HPMC) for inhibiting the transformation of CBZ to CBZ dihydrate on the surface of tablets in aqueous solutions. They postulate that hydroxyl groups from HPMC may hydrogen bond with CBZ at the water binding site leading to inhibition of dihydrate form growth. Tian et al.[9] also studied the conversion of CBZ to CBZ dihydrate and they concluded that hydrogen bonding ability and sufficient hydrophobicity were important

parameters to determine the inhibition ability of various excipients. Wikström *et al*. [10] investigated a number of pharmaceutical excipients as potential TPm formation inhibitors during wet granulation. The majority of excipients tested did not change the transformation of TP. However, polymers such as HPMC and methyl cellulose (MC) could significantly inhibit the transformation of TPa to TPm during wet granulation. Wikström *et al*. [10] suggested that the polymers adsorb to fast-growing surfaces of the monohydrate crystal inhibiting crystal growth and leading to morphological changes.

Pharmacopeial dissolution methods are generally not capable of identifying surface solid state changes occurring during dissolution. This is because standard dissolution techniques require the immersion of the drug (e.g. as a compact) in a flowing dissolution medium with samples of the dissolution medium removed and analyzed for dissolved drug concentration using UV absorption spectroscopy or HPLC [11]. Analyzing solution concentration provides information about how much drug is dissolved, but it does not give any direct information about physical changes of the dissolving dosage form. Direct analysis of the surface of the solid dosage form during dissolution testing can therefore provide improved understanding of dissolution behavior.

In situ dissolution analysis requires analytical techniques that are capable of operating in an aqueous environment. Additionally, the analytical technique must be non-destructive towards the sample and not interfere with the dissolution process. Finally, the technique needs to obtain data at a sufficient temporal resolution (on the order of seconds) to record rapid changes occurring during dissolution. Common solid state analytical techniques such as scanning electron microscopy (SEM), x-ray powder diffraction (XRPD), Near infrared (NIR) and infrared (IR) spectroscopy all have limitations preventing their use *in situ* during dissolution. Infrared radiation used in NIR and IR imaging is strongly absorbed by water limiting their use in aqueous environments [12, 13]. SEM has been used to characterize solid-state changes on the surfaces of dosage forms after dissolution [6, 14]. Debnath et al. [14] investigated XRPD as a tool to depth profile phase changes on samples of IMC and TP during

pharmaceutical processing including post-dissolution analysis. However, due to sample preparation requirements both SEM and XRPD are unsuitable for *in situ* dissolution analysis. Spontaneous Raman spectroscopy on the other hand is suitable for *in situ* analysis and has been used to monitor solid state conversions during dissolution [5, 6]. Spontaneous Raman spectroscopy can generate vibrational spectra covering a wide range of vibrational frequencies in a few seconds. Combining spontaneous Raman spectroscopy with a flow through cell and UV absorption spectroscopy allowed *in situ* analysis of a number of solid state transformations, including transformation from TPa to TPm [6], and the crystallization of amorphous IMC and CBZ [5]. However, non-spatially resolved spontaneous Raman spectroscopy is not capable of identifying where solid state conversions are occurring during dissolution and imaging techniques using spontaneous Raman scattering such as Raman mapping are too slow (s/pixel) for *in situ* dissolution analysis.

Coherent anti-Stokes Raman scattering (CARS) microscopy is an analytical technique capable of *in situ* dissolution analysis. CARS microscopy is described in more detail in chapter one and summarized in [15]. Briefly, CARS microscopy is capable of rapid spectrally- and spatially-resolved imaging allowing the visualization of different solid state forms of drugs based on their Raman vibrational spectra. CARS signal is only produced within the focal volume of the focusing objective making it inherently confocal, providing diffraction limited imaging.

Imaging using CARS microscopy has been performed on a number of pharmaceutical samples focusing on drug release. Windbergs *et al*. [7] and Jurna *et al*. [16] imaged the API distribution in oral lipid dosage forms and monitored the API release during dissolution with a flow through cell setup using TP as a model API.

This chapter describes the development of the CARS microscope dissolution setup allowing simultaneous monitoring of dissolved drug concentration and chemically selective imaging of the surface of the dissolving dosage form. Additionally, hyperspectral CARS imaging pre- and post-dissolution is applied to visually confirm

the solid state conversions observed during dissolution. Theophylline (TP) was the model API used either in a pure form or combined with ethyl cellulose in different dissolution media for these experiments.

3.2 Materials and Methods

3.2.1 Materials

USP grade theophylline (TP, 1,3-dimethyl-7H-purine-2,6-dione) anhydrate and monohydrate were gifted from BASF (Ludwigshafen, Germany). Methyl cellulose powder (400 mPa·s) (MC) and ethyl cellulose powder (22 mPa·s) (EC) were gifted from Colorcon GmbH (Idstein, Germany).

3.2.2 Methods

Compact preparation

Weighed amounts of TPa, TPm, and 50:50 mixture of TPa with EC (0.49 g) were directly compressed using a force feed tablet press (IMA Kilian Pressima, Italy). The upper punch had a pre-compression height of 9.22 mm and a final compression height of 3.02 mm using a compaction force of about 13 kN, resulting in compacts which had a diameter of 12.02 mm and a thickness of about 3 mm.

CARS microscopy

The CARS microscope is described in more detail in chapter two. The dissolution work was conducted with the signal and fundamental laser beam combination focused onto the sample using either a 20X/0.5 NA or 20X/0.75 NA objective. The backscattered CARS signal was collected and using these settings the CARS microscope system had an axial spatial resolution of about 10 μm and a lateral spatial resolution of about 1 μm.

Hyperspectral CARS imaging

Hyperspectral CARS imaging provides a method to rapidly and visually confirm the solid-state form on the surface of an oral dosage form, both pre- and post-dissolution. The method for collecting hyperspectral CARS images has been published in Garbacik et al. [17] and is covered in more detail in chapter two. In this study 512 x 512 pixel hyperspectral images were collected over a range of 100 cm^{-1} with each hyperspectral image taking approximately two minutes to record. CARS spectra shown in this article are pixel intensity profiles across the vibrational frequencies and were extracted from the hyperspectral image data.

In situ CARS dissolution imaging

In situ CARS images (512 x 512 pixels) covering 350 x 350 μm were recorded every 1.12 seconds (roughly 4.3 μs/pixel dwell time) for the duration of the dissolution experiments (15 minutes). All *in situ* CARS images recorded during dissolution testing were recorded around 2952 cm^{-1} and were false colored green. This peak has been assigned to antisymmetric C-H stretching in the methyl groups [18] and provided a strong CARS signal for both TPa and TPm.

CARS microscope dissolution flow cell

Designing and building of the custom CARS microscope dissolution flow cell was required before the dissolution experiments could be conducted. Important aspects that needed to be considered while designing the flow cell included water tightness, microscope objective working distance and tablet dimensions. Water tightness was required because the dissolution medium was used to determine the dissolved drug concentration and also to ensure that no medium leaked on the optical components. The microscope objective working distance defines the maximum allowable distance from the objective to the sample. The objective used for this work has a working distance of 2.1 mm meaning that the tablet in the flow cell could not be further than 2.1 mm from the microscope objective. The tablet dimensions were also an important aspect considered during the design process because the tablet holder had to fit the

tablet perfectly to minimize tablet movement during dissolution and to ensure only one surface of the tablet was available for dissolution. Figure 1 shows the dissolution flow cell used in this work.

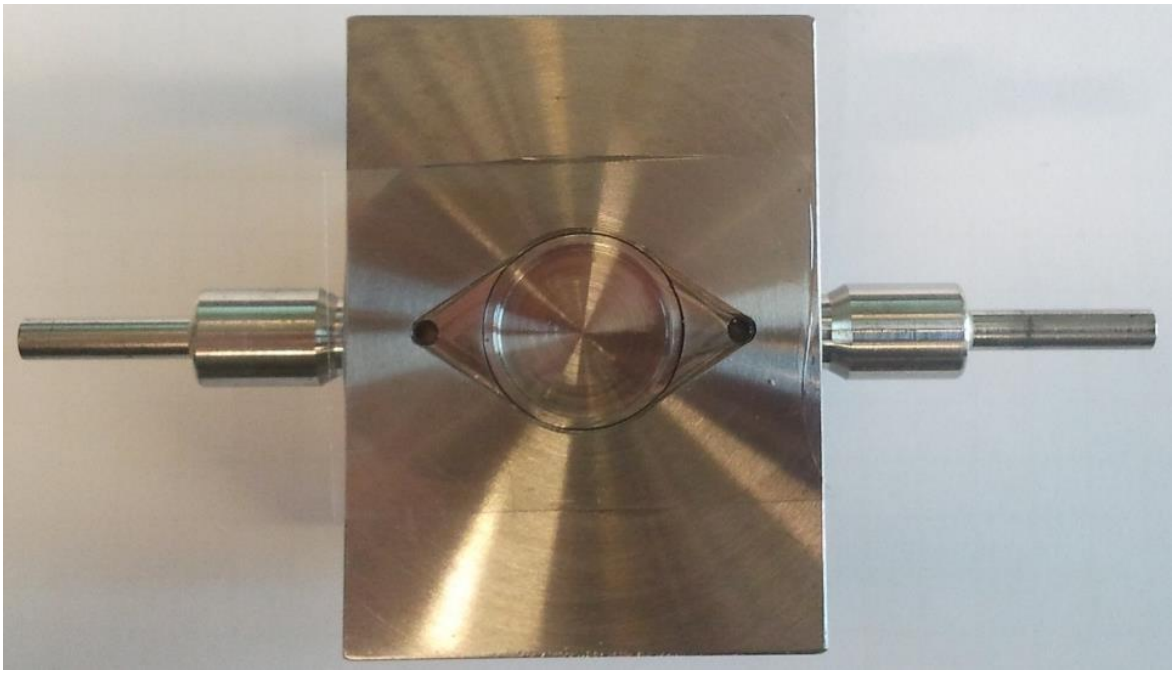

Figure 1. Custom built CARS microscope dissolution flow cell with tablet holder designed to hold flat-faced tablets with 12 mm diameter.

Dissolution setup

A deuterium light source (DT-MINI-2, Ocean Optics, The Netherlands) was connected by an optical fiber to a Z-shaped flow cell (FIA-Z-SMA, Ocean Optics, The Netherlands) with a 10 mm pathlength. An optical fiber connected the Z-shaped flow cell to a CCD spectrometer (USB2000+, Ocean Optics, The Netherlands). Open loop channel flow through intrinsic dissolution was conducted using a peristaltic pump (Reglo, ISMATEC, Germany) which pumped dissolution medium (distilled water or methyl cellulose 0.45 % w/v) through the custom built CARS microscopy dissolution flow cell and through the Z-shaped UV flow cell at a rate of 5 mL/min. UV absorbance was collected at 290 nm every 30 seconds. Dissolution was conducted multiple times on each sample to check for consistency.

3.3 Results and Discussion

3.3.1 Hyperspectral CARS analysis of TPa and TPm

CARS spectra of the C-H stretch region were collected prior to dissolution experiments on pure TPa and TPm to identify an appropriate vibrational frequency at which to record CARS images during dissolution experiments and for comparison to the before and after dissolution hyperspectral scans of the compacts. The C-H stretch region was chosen as TP has an intense signal in that region for both solid state forms (Figure 2). Both TPa and TPm featured a peak at around 2950 cm^{-1} which has been assigned to antisymmetric C-H stretching in the two methyl groups ($\nu_{as}C_{(1,3)}H_3$) [18]. There was a peak shift between the two forms in the C-H stretching region of the spectra at a higher Raman shift, with the TPa peak at around 3120 cm^{-1} and the TPm peak at around 3105 cm^{-1}. This peak has been assigned to the imidazole ring C-H stretching ($\nu C_{(8)}$-H) and the red-shift is due to $C_{(8)}$-H···O intermolecular hydrogen bonding in the TPm form [18, 19]. The peak shift allowed the change of anhydrate to monohydrate to be visualized using hyperspectral imaging. However, the shifting peak was not suitable for single-frequency CARS dissolution imaging because it was not possible to simultaneously image the TPm crystal growth on the surface of a TPa compact.

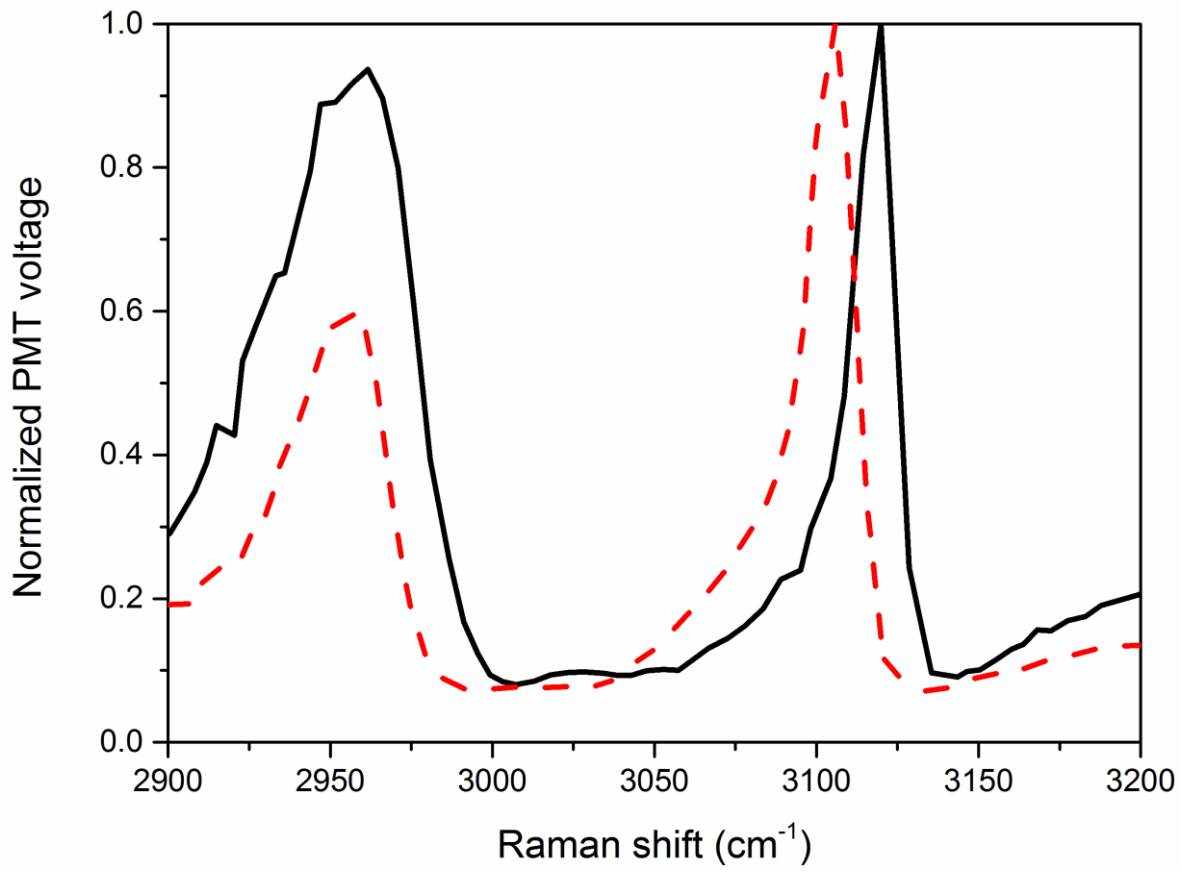

Figure 2. CARS C-H stretch region spectra between 2900 and 3200cm^{-1} for TPa (black line), and TPm (red dashed line).

Since both TPa and TPm produce a strong signal at 2952 cm^{-1}, single-frequency CARS images were recorded at this Raman shift during dissolution experiments to allow visualization of both TPa and TPm simultaneously. Additionally, at 2952 cm^{-1} there is minimal interference due to the presence of water.

Hyperspectral images were recorded before and after dissolution experiments to allow a rapid visual confirmation of the solid-state conversion on the surface of the compact which would be evident as a change in colour. Figure 3A shows the pre-dissolution hyperspectral image for a TPa compact, while Figure 3B shows the post-dissolution hyperspectral image for the same TPa compact recorded after the duration of a dissolution experiment (15 minutes) using water as dissolution medium.

The colour change between Figures 3A and B is due to the $\nu C_{(8)}$-H peak shift in CARS spectra indicating that the TP on the surface has converted to TPm form.

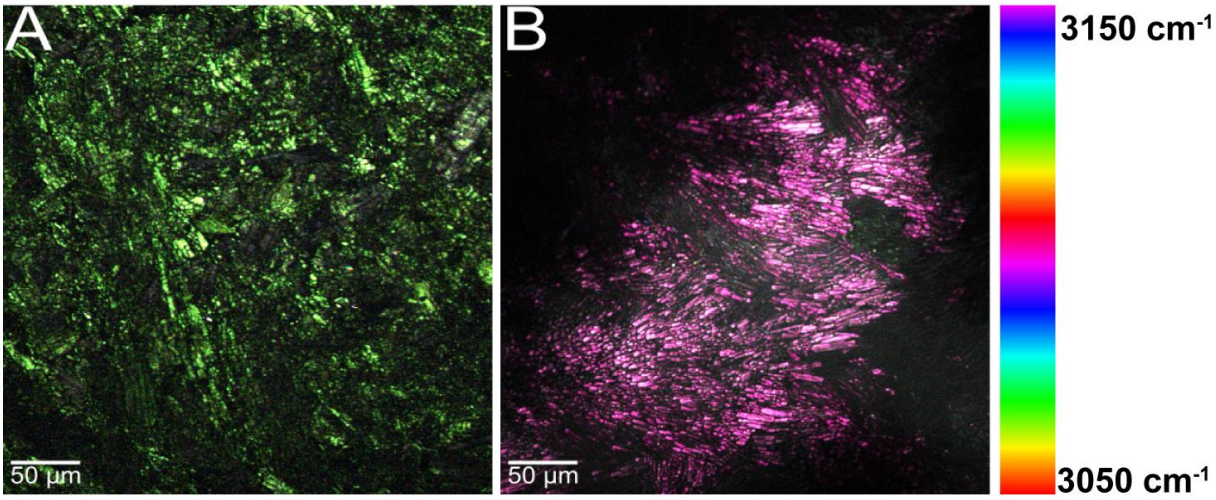

Figure 3. Hyperspectral CARS images recorded between 3050 $cm^{-1}$and 3150 cm^{-1} of a TPa compact before (A) and after (B) dissolution with color map used to project the images where water was used as dissolution medium.

The CARS spectra were collected before and after each dissolution experiment for comparison with the reference spectra (Figure 2) and to confirm the solid-state conversion observed in the dissolution images. Figure 4 shows the pre-dissolution (black line) and post-dissolution (red dashed line) CARS spectra for a TPa compact after dissolution using water as the dissolution medium. The CARS spectra confirm the observed shift in the peak from around 3120 cm^{-1} (before) to 3105 cm^{-1} (after), indicating the conversion from TPa to TPm on the surface of the compact.

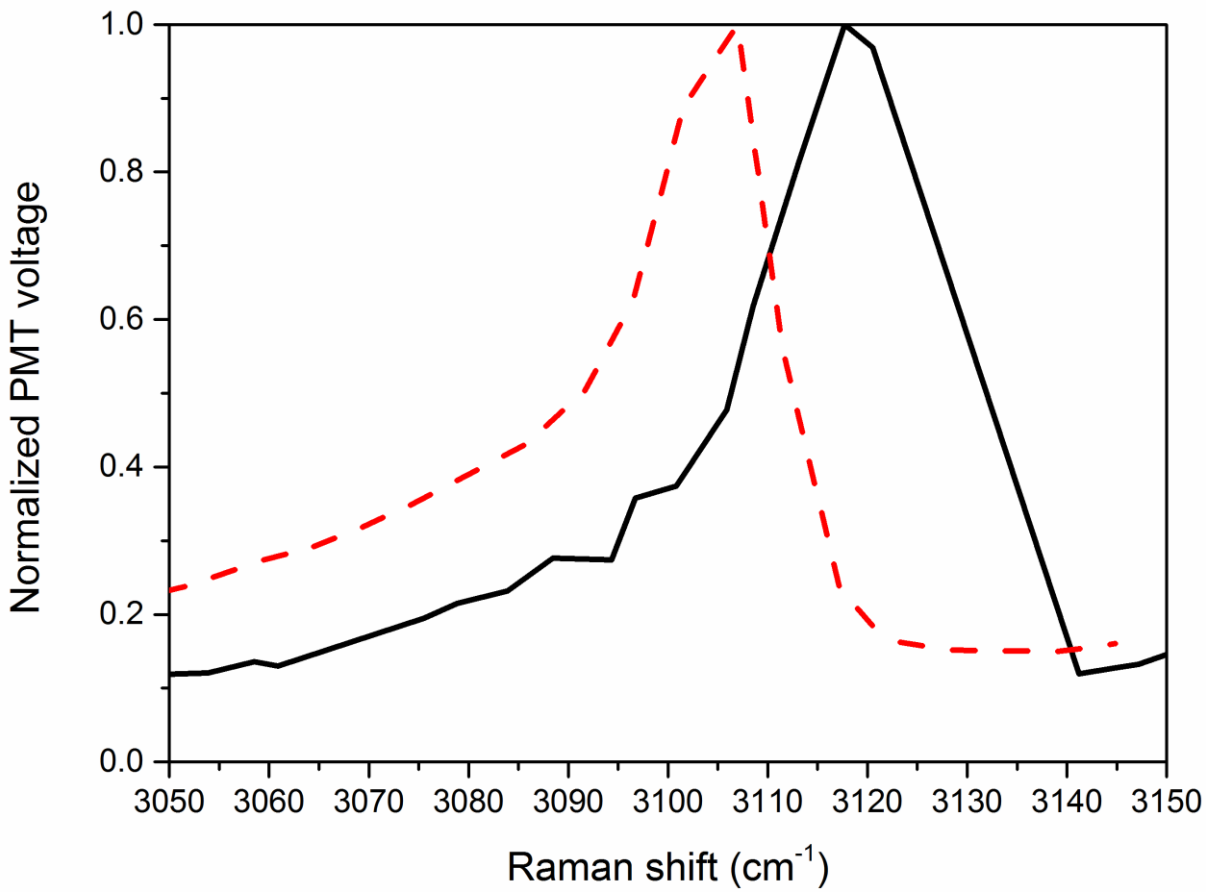

Figure 4. CARS spectra between 3050 and 3150 cm^{-1} for TPa compacts before dissolution (black line) and after dissolution where water was used as dissolution medium (red dashed line).

3.3.2 *In situ* analysis of TP during dissolution testing

3.3.2.1 Theophylline in water dissolution

The first samples to be investigated using the CARS dissolution setup were compacts containing either pure TPa or TPm (CARS results not shown) with water as the dissolution medium. Single-frequency CARS images (512 x 512 pixels) were recorded at 2952 cm^{-1} approximately every second for the duration of the dissolution experiments (15 minutes). Figure 5 shows snapshots of the dissolution imaging from pure TPa dissolution conducted using water as dissolution medium. From Figure 5 it is apparent that the TPm nucleation and crystal growth begins almost immediately after the beginning of the dissolution experiment with TPm crystals (needle shape) growing outwards from two nuclei on the surface of the compact. After two minutes

about half of the field of view is covered in TPm crystals and it appears that most of the field of view is completely covered in TPm after about four minutes. Aaltonen et al.[6] reported observing TPm crystal growth immediately after the beginning of the dissolution experiment with Raman spectroscopy indicating that 100 % of the solid phase of the sample was TPm after around seven minutes.

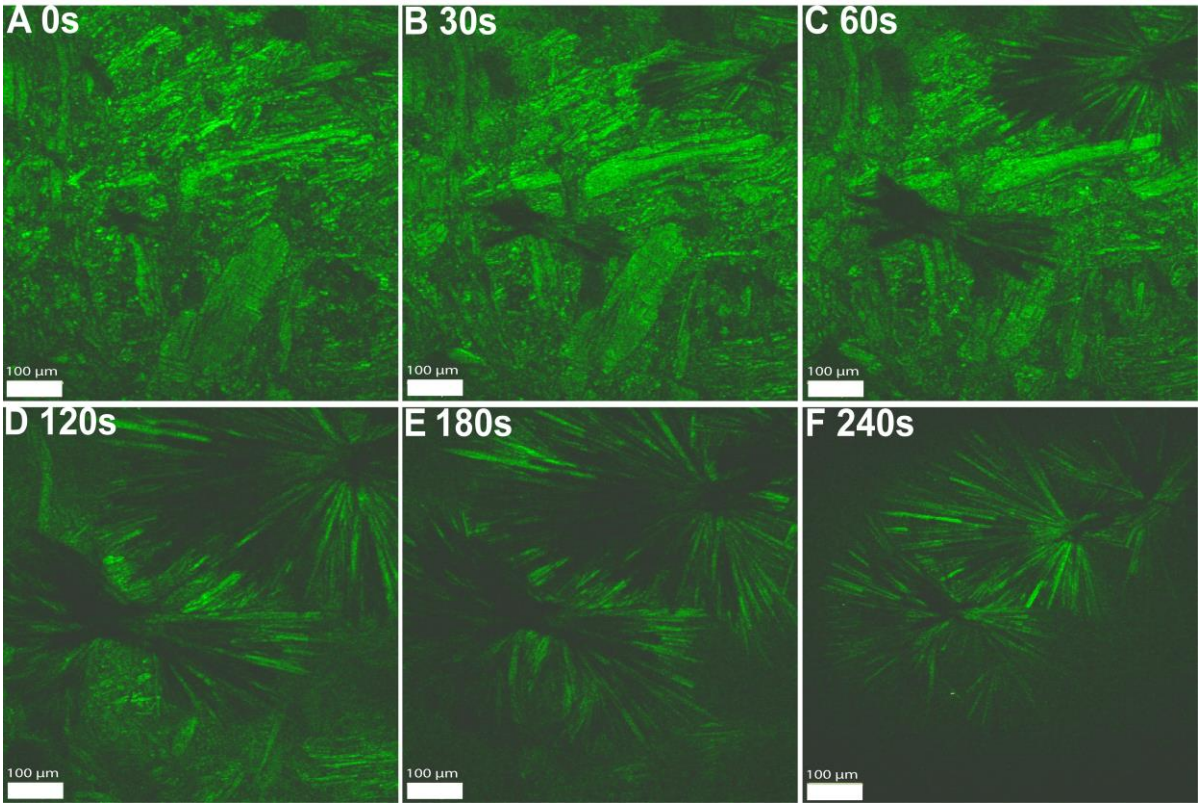

Figure 5. Single-frequency CARS images (2952 cm^{-1}) of TPm crystals growing on the surface of a TPa compact undergoing dissolution using water as the dissolution medium. Still images from a dissolution video show progressive crystal growth.

Ultraviolet spectra were collected every 30 seconds during the dissolution experiment to determine the dissolution rate profiles for TPa and TPm in our channel flow cell system. Figure 6 shows the dissolution profiles for TPa (solid lines) and TPm compacts (dashed lines). From Figure 6 it can be seen that TPa initially increases to peak values of between 150-190 µg/mL while the TPm reaches concentrations of between 70-80 µg/mL. Subsequently, there is a sharp drop in the first few minutes of the TPa dissolution that is not seen for the TPm dissolution. This change in dissolution behavior is due to a solvent mediated transformation wherein the

dissolving TPa (solubility 12 mg/mL at 25 °C [20]) reaches supersaturation which causes precipitation and growth of the more stable but less soluble TPm (solubility 6 mg/mL at 25 °C [20]) crystals that grow on the surface of the TPa compacts during dissolution. The surface growth of TPm on TPa samples undergoing dissolution has also been observed in other studies, using offline XRPD analysis [14] and inline spontaneous Raman spectroscopy [6, 21].

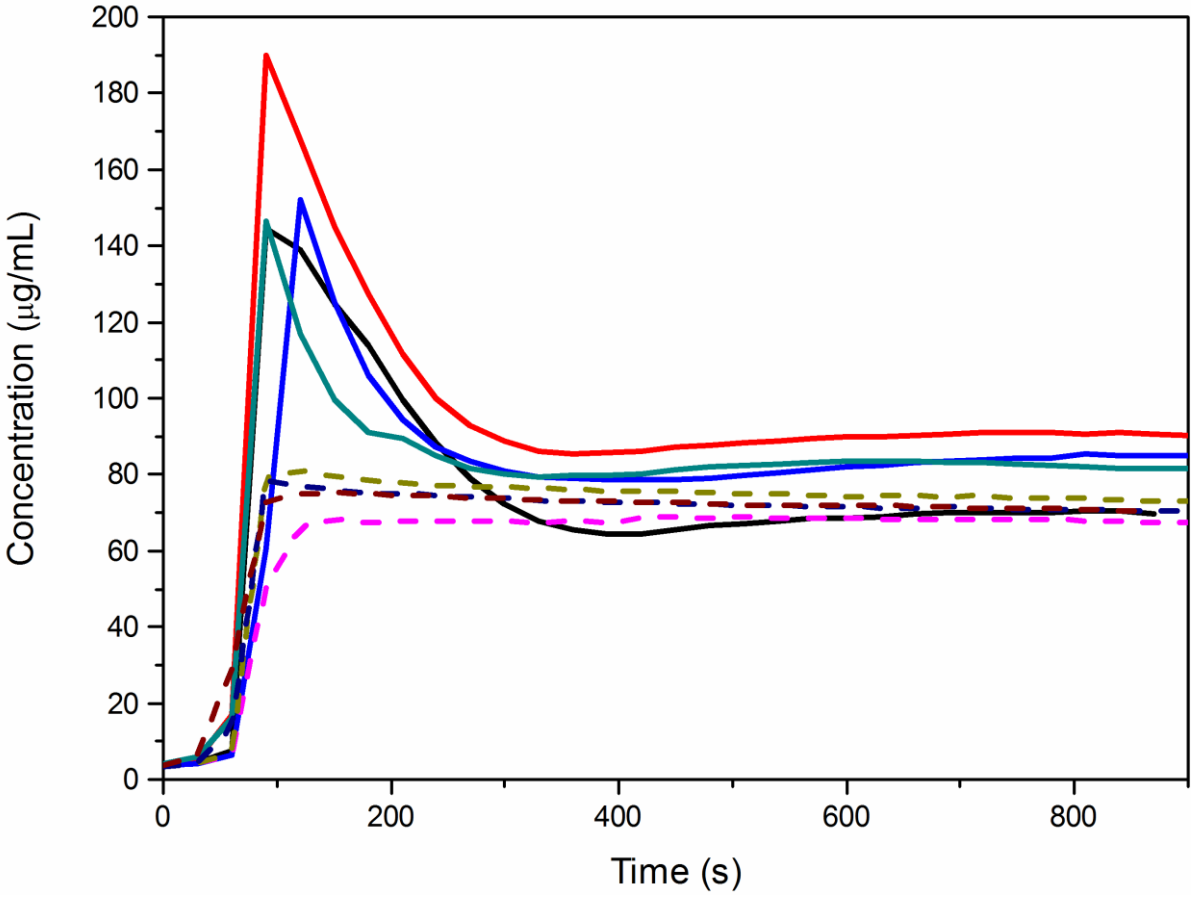

Figure 6. Channel flow through cell dissolution profiles for TPa (solid lines) and TPm (dashed lines) compacts using water as dissolution medium.

The UV data shown in Figure 6 correlate well with the CARS images (Figure 5) that were recorded during the dissolution experiments. The dissolution rate peaked after about two minutes which related to about half of the microscope field of view covered in TPm needle-shaped crystals. After about five minutes the dissolution rate reached a plateau at the same time the crystal growth appeared to completely cover the field of view. Figure 6 shows that the TPm dissolution rate quickly reached a steady state

after one minute and remained there for the duration of the experiment. The steady state dissolution rates were calculated to be 360 ± 37 μg/min/cm^2 and 320 ± 12 μg/min/cm^2 for the compacts prepared from TPa and TPm respectively. The slightly higher dissolution rate (not statistically significant) for the compacts originally composed of TPa after surface conversion to TPm can be attributed to the TPm needle growth resulting in a larger surface area.

3.3.2.2 Theophylline with ethyl cellulose mixture in water dissolution

After performing dissolution using pure TP samples it was decided to try and analyze mixtures with the aim of preventing the TPm crystal growth. One of the mixtures investigated was a 50:50 mixture of TPa with EC. Figure 7 shows selected frames from a dissolution video. At the beginning of dissolution (Figure 7, time 0 s) there are areas of green showing the TP content of the tablet and there are also areas of darkness where there is only EC present on the surface of the tablet. After about 60 seconds there appears to be the beginning of TPm crystal growth on the surface which can be seen as narrow needle-shaped crystals growing outwards from at least one crystal nucleus at the center of the frame (Figure 7, time 60 s). The TPm crystal growth can be much more clearly seen after 130 s (Figure 7, time 130 s). Additionally, at time point 130 s it can be seen that the TPm crystal has not spread entirely across the surface of the tablet. It appears as though the presence of the EC regions has physically blocked the lengthening of the TPm needles. After 250 s it can be seen that the TPm coverage of the surface is not as prominent which suggests that the TPm crystals are themselves beginning to dissolve.

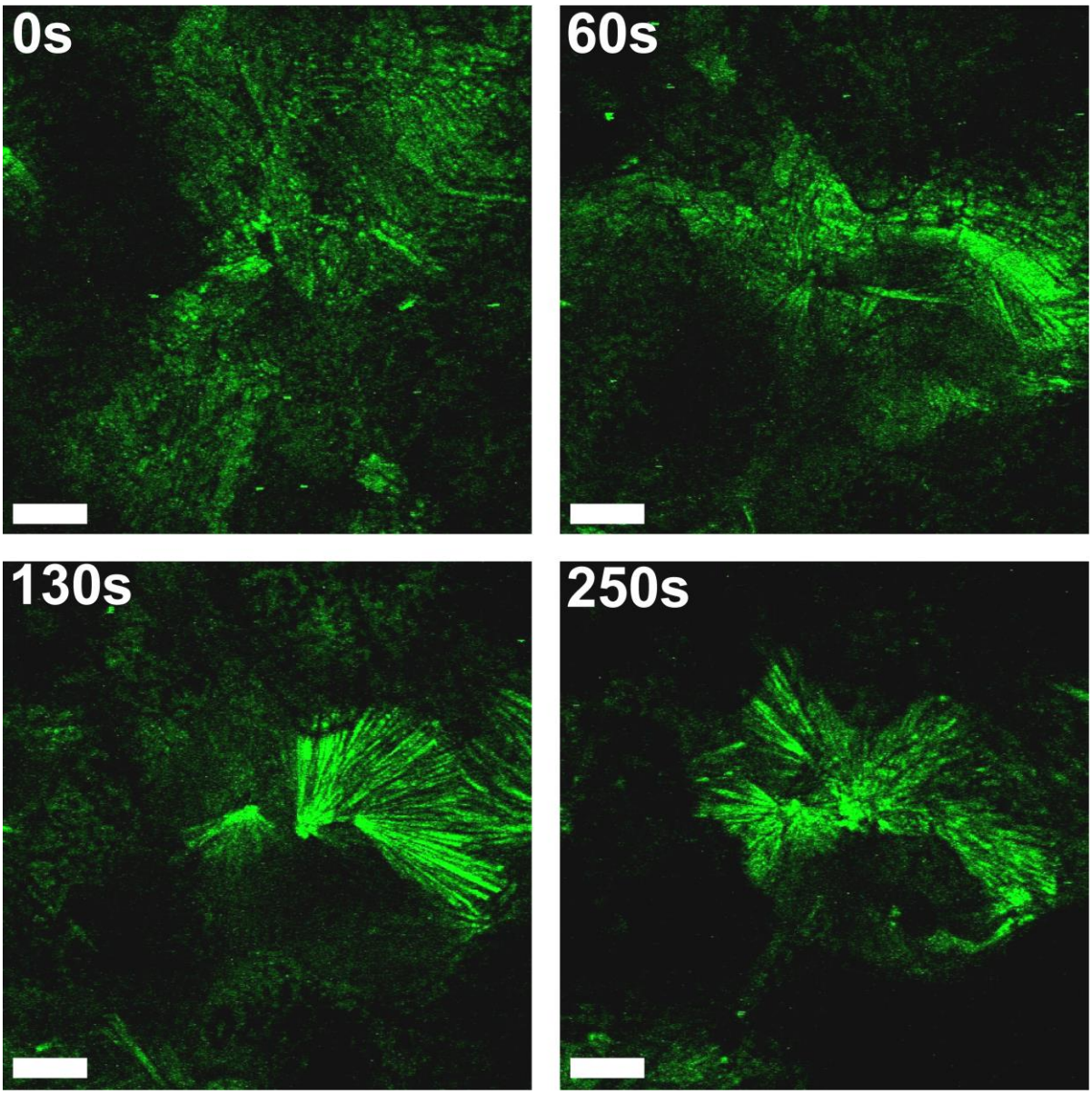

Figure 7. Single-frequency CARS images (2960 cm^{-1}) from a dissolution video for a TPa with EC tablet. The 0 s image is recorded one area of the sample while the 60, 130, and 250 s images are recorded at the same area. Scale bar is 50 µm.

Analysis of the dissolution medium using the inline z-shaped UV flow cell allowed quantitative determination of the drug dissolved during dissolution. Figure 8 shows the dissolution profile for the dissolution of the TPa with EC tablet. The UV dissolution profile (Figure 8) shows that dissolution of TPa begins quickly reaching a maximum concentration of around 90 µg/mL within 120 s, after this time point the dissolution rate begins to decrease. The decrease in the dissolution rate could be due to the

presence of the TPm (solubility 6 mg/mL at 25 °C[20]) crystals on the surface which are less soluble than TPa (solubility 12 mg/mL at 25 °C[20]) and clearly seen in the snapshots from the CARS dissolution video (Figure 7) at this time point. The gradually reducing dissolution rate could also partially be explained by a reduction in TP exposure to the flowing medium. This reduction occurs because EC is practically insoluble in water, so that as the TP dissolves the remaining EC hinders TP exposure to the dissolution medium.

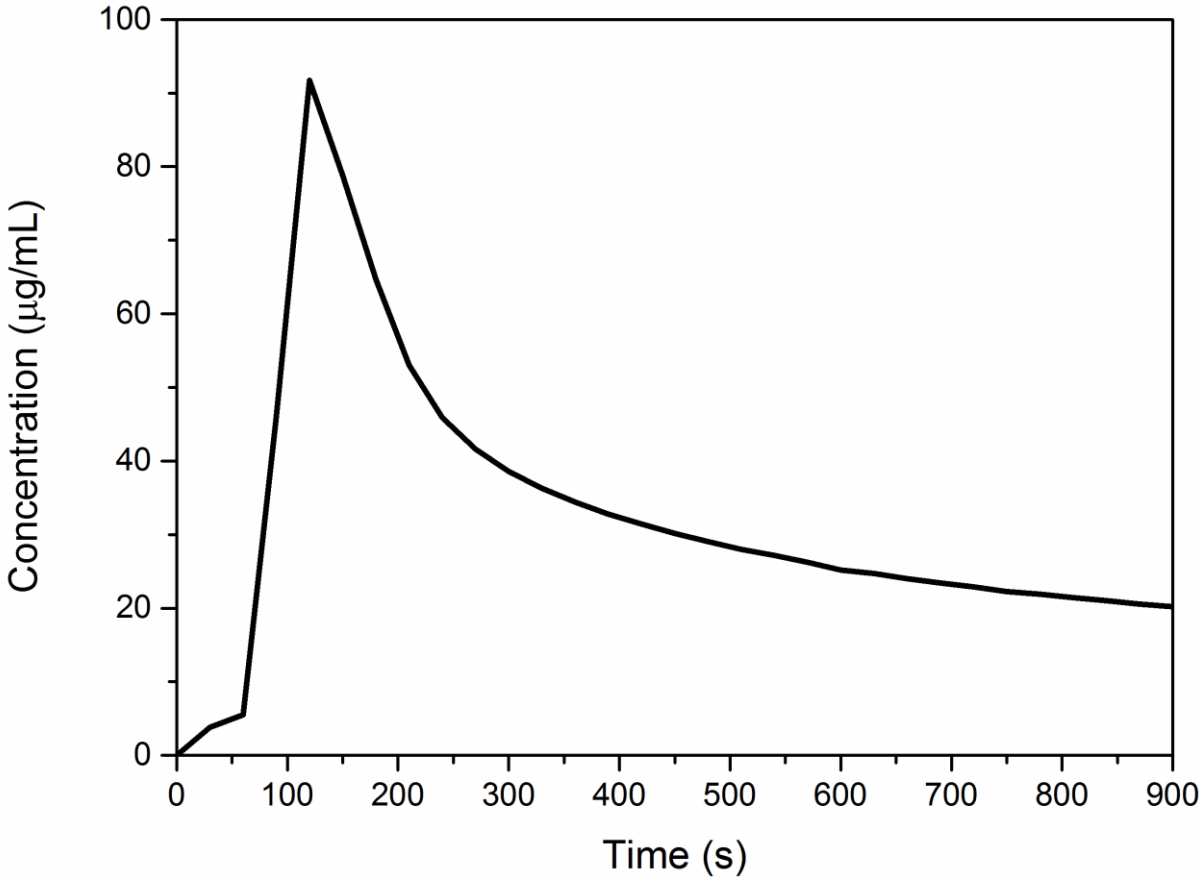

Figure 8. UV dissolution profile. Concentration vs. time plot for a TPa combined with EC tablet showing the concentration of TP in the dissolution medium during the dissolution experiment.

3.3.2.3 Dissolution of theophylline in methyl cellulose solution

As the combination of TPa with EC was unsuccessful in preventing TPm crystal growth it was decided to try another strategy to prevent the TPm growth. In the literature, Wikström et al. [10] reported MC solution delaying TPm crystal growth

during high-shear wet granulation. The following step was to perform dissolution testing using MC solution as the dissolution medium.

In situ CARS imaging identified delayed TPm crystal growth on the surface of TPa compacts undergoing dissolution using a MC solution (0.45 % w/v) as the dissolution medium. Figure 9 shows *in situ* single-frequency CARS snapshots taken from a dissolution video. The TPm crystal growth was delayed as it was first observed after approximately 300 seconds (5 minutes) and the surface coverage with TPm was incomplete after the duration of the experiment (15 minutes). Additionally the TPm crystals were of a different morphology than previously seen when using water as the dissolution medium. Instead of the thin needle-like structure seen growing in water, there was a broad almost sheet-like growth along the surface of the compact.

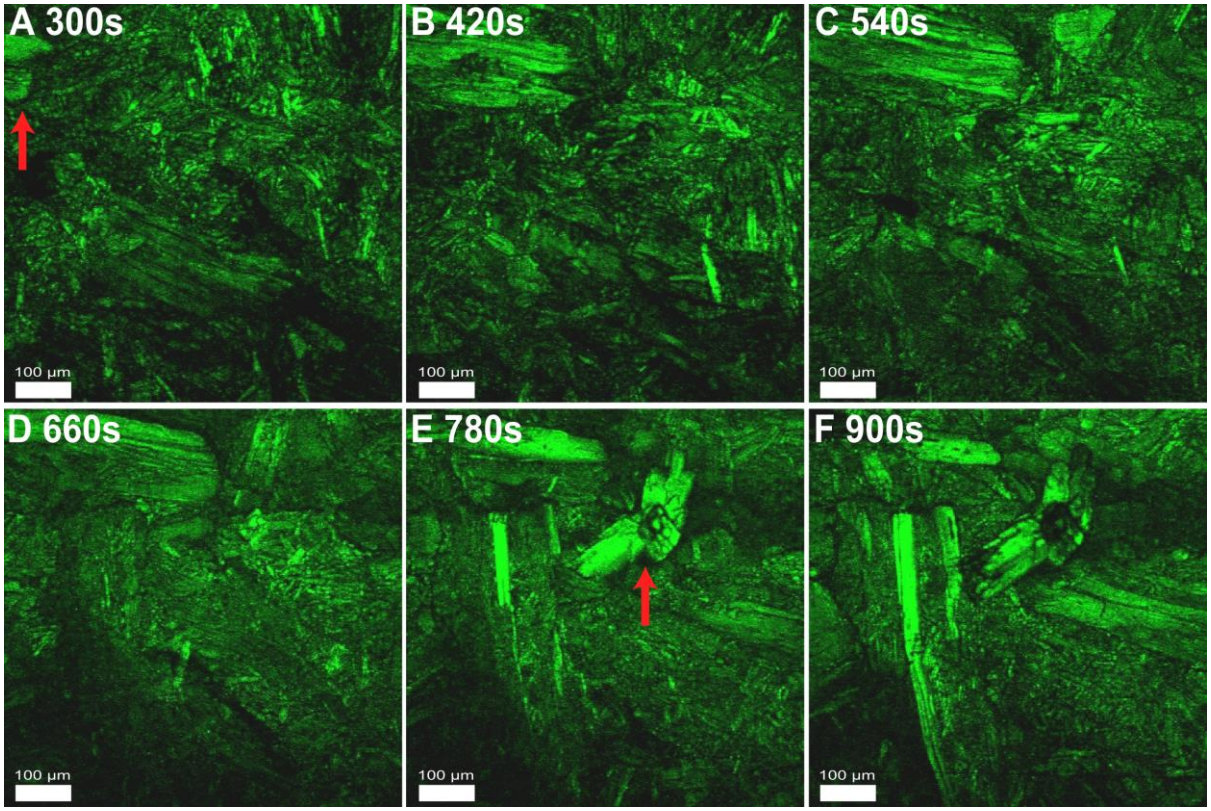

Figure 9. Single-frequency CARS images (2952 cm^{-1}) of TPm crystals growing on the surface of a TPa compact undergoing dissolution using MC solution (0.45 % w/v) as dissolution medium. Red arrows indicate areas of TPm crystal growth. Still images from a dissolution video show delayed crystal growth and different crystal morphology. Scale bar is 100 µm.

The delayed onset of crystal growth and different morphology suggests that the polymer affects both nucleation and crystal growth. It has been suggested that the polymer adsorbs to the surface of the TPa particles and this leads to inhibition of heterogeneous nucleation, while the changed crystal morphology is likely to be due to preferential adsorption to specific crystal faces of TPm, which, in turn, affects their relative growth rates [10].

The delayed TPm crystal growth seen in the CARS dissolution imaging (Figure 9) was expected to affect the TPa dissolution rate and Figure 10 shows that this was the case. Figure 10 shows the dissolution profiles for TPa and TPm compacts undergoing dissolution using MC solution as the dissolution medium. From Figure 10 it can be seen that the characteristic decrease in dissolution rate associated with TPm growth on the surface of TPa compacts (Figure 6) is no longer seen. Instead the TPa compacts reach a concentration of about 150 µg/mL and remain there for the duration of the experiment. The dissolution behavior of the TPm compacts appear minimally affected by the use of the MC dissolution medium as they reach a concentration of about 80 µg/mL and remain there for the duration of the experiment. This concentration is the same as was observed for water without the polymer, revealing that the solubility of the drug (in the same solid state form) is not affected by the polymer in solution, and therefore the different dissolution profiles obtained with and without polymer solution are not solubility mediated.

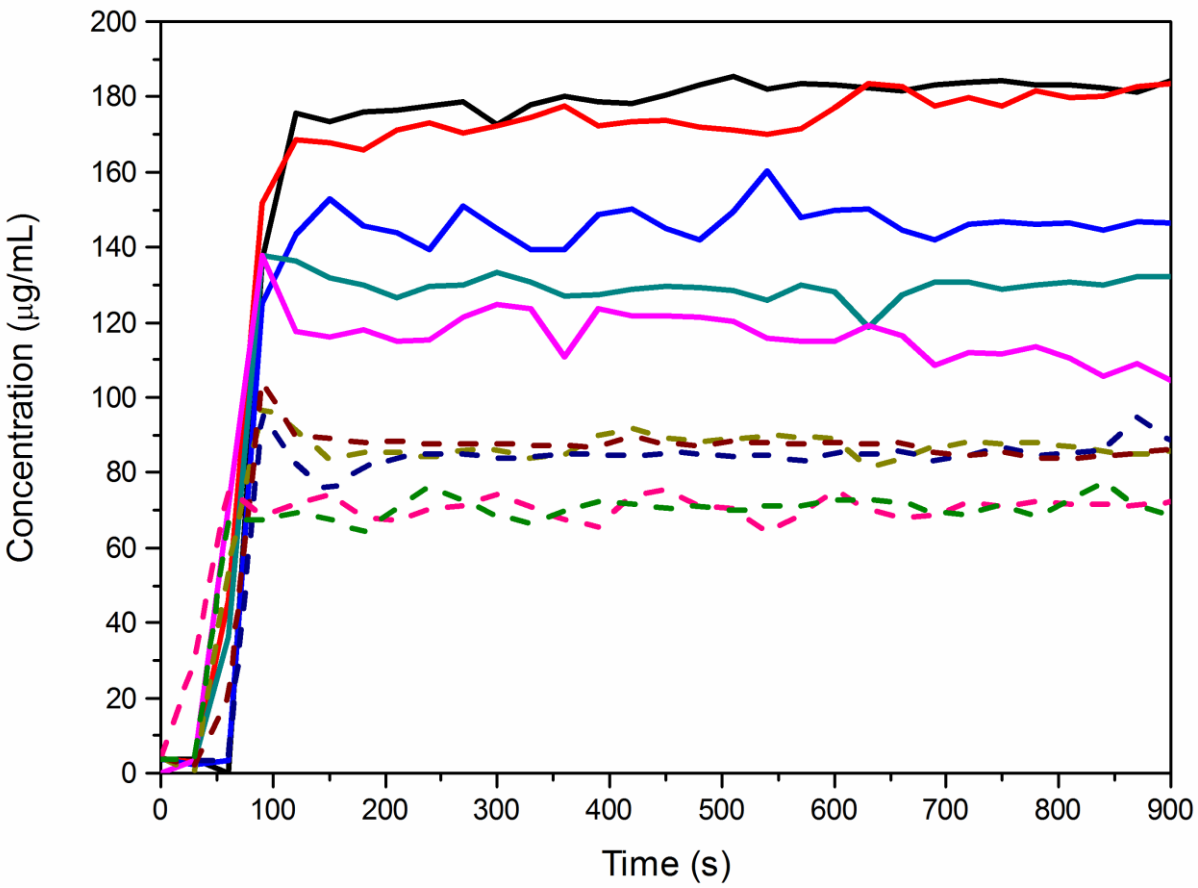

Figure 10. Channel flow through cell dissolution profiles for TPa (solid lines) and TPm (dashed lines) using MC solution as dissolution medium.

The steady state intrinsic dissolution rates were calculated to be 700 ± 130 µg/min/cm^2 and 350 ± 40 µg/min/cm^2 for the compacts prepared from TPa and TPm respectively (assuming both compacts had a perfectly planar surface). Since the solubility of the TPa is twice that of TPm in water at 25 °C [20], a two-fold increase in the dissolution rate of the compact prepared from TPa would theoretically only be expected if there were no conversion to the TPm. However, an increase in surface area of the compacts prepared from TPa after TPm formation was observed in water which affected the dissolution behavior, and therefore a surface area increase can also be expected to affect the dissolution profiles in the polymer solution. Additionally, from Figure 10 there are noticeable fluctuations in the steady state concentrations (when compared to Figure 6) of both TPa and TPm this is attributed to bubbles in the dissolution medium not removed by sonication.

The inherent confocality, chemical specificity, and speed provided by CARS microscopy increases the spatial and chemical resolution of the system providing advantages over existing approaches including traditional IR microscopy and Raman microscopy based on spontaneous Raman scattering. The biggest advantage when compared to traditional optical microscopy is the fact that the detected signal is generated when the excitation beams match the Raman vibrational mode for the chemical of interest this provides chemical selectivity. The inherent confocal nature means that the morphological information is resolved to approximately 10 µm in the depth direction, a resolution that is not obtained with traditional optical microscopy.

3.4 Conclusions and Outlook

CARS microscopy was used to image *in situ* solid-state conversions of samples during dissolution in real time. The combination of CARS microscopy with flow through UV absorbance spectroscopy allowed the visualized polymorphic conversion to be correlated with changes in dissolution rates. Additionally the inhibition of TPm crystal growth due to the presence of MC was correlated with changes in dissolution rate for TPa compacts. Hyperspectral CARS microscopy provided a rapid visual technique to confirm the polymorphic conversion that occurred during dissolution. The combination of the rapid analysis and chemical selectivity of CARS and hyperspectral CARS with UV absorption spectroscopy has the potential to allow improved characterization of solid dosage forms undergoing dissolution. CARS with UV absorption spectroscopy allows further in depth analysis on dosage forms exhibiting unexpected dissolution profiles, including failed dissolution tests. Improved characterization of solid dosage forms undergoing dissolution will help in the development of formulations where dissolution profiles are especially important. Formulations such as those containing a poorly soluble APIs and controlled release formulations, where bioavailability is dissolution- or release-rate limited will benefit from improved characterization.

3.5 References

1. Fussell, A., et al., *In situ dissolution analysis using coherent anti-Stokes Raman scattering (CARS) and hyperspectral CARS microscopy.* European Journal of Pharmaceutics and Biopharmaceutics, 2013. **85**(3, Part B): p. 1141-1147.
2. Fussell, A.L., et al., *Coherent anti-Stokes Raman scattering (CARS) microscopy visualizes pharmaceutical tablets during dissolution.* Journal of visualized experiments, 2014.
3. Davey, R.J., et al., *Rate controlling processes in solvent-mediated phase transformations.* Journal of Crystal Growth, 1986. **79**(1–3, Part 2): p. 648-653.
4. Wikström, H., et al., *Toward an Understanding of the Factors Influencing Anhydrate-to-Hydrate Transformation Kinetics in Aqueous Environments.* Crystal Growth & Design, 2008. **8**(8): p. 2684-2693.
5. Savolainen, M., et al., *Better understanding of dissolution behaviour of amorphous drugs by in situ solid-state analysis using Raman spectroscopy.* European Journal of Pharmaceutics and Biopharmaceutics, 2009. **71**(1): p. 71-79.
6. Aaltonen, J., et al., *In situ measurement of solvent-mediated phase transformations during dissolution testing.* Journal of Pharmaceutical Sciences, 2006. **95**(12): p. 2730-2737.
7. Windbergs, M., et al., *Chemical Imaging of Oral Solid Dosage Forms and Changes upon Dissolution Using Coherent Anti-Stokes Raman Scattering Microscopy.* Analytical Chemistry, 2009. **81**(6): p. 2085-2091.
8. Katzhendler, I., R. Azoury, and M. Friedman, *Crystalline properties of carbamazepine in sustained release hydrophilic matrix tablets based on hydroxypropyl methylcellulose.* Journal of Controlled Release, 1998. **54**(1): p. 69-85.
9. Tian, F., et al., *The influence of various excipients on the conversion kinetics of carbamazepine polymorphs in aqueous suspension.* Journal of Pharmacy and Pharmacology, 2007. **59**(2): p. 193-201.
10. Wikstrom, H., W.J. Carroll, and L.S. Taylor, *Manipulating theophylline monohydrate formation during high-shear wet granulation through improved*

understanding of the role of pharmaceutical excipients. Pharmaceutical Research, 2008. **25**(4): p. 923-935.

11. United States Pharmacopeial Convention, ed. *The United States Pharmacopeia*. 2009: Rockville.
12. Reich, G., *Near-infrared spectroscopy and imaging: Basic principles and pharmaceutical applications.* Advanced Drug Delivery Reviews, 2005. **57**(8): p. 1109-1143.
13. Coutts-Lendon, C.A., et al., *The use of FT-IR imaging as an analytical tool for the characterization of drug delivery systems.* Journal of Controlled Release, 2003. **93**(3): p. 223-248.
14. Debnath, S., P. Predecki, and R. Suryanarayanan, *Use of Glancing Angle X-Ray Powder Diffractometry to Depth-Profile Phase Transformations During Dissolution of Indomethacin and Theophylline Tablets.* Pharmaceutical Research, 2004. **21**(1): p. 149-159.
15. Evans, C.L. and X.S. Xie, *Coherent anti-stokes Raman scattering microscopy: chemical imaging for biology and medicine.* Annu Rev Anal Chem (Palo Alto Calif), 2008. **1**: p. 883-909.
16. Jurna, M., et al., *Coherent anti-Stokes Raman scattering microscopy to monitor drug dissolution in different oral pharmaceutical tablets.* Journal of Innovative Optical Health Sciences, 2009. **2**(1): p. 37-43.
17. Garbacik, E.T., et al., *Rapid identification of heterogeneous mixture components with hyperspectral coherent anti-Stokes Raman scattering imaging.* Journal of Raman Spectroscopy, 2012. **43**(5): p. 651-655.
18. Nolasco, M.M., A.M. Amado, and P.J.A. Ribeiro-Claro, *Computationally-assisted approach to the vibrational spectra of molecular crystals: Study of hydrogen-bonding and pseudo-polymorphism.* ChemPhysChem, 2006. **7**(10): p. 2150-2161.
19. Ribeiro-Claro, P.J.A. and P.D. Vaz, *Towards the understanding of the spectroscopic behaviour of the C-H oscillator in C-H center dot center dot center dot O hydrogen bonds: the effect of solvent polarity.* Chemical Physics Letters, 2004. **390**(4-6): p. 358-361.
20. Rodríguez-Hornedo, N., D. Lechuga-Ballesteros, and W. Hsiu-Jean, *Phase transition and heterogeneous/epitaxial nucleation of hydrated and anhydrous*

theophylline crystals. International Journal of Pharmaceutics, 1992. **85**(1-3): p. 149-162.

21. Lehto, P., et al., *Simultaneous measurement of liquid-phase and solid-phase transformation kinetics in rotating disc and channel flow cell dissolution devices.* International Journal of Pharmaceutics, 2008. **363**(1–2): p. 66-72.

Chemical imaging of adhesive mixtures for inhalation using CARS microscopy

Chapter four

An adhesive mixture for inhalation is a formulation technique developed to improve drug delivery to the airways by ensuring the drug released from the inhaler is of an optimal particle size for delivery. CARS microscopy is a chemically selective imaging technique capable of discriminating between different pharmaceutically relevant chemicals based on differences in their Raman spectra. In this chapter adhesive mixtures consisting of lactose carrier particles coated with one of two model drugs namely budesonide or salmeterol are investigated using CARS microscopy. CARS was used initially to identify the drug distribution on the surface of carrier particles. Image analysis was then performed to determine the drug particle size. Finally correlative imaging was performed with CARS images and scanning electron microscopy images recorded to allow a direct comparison between the two techniques. The content of this chapter is based upon work published in Fussell et al.[1] and was performed in collaboration with Floris Grasmeijer from the Rijksuniversiteit Groningen.

4.1 Introduction

Adhesive mixtures for inhalation are pharmaceutical systems that are designed to increase drug penetration into the airways by ensuring that the active pharmaceutical ingredient (API) is of an optimal particle size for drug delivery to the lungs. These powder mixtures contain API particles in the aerodynamic size range of 1-5 µm adhered on the surface of relatively coarse alpha-lactose monohydrate particles. The API particles need to be within this size range to ensure the API can effectively reach the target deposition sites in the airways with minimal risk of being swallowed or exhaled [2, 3]. Figure 1 illustrates the effect of particle size on the deposition of particles in the airways. The lactose excipient dilutes the drugs and improves the flowability of the powder, which enables reproducible dose delivery for doses as low as only a few micrograms. During mixing, the small drug particles will adhere spontaneously to the large lactose 'carrier' particles, predominantly by means of Van der Waals forces. The adhesive behavior provides improved content uniformity and physical stability of the mixtures [4, 5], but the coated carrier particles are too large for drug delivery to the airways. This means that for effective drug delivery the API particles are required to detach from the carrier particle during inhalation and disperse into the inhaled air stream.

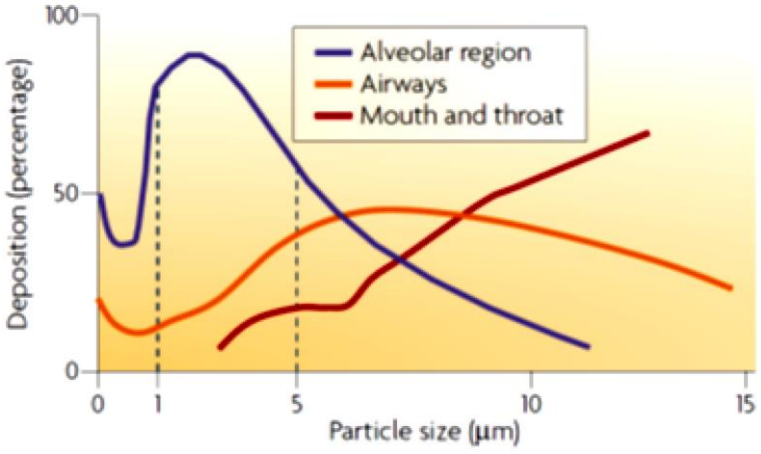

Figure 1. Graph illustrating the effect of particle size on the deposition of particles in the human respiratory tract. Figure reproduced from Patton and Byron [6].

There is a lot of research into which formulation variables are most important for determining performance of the adhesive mixtures but due to conflicting results there is still work to be done to identify critical mixture properties [7]. Two formulation variables that are thought to be important include particle size distribution of API particles on the carrier surface and the spatial distribution of the API particles over carrier surface sites with different binding activities [8-10]. API particles may agglomerate during the mixing process (either alone or with the fine lactose particles also in the mixture), which changes the size distribution of the adhering particles. The surface of the lactose carrier particle is rough on the micrometer scale resulting in particle binding sites with a wide range of binding activity. This means that some API particles are more readily released from the surface than others. These variables influence the drug-carrier interaction forces as well as the separation forces during inhalation, and ultimately the performance of the adhesive mixture.

Scanning electron microscopy (SEM) is a standard imaging technique for characterizing the appearance of adhesive mixtures. SEM is a high resolution imaging technique that has been used to study the morphology of particles in adhesive mixtures for inhalation [11]. However, one of the drawbacks to SEM is that it is not a chemically selective imaging technique making it difficult to distinguish drug particles from fine lactose excipient particles (known as fines), which are similar in size and always present in the adhesive mixture formulation. Therefore, there is a need to accurately assess the composition of agglomerates and to identify the spatial distribution of the API on the surface of the carrier particles.

Coherent anti-Stokes Raman Scattering (CARS) microscopy is a third order non-linear optical technique that is capable of rapid chemically selective imaging based on the same molecular vibrational frequencies as spontaneous Raman techniques. Coherent Raman imaging techniques such as CARS microscopy have about 100 times faster imaging speed when compared to spontaneous Raman mapping techniques [12].

CARS microscopy has been widely applied in biological and medical imaging [13, 14], but applications for pharmaceutical formulations are much fewer. Early work by Pautot et al. [15] focused on using CARS to analyze the composition of emulsions while Kang et al. [16-18] imaged *in situ* release of paclitaxel from polymeric films in a static medium using CARS microscopy.

CARS microscopy provides chemically selective imaging but it is an optical imaging technique, which means that the resolution of the technique is limited to the diffraction limit (around 500 nm for 1064 nm light). This is not the case for SEM imaging which uses an electron beam so SEM is capable of much higher resolution (around 1 nm). Therefore, a combination of a high resolution imaging technique like SEM with a chemically selective imaging technique such as CARS may greatly improve analysis of adhesive mixtures.

Combining the imaging modalities of light microscopy and electron microscopy is well-established in the area of biomedical sciences, with fluorescence microscopy commonly being combined with scanning electron microscopy (SEM). Correlative light and electron microscopy (CLEM) allows a cell to be imaged from the micron to nanometer scale while maintaining spatial orientation [19]. Additionally, spontaneous Raman microscopy [20] and spectroscopy [21] have been combined with SEM. CARS microscopy has also been combined with electron microscopy [22, 23], but has not yet been demonstrated in a correlative manner with SEM. Here results are presented that combine CARS microscopy with SEM in a correlative manner, allowing a direct comparison of images recorded by both modalities.

In this chapter CARS microscopy is used for chemically selective imaging of micronized API that is distributed over the surface of lactose carrier particles. Image analysis was performed using Image J software in an attempt to determine the drug particle distribution which is compared to the standard method of laser diffraction.

Additionally, correlative CARS and SEM were collected allowing a direct comparison between the images obtained using CARS microscopy with those from scanning electron microscopy.

4.2 Materials and Methods

4.2.1 Materials

Alpha lactose monohydrate (Pharmatose 80M) was donated by DFE Pharma (Goch, Germany). The drugs used in this work are micronized salmeterol xinafoate (Novartis, Germany) and budesonide (Fagron, The Netherlands).

4.2.2 Methods

Mixture preparation

All drugs were passed through a 90 μm sieve to break up larger agglomerates prior to mixing with the lactose carrier. Carrier size fractions of 63-90 μm and 250-315 μm were sieved from the Pharmatose starting material (Retsch AS 200 control, Germany). The carrier fractions were subsequently subjected to an air jet sieving process to remove as many residual contaminating lactose particles (known as fines) as possible from the carrier particle surface (Alpine AS200, Augsburg, Germany). Budesonide (0.4% w/w) was mixed for 10 minutes at 90 rpm with the 250-315 μm carrier material using a Turbula blender (WA Bachhofen, Basel, Switzerland). Salmeterol (1.48% w/w) was mixed with the 63-90 μm carrier fraction for either 0.5 or 600 minutes using the same mixer and mixing intensity.

Hyperspectral and *z*-stacked CARS methods

CARS microscope setup

The CARS microscopy system is covered in more detail in chapter two and published elsewhere [24]. For this work the 60X/1.2 NA objective was used for the drug distribution and particle size measurements while the 40X/0.9 NA objective was used

for the correlative CARS and SEM imaging. All of the images presented in this chapter are from backscattered CARS signal. The CARS microscope system using the 60X objective had an axial spatial resolution of about 1 μm and a lateral spatial resolution of about 0.4 μm while the lateral resolution for the 40X objective is about 0.7 μm and the axial resolution around 3 μm.

Hyperspectral imaging

Hyperspectral CARS imaging provides a rapid method to extract the CARS intensity profile (CARS spectra) over range of wavenumbers allowing the identification of peaks suitable for recording chemically specific CARS images. The method for conducting hyperspectral imaging is covered in chapter two and was published previously [24]. Hyperspectral scans were recorded over the range of 2800-3100 cm^{-1} using a step size of about 4 cm^{-1} and taking about 4 minutes to collect.

Z-stacked imaging

Z-stacked imaging was conducted by stepping the microscope objective in the *z* direction in increments of 1 μm. Each *z*-stacked image (512x512 pixels) covers 120x120 μm, consists of about 20 slices and took about 1 minute to record. All CARS images in this chapter are z-stacked images that are projected using a maximum intensity projection.

Particle size analysis using laser diffraction

The particle size distribution of the primary budesonide particles was measured prior to mixing with a HELOS BF diffractometer using a RODOS dry disperser at 3 bar (Sympatec, Clausthal-Zellerfeld, Germany). The diffractometer was equipped with a 100 mm lens and calculations were performed based on the Fraunhofer theory. Increasing the dispersion pressure to 5 bar did not affect the particle size distribution of the drug, indicating that the particle size distribution of the primary particles was measured at 3 bar. To compare the RODOS data with the results from the analysis

using Image J (see further) laser diffraction particle sizes (volume equivalent sphere diameter) were recalculated to projected surface areas according to

$$SA = ¼ * \pi * d_{drug}^2. \quad (4.1)$$

Particle size analysis using Image J

Particle size analysis was performed using the particle analyzer command available in the Image J software (http://rsbweb.nih.gov/ij/) according to the following steps. The image file was first opened by Image J and the scale bar from the image was used to calibrate the software scale in image J. The image was then converted to 8 bit type and converted to binary using the inbuilt automated routine based on the IsoData algorithm [25]. The scale bar was then removed from the image before setting the particle analyzer command to calculate the number and area for particles with an area between 0-infinity μm^2.

Correlative CARS and SEM methods

Samples were mounted on a glass microscope slide using double-sided adhesive tape and suspended in the air above a 40X/0.9NA objective. Carrier particles of interest were identified using the transmission signal on the CARS microscope. *Z*-stacked CARS images (512x512 pixels) were recorded for both the lactose carrier particle (2888 cm^{-1}) and the drug (budesonide, 3046 cm^{-1}, salmeterol, 3050 cm^{-1}) loaded onto the surface. After CARS imaging, the glass microscope slide was removed from the CARS microscope and mounted on double-sided carbon tape and placed on the SEM sample holder. The samples were sputter coated with 20 nm of a gold/palladium alloy. SEM images were then obtained at an acceleration voltage of 3 kV (JSM-6301F, Jeol, Japan).

4.3 Results and Discussion

4.3.1 CARS spectra

Hyperspectral CARS images of the pure chemical compounds were recorded to identify the key vibrational bands that would allow selective imaging of the adhesive mixtures. Hyperspectral scans covered the wavenumber region from 2800-3100 cm^{-1}, corresponding to the C-H stretch region. Figure 2 shows the CARS spectra extracted from the hyperspectral data for alpha lactose monohydrate (green), budesonide (dashed red) and salmeterol (dash-dot black). The frequencies chosen for single wavelength imaging were 2888 cm^{-1} (lactose), 3046 cm^{-1} (budesonide), and 3050 cm^{-1} (salmeterol).

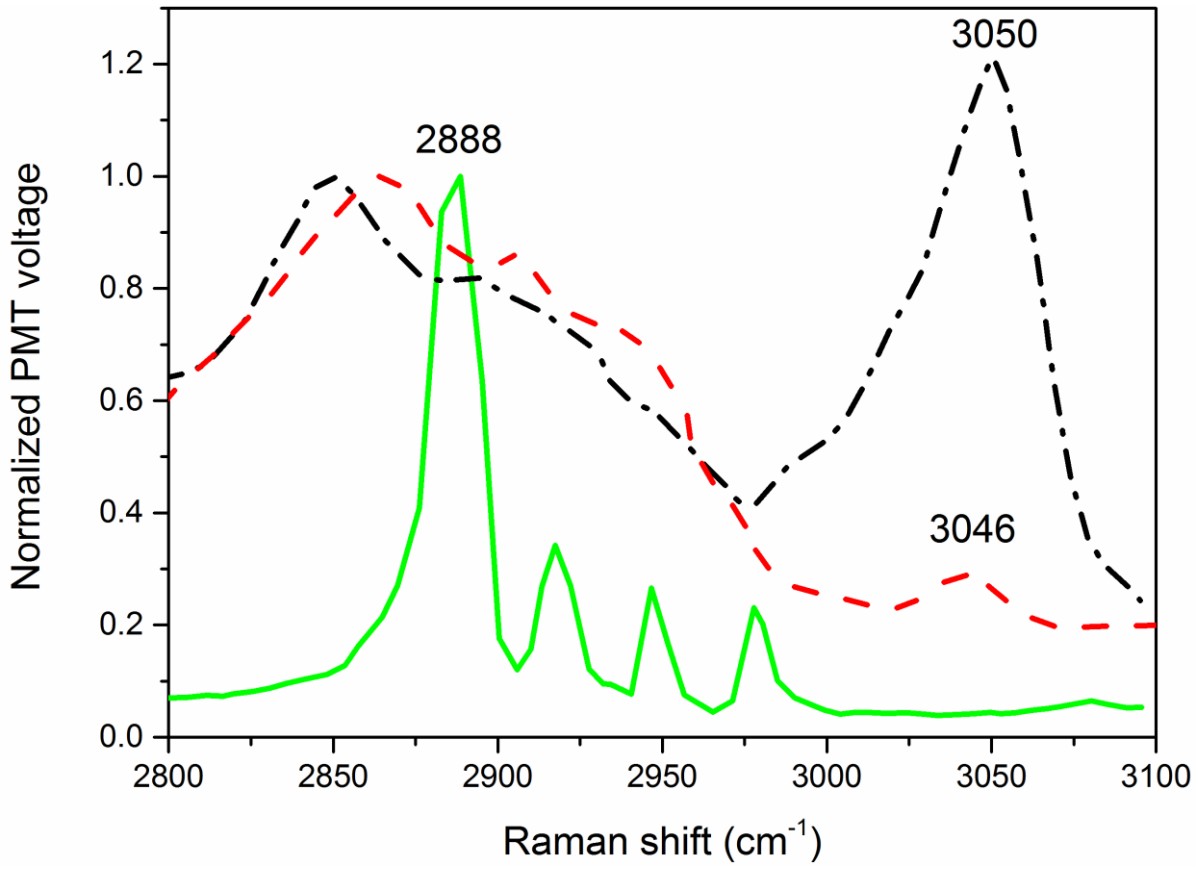

Figure 2. CARS spectra extracted from hyperspectral data covering the CH stretching range from 2800-3100 cm^{-1} for lactose (solid green), budesonide (dashed red) and salmeterol (dash-dot black).

4.3.2 Drug distribution

CARS microscopy allows chemically selective imaging based on Raman vibrational resonances. This makes CARS ideal for studying the distribution of drug on the surface of lactose carrier particles, because different components of the same sample can be imaged by only tuning the frequency difference between the two lasers. Figure 3A shows a *z*-stacked (20 slices, 1 µm slice) CARS image (512x512 pixels) collected at 3046 cm^{-1} which is selective for budesonide. Figure 3B shows a *z*-stacked image (512x512 pixels) of the same area as Figure 3A recorded at 2888 cm^{-1} which is selective for lactose. Figure 3C shows the overlaid *z*-stacked images from figures 3A and 3B, while Figure 3D shows the corresponding transmission light image. From Figure 3C it can be seen that the budesonide (red) is distributed in clusters covering the surface of the lactose particles. Comparing the CARS image in figure 2C with the transmission image in figure 3D highlights the power of this technique, as the transmission image suggests little more than a rough surface and does not reveal the localized distribution of the drug on the surface.

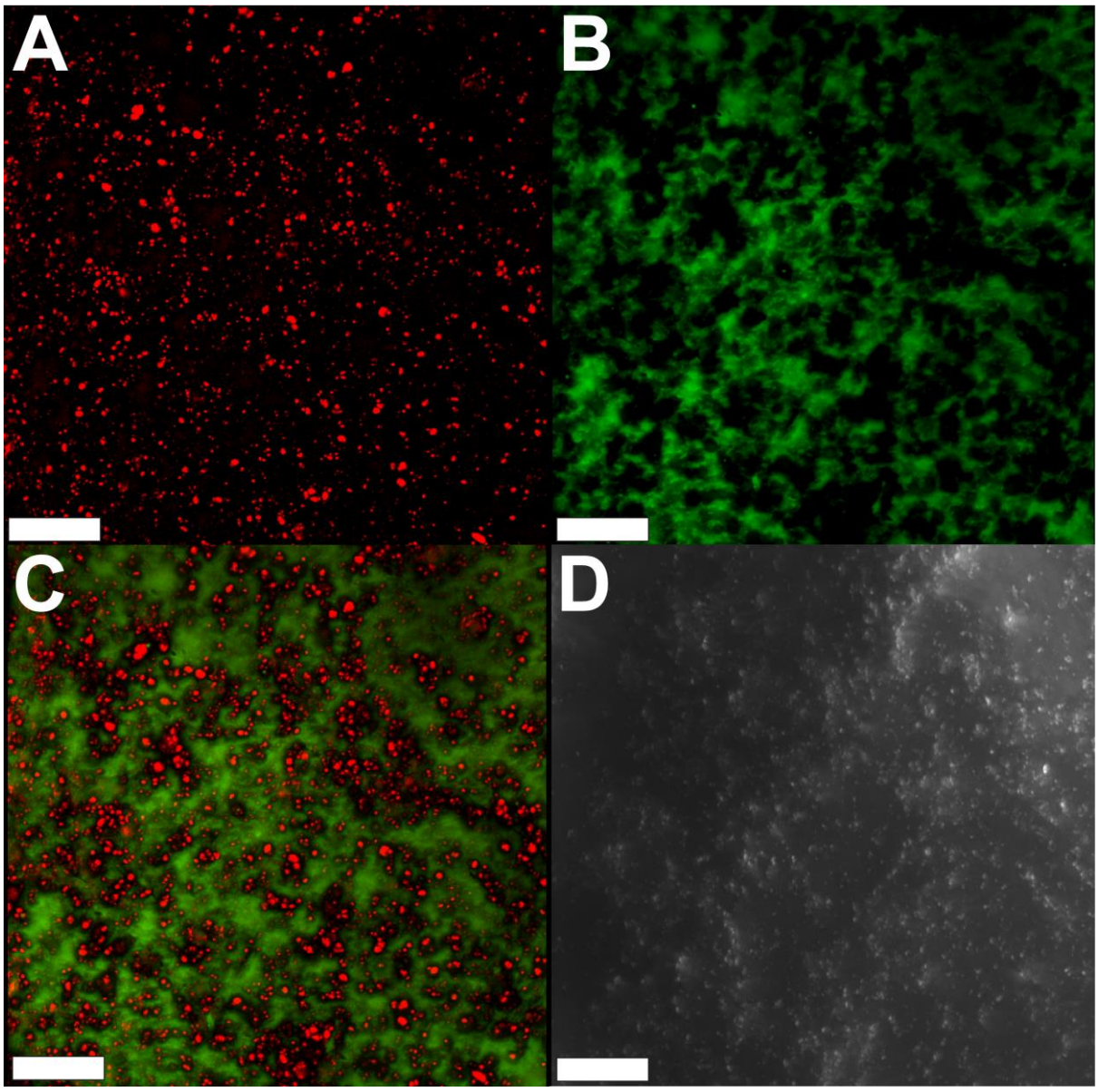

Figure 3. Projected Z-stack CARS images A) budesonide (3046 cm^{-1}), B) lactose (2888 cm^{-1}), C) overlay image showing distribution of budesonide on the surface of a lactose carrier particle, and D) transmission light image. Scale bars represent 20 µm.

CARS microscopy is inherently confocal with signal generated only within the focus of the objective; this feature provides the ability to record *z*-depth stacked images to gain a greater understanding of the drug distribution on the rough surface of the lactose carrier particles. Figure 4 shows frames from a *z*-stacked image (512x512 pixels) of a budesonide (red) loaded lactose carrier particle (green) starting from 0 µm depth and stepping every 2 µm until a depth of 10 µm. In addition to drug

penetration depth figure 4 also provides information about surface curvature of the carrier particle because the focus can be seen shifting from the center towards the edge of the image as the *z*-stack progresses. This representation may offer the possibility to image changes in the depth of the drug in a multi-layer of drug and added lactose fines when, for example, studying the effect of the order in which the different fine components are added to the blend.

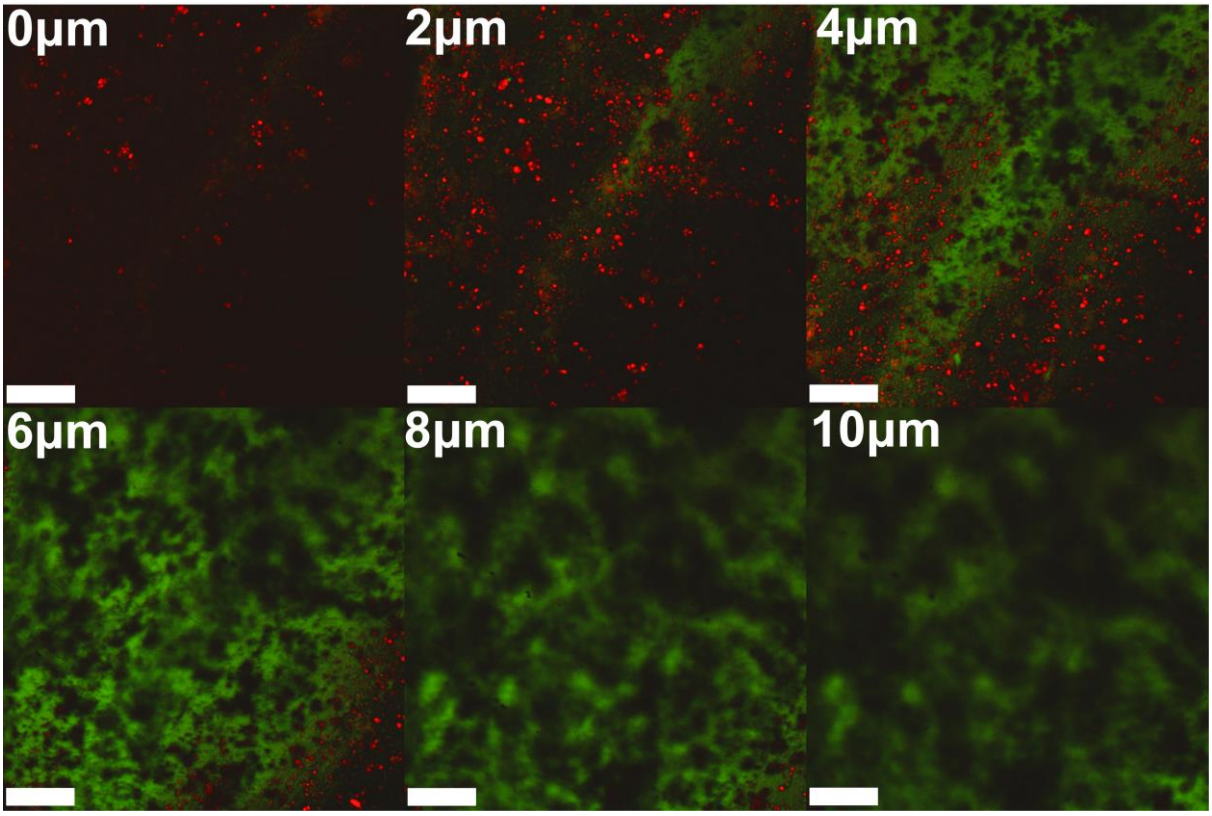

Figure 4. Frames from a Z-stacked video for a lactose carrier particle (green) loaded with budesonide (red). Scale bars represent 20 µm.

4.3.3 Particle size analysis

The particle size distribution is a critical parameter for the formulation of inhalation therapeutics. If the particles are too large they will impact in the oropharynx and subsequently swallowed, while on the other hand if the particles are too small they are likely to be exhaled [6]. It is generally accepted that the optimal aerodynamic diameter for particle inhalation roughly lies between 1-5 µm (depending on the

precise target deposition site and the inhalation flow rate) [2, 3]. The Image J particle analysis command calculates the particle area by setting a threshold intensity which is then removed and the remaining pixels are counted to give an area in μm^2. Figure 5A shows the original CARS image (reproduced from Figure 3A) prior to particle size analysis. Figure 5B shows the background removed image with only the drug particles (black) remaining. Figure 5C is a histogram representing the pixel intensity distribution for all of the pixels in Figure 5A with a dashed blue line indicating the threshold used by the binary algorithm to remove background signal. From the histogram it was calculated that about 30% of the total pixel intensity is retained in the binary image which contains only 6% of the number of pixels (Figure 5B). It is expected that the majority of the pixels in Figure 5A are background because the drug is only present in the sample at a concentration of 0.4 %w/w. Although it is possible to have a higher apparent surface concentration due to poor mixing it is still expected that the carrier particle dominates the imaging area. Figure 5D is a plot showing the distribution of particle size comparing the distributions determined using Image J particle analysis (striped black) and laser diffraction (solid red) methods. The PSD obtained with Image J analysis reports 68% of the particles to have a median projection area of 0.4 μm^2, while laser diffraction analysis results in a PSD with 94% of the primary particles within the same size class. The larger particle sizes measured with Image J analysis can be attributed to agglomeration of the primary particles during mixing. Additionally, due to the 0.4 μm^2 area being around the resolution limit for the CARS technique it is possible that some smaller particles would be missed during the binary conversion as the particle counting algorithm calculated a large number of particles lower than the microscope resolution.

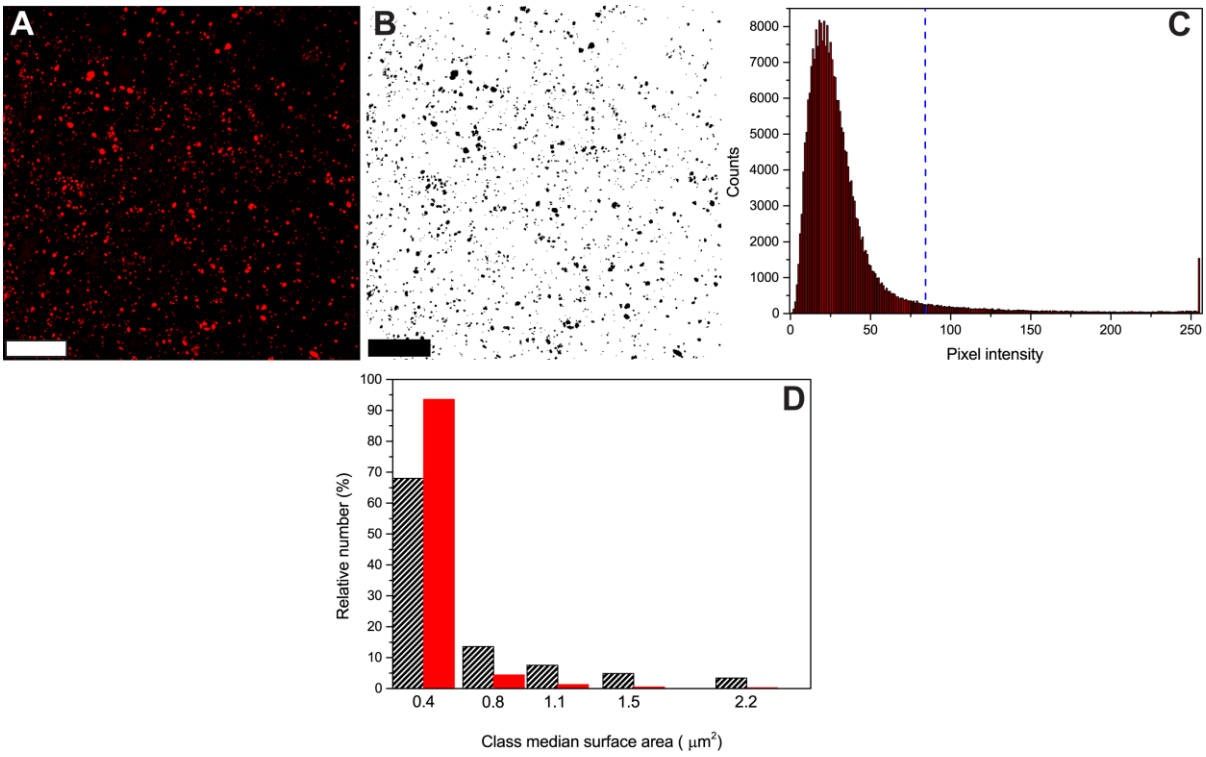

Figure 5. A) Original CARS image of a budesonide coated lactose carrier particle, B) binary representation of the CARS image containing the particles C) histogram showing pixel intensity with blue dashed line indicating the threshold used for the binary conversion, and D) particle size distribution from Image J analysis (striped black) and laser diffraction analysis (solid red). Scale bars represent 20 μm.

4.3.4 Correlative CARS and SEM imaging

Combining SEM with CARS microscopy provides the advantages of the high resolution available with SEM and chemically specific imaging provided by CARS. With the combined techniques it is possible to image the spatial distribution of the drug on the carrier surface and to relate this to morphological characteristics of the drug and carrier particles. This is particularly useful when the drug particles do not deviate in size or shape from fines originating from the excipient particles, or when the mixing process causes the drug particles to change in such a way that they cannot be identified by comparison with the starting material. Figure 5 shows high magnification SEM images of the pure starting materials prior to mixing. Figure 6A is a lactose carrier particle covered in fines while Figure 6B shows the plate-like shape of salmeterol.

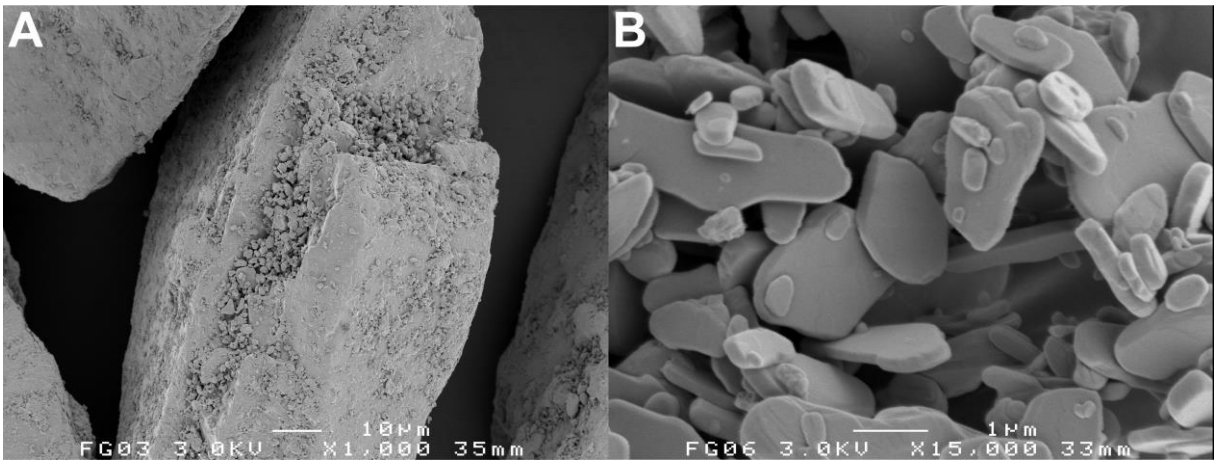

Figure 6. High magnification SEM images of the sieved pure lactose carrier (A) and micronized salmeterol (B) prior to mixing.

Figure 7 shows the result of correlative CARS and SEM imaging of the salmeterol blends prepared by 0.5 and 600 minutes of mixing. After only 0.5 minutes of mixing, the characteristic plate-like shape of the salmeterol particles is still intact, allowing the identification of the drug particles on the carrier surface by only high resolution SEM imaging. The seemingly random distribution of drug particles is confirmed by CARS. Interestingly, upon close examination not all particles that may be identified as drug particles based on their plate-like shape by SEM imaging are identified as such by CARS. It is possible that due to high carrier surface roughness combined with a large *z*-stack step size (1µm) CARS imaging missed some of the drug particles observed using SEM. Therefore, CARS imaging can possibly be further optimized by reducing the image scanning speed and by using smaller step size for *z*-stacked imaging, thereby improving the correlation with SEM imaging. As described previously [26], prolonged mixing causes plastic deformation and aggregation of the drug particles and they can therefore not be identified as drug particles with certainty by comparison with the drug starting material. CARS in this case confirms that the modified particles consist of salmeterol. It was also described that salmeterol forms a film on the carrier surface in addition to the spherical agglomerates after such long mixing times. However, this film formation is not observed with CARS, which may be due to the film thickness being below the resolution limit for CARS microscopy.

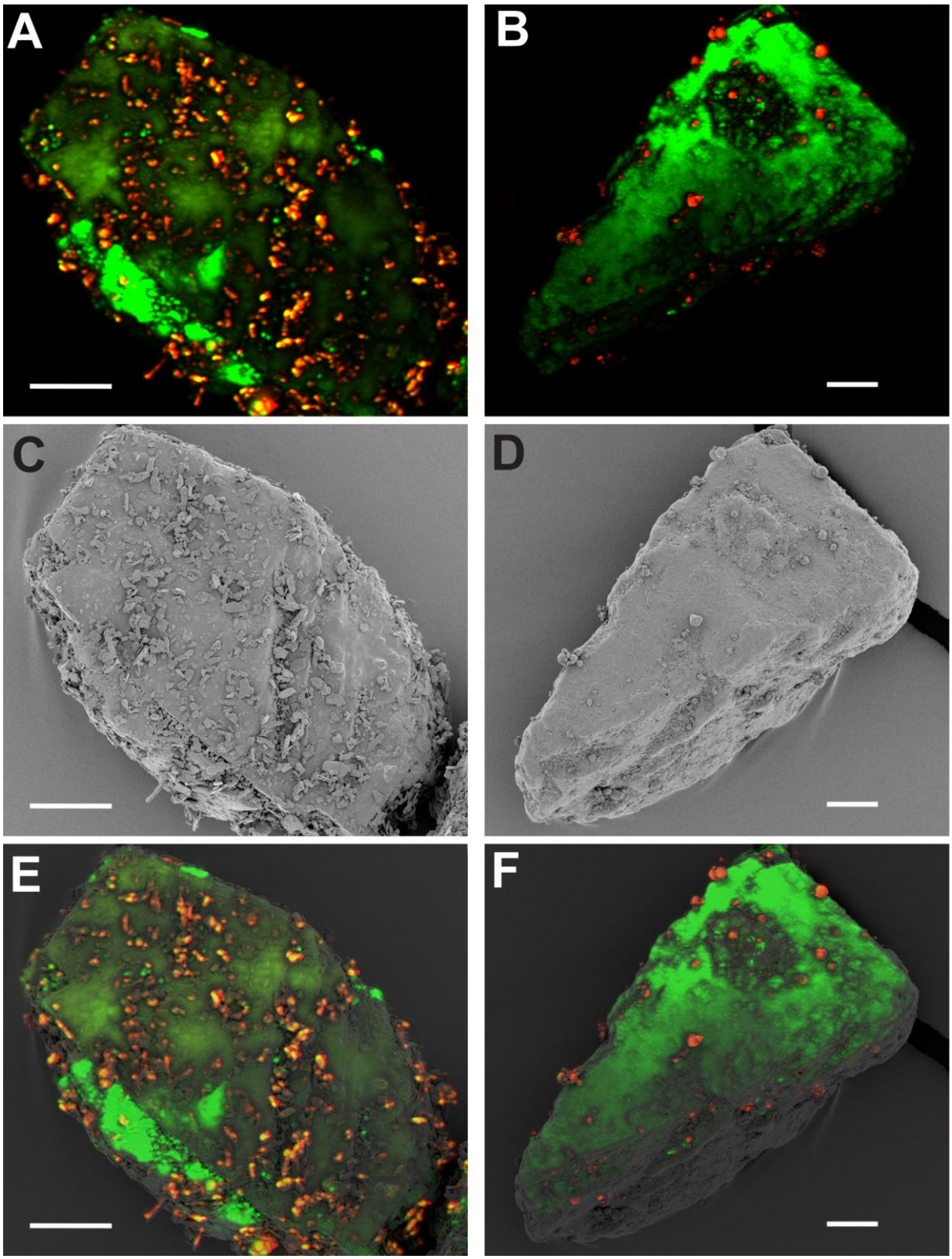

Figure 7. CARS (A+B), SEM (C+D) and CLEM images (E+F) of salmeterol mixtures after 0.5 (left) and 600 minutes of mixing (right). Scale bars represent 20 µm.

4.4 Conclusions and Outlook

CARS microscopy provides chemically selective imaging and is able to rapidly image the distribution of micronized budesonide and salmeterol over the surface of lactose carrier particles. Particle size measurements using the particle size analysis tool from Image J software in this study calculated a slightly larger particle size than that determined using the laser diffraction technique. However, further work is required to validate the binary conversion algorithm to ensure that it is not rejecting small drug particles. CLEM by combining CARS and SEM is a promising tool for the study of adhesive mixtures for inhalation. A further optimization and validation of the CLEM technique and the Image J particle counting algorithm are required to ensure that all drug particles are observed.

4.5 References

1. Fussell, A.L., et al., *CARS microscopy as a tool for studying the distribution of micronised drugs in adhesive mixtures for inhalation.* Journal of Raman Spectroscopy, 2014.
2. Newman, S.P., *Aerosol Deposition Considerations in Inhalation-Therapy.* Chest, 1985. **88**(2): p. S152-S160.
3. Usmani, O.S., M.F. Biddiscombe, and P.J. Barnes, *Regional Lung Deposition and Bronchodilator Response as a Function of {beta}2-Agonist Particle Size.* Am. J. Respir. Crit. Care Med., 2005. **172**(12): p. 1497-1504.
4. Hersey, J.A., *Ordered mixing: A new concept in powder mixing practice.* Powder Technology, 1975. **11**(1): p. 41-44.
5. Staniforth, J.N., *British Pharmaceutical Conference Science Award Lecture 1986: Order out of chaos.* Journal of Pharmacy and Pharmacology, 1987. **39**(5): p. 329-334.
6. Patton, J.S. and P.R. Byron, *Inhaling medicines: delivering drugs to the body through the lungs.* Nature Reviews Drug Discovery, 2007. **6**(1): p. 67-74.
7. Marriott, C. and H.W. Frijlink, *Lactose as a carrier for inhalation products: breathing new life into an old carrier.* Advanced Drug Delivery Reviews, 2012. **64**(3): p. 217-219.
8. Kulvanich, P. and P.J. Stewart, *The effect of particle size and concentration on the adhesive characteristics of a model drug-carrier interactive system.* Journal of Pharmacy and Pharmacology, 1987. **39**(9): p. 673-8.
9. Dickhoff, B.H.J., et al., *The effect of budesonide particle mass on drug particle detachment from carrier crystals in adhesive mixtures during inhalation.* European Journal of Pharmaceutics and Biopharmaceutics, 2002. **54**(2): p. 245-248.
10. Young, P.M., et al., *The influence of dose on the performance of dry powder inhalation systems.* International Journal of Pharmaceutics, 2005. **296**(1–2): p. 26-33.
11. Shur, J. and R. Price, *Advanced microscopy techniques to assess solid-state properties of inhalation medicines.* Advanced Drug Delivery Reviews, 2012. **64**(4): p. 369-382.

12. Slipchenko, M.N., et al., *Vibrational imaging of tablets by epi-detected stimulated Raman scattering microscopy.* Analyst, 2010. **135**(10): p. 2613-2619.
13. Krafft, C., et al., *Raman and coherent anti-Stokes Raman scattering microspectroscopy for biomedical applications.* Journal of Biomedical Optics, 2012. **17**(4): p. 040801-15.
14. Evans, C.L. and X.S. Xie, *Coherent anti-stokes Raman scattering microscopy: chemical imaging for biology and medicine.* Annu Rev Anal Chem (Palo Alto Calif), 2008. **1**: p. 883-909.
15. Pautot, S., et al., *Spontaneous formation of lipid structures at oil/water lipid interfaces.* Langmuir, 2003. **19**(24): p. 10281-10287.
16. Kang, E., et al., *In Situ Visualization of Paclitaxel Distribution and Release by Coherent Anti-Stokes Raman Scattering Microscopy.* Analytical Chemistry, 2006. **78**(23): p. 8036-8043.
17. Kang, E., et al., *Paclitaxel distribution in poly(ethylene glycol)/poly(lactide-co-glycolic acid) blends and its release visualized by coherent anti-Stokes Raman scattering microscopy.* Journal of Controlled Release, 2007. **122**(3): p. 261-268.
18. Kang, E., et al., *Application of coherent anti-stokes Raman scattering microscopy to image the changes in a paclitaxel–poly(styrene-b-isobutylene-b-styrene) matrix pre- and post-drug elution.* Journal of Biomedical Materials Research Part A, 2008. **87A**(4): p. 913-920.
19. Giepmans, B.N.G., *Bridging fluorescence microscopy and electron microscopy.* Histochemistry and Cell Biology, 2008. **130**(2): p. 211-217.
20. Ghosal, S. and J. Wagner, *Correlated Raman micro-spectroscopy and scanning electron microscopy analyses of flame retardants in environmental samples: a micro-analytical tool for probing chemical composition, origin and spatial distribution.* Analyst, 2013. **138**(13): p. 3836-3844.
21. Namba, Y., E. Heidarpour, and M. Nakayama, *Size Effects Appearing in the Raman-Spectra of Polycrystalline Diamonds.* Journal of Applied Physics, 1992. **72**(5): p. 1748-1751.
22. Foston, M., et al., *Chemical, ultrastructural and supramolecular analysis of tension wood in Populus tremula x alba as a model substrate for reduced recalcitrance.* Energy & Environmental Science, 2011. **4**(12): p. 4962-4971.

23. Perney, N.M., et al., *Polyglutamine Aggregate Structure In Vitro and In Vivo; New Avenues for Coherent Anti-Stokes Raman Scattering Microscopy.* Plos One, 2012. **7**(7).
24. Garbacik, E.T., et al., *Rapid identification of heterogeneous mixture components with hyperspectral coherent anti-Stokes Raman scattering imaging.* Journal of Raman Spectroscopy, 2012. **43**(5): p. 651-655.
25. Ridler T.W. and C. S., *Picture Thresholding Using an Iterative Selection Method.* Systems, Man and Cybernetics, IEEE Transactions on, 1978. **8**(8): p. 630-632.
26. Grasmeijer, F., et al., *Mixing Time Effects on the Dispersion Performance of Adhesive Mixtures for Inhalation.* PLoS ONE, 2013. **8**(7): p. e69263.

Drug distribution in ordered mesoporous silica imaged using CARS microscopy

Chapter five

Drug loaded mesoporous silica microparticles are a formulation technique designed to stabilize the amorphous form of poorly water soluble drugs. Loading these drugs into porous silica aims to disperse the drug in small volumes into the pores with the walls of the pores acting as a physical barrier preventing the drug from crystallizing. One of the concerns with this technique is inefficient or incomplete loading with a large number of pores remaining empty after the loading process. Another issue is the possibility of unloaded drug crystallizing on the surface of the microparticles. In this chapter chemically selective CARS microscopy is used to investigate mesoporous MCM-41 silica microparticles loaded with one of two model drugs by two different loading methods. The content of this chapter is based upon work submitted in Fussell et al [1].

5.1 Introduction

Poorly water soluble drugs are an ever increasing problem in drug development with estimates suggesting that around 50% of all drugs under development are affected [2]. A large area of research is devoted to increasing solubility and dissolution rate for poorly water soluble drugs. The amorphous form is a promising approach to increase the apparent solubility and dissolution rate of many drugs. However, as the amorphous form is thermodynamically high-energy, drugs in this form may crystallize during storage and/or administration. Attempts have been made to stabilize the amorphous form by using, for example, solid dispersions [3, 4], co-amorphous formulations [5], as well as drug loaded mesoporous silica [6, 7] and silicon [8, 9]. There is particular interest in identifying drug loading efficacy and distribution of mesoporous materials making CARS microscopy a potentially powerful tool in studying these materials.

Mesoporous materials contain nanosized pores between 2–50 nm [10-12], allowing the loading of drug molecules inside the pores. Incorporation of drug into the pores can be performed using solvent deposition methods [6, 9, 13], mechanical activation methods [14, 15] or vapor-phase mediated mass transfer [12]. The solvent deposition method is based on dissolving the drug into an organic solvent at a high concentration and mixing the solvent with the mesoporous silica allowing the drug to migrate through diffusion into the pores of the mesoporous silica particles. This process is followed by a solvent removal step where the excess solvent is removed, leaving the remaining drug loaded in the mesoporous silica.

Characterization of drug loaded mesoporous silica has had some analytical challenges. Techniques such as X-ray powder diffraction (XRPD) [13, 16, 17], Fourier transform infrared spectroscopy (FT-IR) [13, 16, 18], differential scanning calorimetry (DSC) [13, 16, 19, 20] and thermogravimetric analysis (TGA) [13, 16, 20, 21] are commonly used to determine the solid state form of the drug and the extent of the loading process in the loaded mesoporous silica. Other techniques such as Raman spectroscopy [22], and X-ray photoelectron spectroscopy (XPS) [22, 23] have also

been used in the study of drug loaded mesoporous silica or silicon samples. Vanea and Simon [22] combined Raman spectroscopy and XPS to study zinc containing silica microparticles loaded with insulin. They confirmed the loading of insulin using XPS and determined the biologically active conformation with Raman spectroscopy. However, these techniques do not provide any spatial information about the distribution of the drug within the mesoporous silica, or indeed whether any drug is present on the surface or as separate particles. Therefore, there is a need for spatially resolved analysis that provides information on both drug distribution and solid state form.

Time-of-flight secondary-ion mass spectroscopy (ToF-SIMS) is a spatially resolved surface sensitive technique which has been used to investigate the penetration of proteins into silicon wafers [24]. As ToF-SIMS is a surface technique sensitive to the first monolayer of a sample it is not suitable for completely non-destructive imaging the three dimensional (3D) distribution of drug loaded silica microparticles [25]. Hellstén *et al.* [26] published the first use of spontaneous Raman spectroscopic mapping to map the distribution of indomethacin loaded in SBA-15 and MCM-41 silica. Additionally, they used partial least squares analysis of the Raman spectra and were able to determine the solid state form of the loaded drug. However, spontaneous Raman spectroscopic imaging is a slow imaging method with image acquisition speed of around 30 seconds for an area of 100 μm^2, depending on the material being imaged [26]. In addition the axial resolution of the technique is usually in the order of several micrometers, which can limit the ability to obtain spatially resolved information in three dimensions.

Coherent Raman techniques such as coherent anti-Stokes Raman scattering (CARS) and stimulated Raman scattering can image up to video rate speeds allowing fast image acquisition. A summary of the CARS microscopy technique is provided elsewhere [27] and is covered in more detail in chapter one. Briefly, CARS microscopy is a non-linear optical imaging technique which provides rapid chemically selective imaging of different drugs and solid-state forms of drugs based on spectral

differences in their Raman spectra. As the CARS process is non-linear it is inherently confocal with diffraction limited resolution in three dimensions.

CARS microscopy has recently gained interest in imaging pharmaceutical formulations. Some of the early work involved using CARS to image the composition of dodecane emulsions [28]. Windbergs *et al*. [29] and Jurna *et al*. [30] performed CARS on lipid-based oral dosage forms where they imaged the distribution of the drug theophylline and monitored the release in real time during dissolution using a flow-through cell setup. Fussell *et al.* [31] extended this dissolution concept by building an intrinsic flow-through dissolution setup which allowed correlation of surface solid-state changes occurring during dissolution with changes in drug dissolution rate. Slipchenko *et al.* [32] and Hartshorn *et al.* [33] focused on studying complex oral dosage forms containing APIs combined with a number of excipients. Slipchenko *et al.* [32] applied stimulated Raman scattering for their work while Hartshorn *et al.* [33] applied broadband CARS. Both groups reported that their respective optical techniques were capable of rapidly imaging the distribution of the API and excipients on the surface of the tablet.

In this chapter, CARS microscopy is presented as an analytical tool to image drug distribution within drug loaded ordered mesoporous silica. CARS microscopy is used for chemically selective imaging of the 3D distribution of the model drugs, griseofulvin and itraconazole, loaded in ordered mesoporous MCM-41 silica microparticles. Loading of the drugs was studied using two different solvent deposition methods (immersion and rotary evaporation) in two different silica particle size ranges (63–90 µm and 100–125 µm) and it was aimed to identify any differences in drug distribution based on different loading methods or particle sizes. Additionally, hyperspectral CARS microscopy is applied to evaluate the solid state form of the drug loaded in the microparticles.

5.2 Materials and methods

5.2.1 Materials

Synthesis of the mesoporous MCM-41 material was carried out in a 300 mL autoclave as described elsewhere [34, 35], using fumed silica (SiO_2, 99.9%), tetramethylammonium silicate ($(CH_3)_4N(OH)\cdot 2SiO_2$, 99.99%), sodium silicate ($Na_2O_7Si_3,SiO_2$, 27%), ethyltrimethylammonium bromide ($CH_3(CH_2)_{15}N(CH_3)_3Br$, 99%) (all from Sigma–Aldrich, USA) and distilled water. The autoclave was kept in a large oven and the synthesis of MCM-41 was performed at 100 °C. The autoclave was then taken out of the oven and quenched. Mesoporous silica MCM-41 was filtered and washed with distilled water. Drying of the sample was carried out at 110 °C for 12 h and calcined at 550 °C for 10 h.

The synthesized mesoporous silica materials were ground using a ball mill and the resulting fine powder was passed through mesh test sieves (63 and 90 μm; 100 and 125 μm) using a sieve shaker apparatus (Fritsch GmbH, Idar-Oberstein, Germany), to achieve particle size fractions of 63–90 and 100–125 μm.

Itraconazole (Orion Pharma, Finland) and griseofulvin (Sigma-Aldrich, USA) were used as model drugs. The stable crystalline forms were used as received (Cambridge Structural Database reference codes GRISFL and TEHZIP for griseofulvin and itraconazole respectively). Amorphous itraconazole and griseofulvin were prepared by quench cooling of the melt and analyzed immediately after preparation.

5.2.2 Methods

Drug loading using immersion method

The mesoporous silica particles were loaded using a similar approach as described in Limnell *et al.* [17]. Solutions of griseofulvin (40 mg/mL) and itraconazole (235.5 mg/mL) dissolved in dichloromethane were prepared. Weighed samples (20 mg) of mesoporous MCM-41 (63–90 and 100–125 μm) were added to the solutions and stirred by magnetic stirrer for 90 min. After stirring, the samples were centrifuged for 4 min at 8000 rpm and the supernatant was removed. The samples were washed by

the addition of 500 µL of distilled water and centrifuged for 4 min at 8000 rpm. The samples were then dried in a vacuum oven at 40 °C for 2 h.

Drug loading using rotary evaporation

The mesoporous silica microparticles were loaded using a similar approach as described in Limnell *et al.* [17]. Solutions of griseofulvin (10 mg/mL) and itraconazole (10 mg/mL) dissolved in dichloromethane were prepared. Weighed samples (20 mg) of mesoporous MCM-41 (63–90 or 100–125 µm) were added to the solutions and shaken for 90 min. The samples were then evaporated using the Rotavap (Büchi, Switzerland) with the water bath set at 32 °C. The samples were dried in a vacuum oven at 40 °C for 2 h.

Characterization methods

Thermogravimetric analysis (TGA)

The drug payloads loaded in the mesoporous MCM-41 were studied with TGA. TGA was performed on a TGA-7 instrument (PerkinElmer, Waltham, MA, USA) with a heating rate of 10 °C/min under a N_2 gas purge of 40 mL/min. Alumel, nickel, perkalloy and iron were used to calibrate the TG temperature scale. Approximately 3-5 mg of sample was used for analysis.

CARS microscopy

The CARS microscopy system is described in detail elsewhere [36] and covered in more detail in chapter two. CARS imaging in this chapter was conducted using either a 40×/0.9 NA (correlative CARS with SEM imaging) or a 60×/1.2 NA (*z*-stacked and hyperspectral imaging) objective. The CARS microscope system using the 60× objective had a lateral spatial resolution of about 0.4 µm and an axial spatial resolution of about 1 µm while the lateral resolution for the 40× objective is about 0.7 µm and the axial resolution around 3 µm.

Hyperspectral CARS imaging

Hyperspectral CARS imaging provides a rapid method to extract the CARS intensity profile (CARS spectra) over a range of wavenumbers allowing the identification of peaks suitable for recording chemically specific CARS images. The method for conducting hyperspectral imaging has been described previously [36] and more information can be found in chapter two. Hyperspectral scans were recorded over the range of 2800–3100 cm^{-1} using a step size of about 4 cm^{-1} with a collection time of about 4 min. CARS spectra of the pure chemicals were collected from one region of interest while the spectra from the silica samples were the average of five regions of interest extracted from the hyperspectral data.

Z-stacked CARS analysis

Z-stacked imaging was conducted by stepping the microscope objective in the *z*-direction in increments of 1 μm. Each *z*-stacked image (512×512 pixels) consisted of between 40 and 80 slices depending on sample thickness and level of zoom and took between 1–3 min to record. For this work a total of 74 *z*-stacked images covering an area of about 11 mm^2 were recorded.

Scanning electron microscopy (SEM)

The MCM-41 silica microparticles were coated with an 18 nm thick layer of AuPd prior to SEM imaging. SEM imaging (Nova 600, FEI Company, USA) was performed using a voltage of 2 kV and a current of 0.59 nA.

5.3 Results and discussion

5.3.1 Thermogravimetric analysis of drug loading

Thermogravimetric analysis is a thermal analytical technique that requires a precision balance combined with a heating furnace to simultaneously weigh the sample while heating the sample at a controlled rate [37]. Calculation of the loaded drug is possible using TGA because during heating the drug decomposes and desorbs from the pores. This desorption results in a temperature dependent weight decrease [38]. The prepared mesoporous silica samples and their corresponding drug loading degrees analyzed by TGA are shown in Table 1. MCM-41 silica was used in two different particle size ranges (63–90 or 100–125 µm) and was loaded with one of two poorly water–soluble model drugs (griseofulvin or itraconazole) using either the immersion or rotary evaporation method. The TGA results identify a consistently higher loading degree (w-%) for the immersion method, irrespective of the particle size or drug, with drug loading degrees between 23.8 w-% (griseofulvin, 100–125 µm) and 67.3 w-% (itraconazole, 100–125 µm) for immersion, and 16.5 w-% (griseofulvin, 63–90 µm) and 17.5% w-% (itraconazole, 100–125 µm) for rotary evaporation. Additionally, the itraconazole samples had a higher loading degree when compared to the corresponding griseofulvin samples. This could, at least partly, be explained by the higher starting concentration used for the itraconazole than griseofulvin in the immersion experiments. There did not appear to be any difference in the loading degrees due to differences in particle size. This could be due to the fact that for both particle size ranges, the ordered pores are of the same diameter, with each pore continuing the complete length of the particle [34, 35].

Table 1. Loading degree of drug-loaded mesoporous MCM-41 microparticles.

Particle size (μm)	Loaded drug	Method	Loading degree, w-% (TGA results)
100-125	Griseofulvin	Rotavap	16.8
100-125	Griseofulvin	Immersion	23.8
100-125	Itraconazole	Rotavap	17.5
100-125	Itraconazole	Immersion	67.3
63-90	Itraconazole	Rotavap	17.1
63-90	Itraconazole	Immersion	54.5
63-90	Griseofulvin	Rotavap	16.5
63-90	Griseofulvin	Immersion	26.6

5.3.2 Hyperspectral CARS imaging of pure compounds

Hyperspectral scans were conducted initially for the pure drugs (in crystalline form) and the pure unloaded MCM-41 particles to determine suitable Raman shifts for imaging the drug distribution. Figure 1 shows CARS spectra extracted from hyperspectral scans for griseofulvin (A) and itraconazole (B). There was no notable CARS signal observed for the pure MCM-41 samples. The vibrational frequency of 2910 cm^{-1} (CH_3 stretch [39]) was chosen to image the griseofulvin samples, while 3070 cm^{-1} (aromatic CH stretch [39]) was chosen for the itraconazole samples. These frequencies allowed chemically specific imaging of the drug loaded MCM-41 samples with strong CARS signal from the drug and negligible interference from the MCM-41 microparticles.

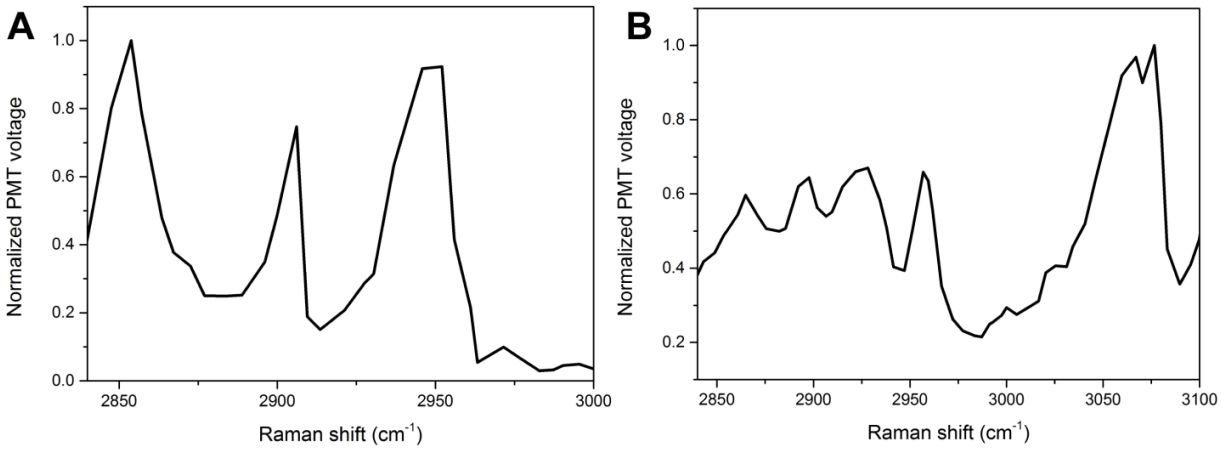

Figure 1. CARS spectra extracted from hyperspectral scans from pure griseofulvin (A) and itraconazole (B).

5.3.3 *Z*-stacked CARS imaging of the MCM-41 microparticles

Unloaded MCM-41 microparticles

As CARS signal is generated only within the focal volume of the objective, it is an inherently confocal technique which allows for three dimensional (3D) optical sectioning of the sample by moving the focusing objective in a step–wise manner. This 3D imaging capability allowed selective imaging of the drug distribution within the drug loaded MCM-41. Before imaging the drug distribution of the loaded silica samples it was decided to first perform imaging on the pure unloaded MCM-41 microparticles at the vibrational frequencies chosen for drug imaging to ensure that there was no interfering signal from the microparticles. Figure 2 shows *z*-stacked CARS images (2A and 2C) and corresponding transmission images (2B and 2D) for unloaded MCM-41 recorded at 3070 cm^{-1} (2A) (frequency for itraconazole) and 2910 cm^{-1} (2C) (frequency for griseofulvin). Looking at Figures 2A and 2C it is clear that there is only faint noise suggesting that there is no unwanted CARS signal generated from the MCM-41.

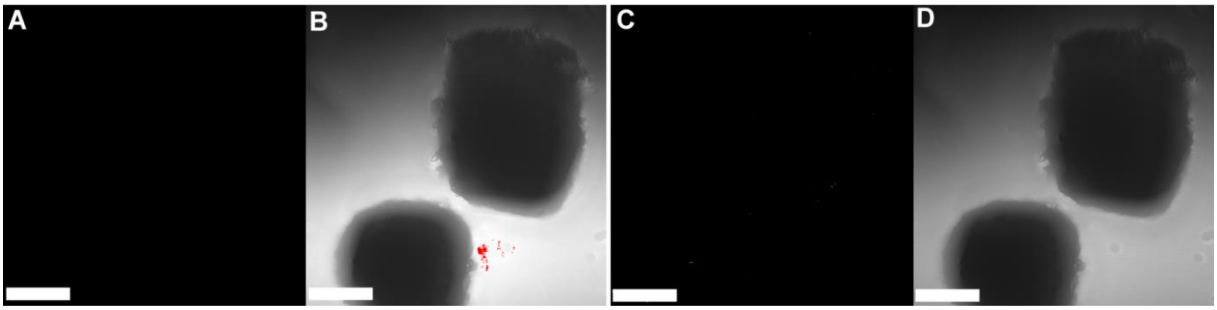

Figure 2. Z-stacked CARS images (A and C) and corresponding transmission images for unloaded MCM-41 recorded at 3070 cm^{-1} (A and B) and 2910 cm^{-1} (C and D) representing the frequencies chosen for imaging itraconazole and griseofulvin respectively. Scale bars are 50 µm.

Itraconazole loaded MCM-41 microparticles

The first drug loaded MCM-41 silica microparticles to be investigated were 100-125 µm in size and loaded with itraconazole. A total of 34 *z*-stacked images were recorded for itraconazole loaded MCM-41 silica microparticles covering an area of around 5.5 mm^2. Figure 3 shows one of the projected *z*-stack images for itraconazole loaded MCM-41 using the immersion method to load the MCM-41. Figure 3A shows the CARS signal from the drug, while Figure 3B shows the transmission image outlining the nodule like surface of the MCM-41 [35] and Figure 3C shows the overlaid image from Figures 3A and 3B. From Figure 3 it can be seen that there is very good overlap between the MCM-41 microparticle outlines seen in Figure 3B and the CARS signal from the drug. This indicates a good loading of drug into the pores of the MCM-41 microparticles throughout the particles. However, there are some small areas (marked using red arrows) around the edge where no drug signal was found in the CARS images, but the transmission images suggest that there is MCM-41 present. Although the TGA results (Table 1) suggest a high loading degree (67.3 w-% for this sample) there still appear to be small areas of unloaded silica, but it could also be due to the *z*-stack images not extending deep enough into the sample to record a CARS signal from these particles.

The *z*-projection, in Figure 3D, shows the drug signal as a function of depth for the plane of interest shown by the red line in Figure 3A. The *z*-stacked image covers a depth of 30 μm but in this plane the drug signal is only observed to a depth of 20 μm. The signal is less intense than in Figure A because it represents the signal from a single plane (not the cumulative signal of multiple planes).

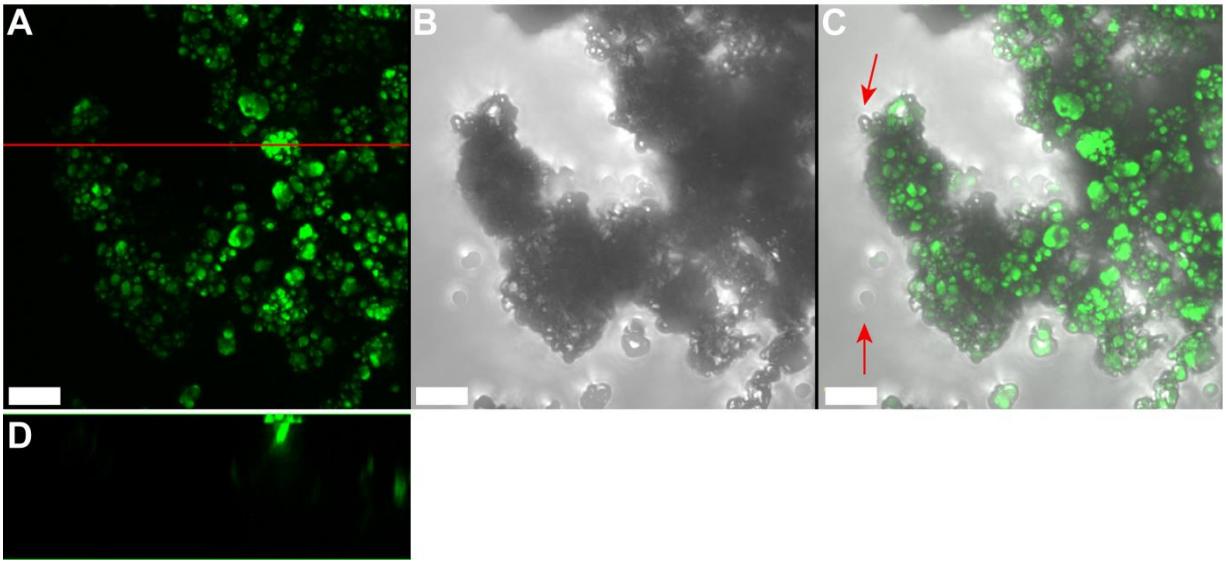

Figure 3. Z-stacked image from itraconazole loaded MCM-41 (100–125 μm) using immersion method. (A) CARS image recorded at 3070 cm^{-1} with red line indicating depth profile position, (B) transmission image, (C) overlaid A and B showing drug distribution with red arrows indicating poor loading, and (D) the z depth profile showing a depth of 30 μm. Scale bars are 10 μm.

Griseofulvin loaded MCM-41 microparticles

The results for the *z*-stacked CARS imaging of the griseofulvin loaded MCM-41 are very similar to those seen for itraconazole (Figure 3). A total of 30 *z*-stacked images were recorded for griseofulvin loaded MCM-41 silica microparticles covering an area of around 4.5 mm^2. Figure 4 contains *z*-stacked images of griseofulvin loaded using the immersion method showing large areas of MCM-41 (seen in transmission image) that do not produce drug signal (seen in CARS image) suggesting that these areas are not loaded with drug. This may be associated with the low drug loading (Table 1)

— the TGA result reports a loading degree of only 23.8 w-% for this sample. The depth projection (figure 4D) shows the drug signal as a function of depth for the area of the sample labelled with a red line (figure 4A). The whole image covers a depth of 46 µm, but in the selected region the drug signal can be seen only to a depth of about 10 µm with the remainder of the image showing no drug signal.

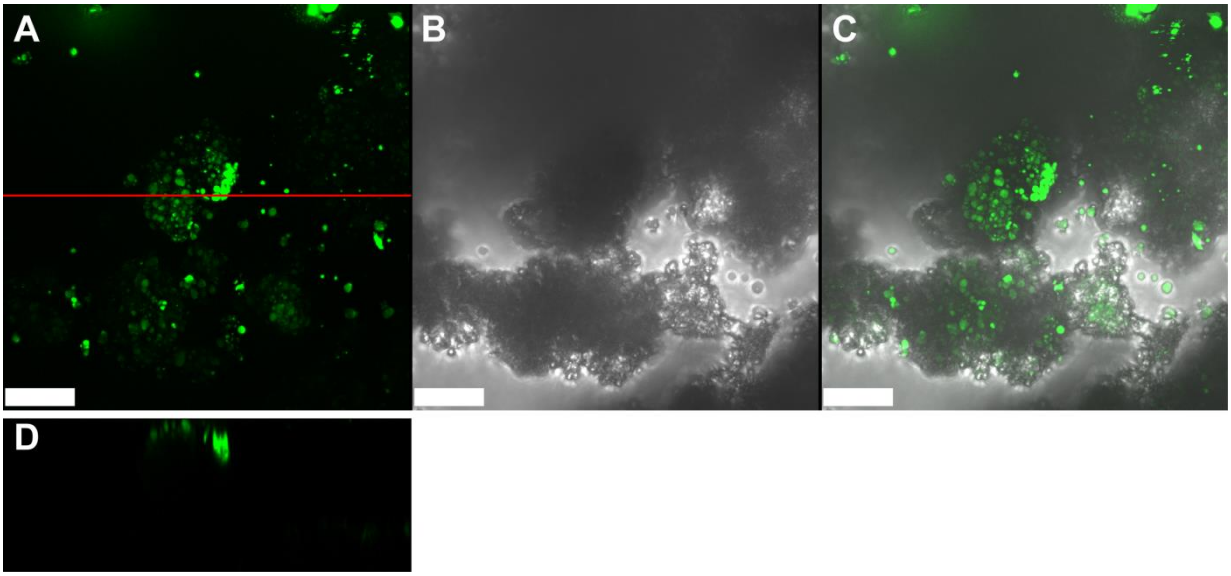

Figure 4. Z-stacked image of griseofulvin loaded MCM-41 (100–125 µm) using immersion method. (A) CARS image recorded at 2910 cm^{-1} with red line indicating depth profile position, (B) transmission image, (C) overlaid A and B showing drug distribution within the silica microparticles and (D) the z depth profile showing a depth of 46 µm. Scale bars are 20 µm.

5.3.4 Correlative light and electron microscopy (CLEM)

CLEM imaging combines the chemically specific imaging provided by CARS microscopy with the high resolution imaging provided by SEM imaging. CLEM imaging was performed to gain further understanding of the 3D structure and the morphology of the drug loaded MCM-41 silica microparticles. Figure 5A shows a CARS image for an itraconazole loaded MCM-41 microparticle, 5B shows the corresponding SEM image for the same MCM-41 microparticle, 5C shows a CARS image for a griseofulvin loaded MCM-41 microparticle and 5D shows the corresponding SEM image. From the SEM images it can be seen that the surface is

rough with nodule-like protrusions [35] which are also clearly visible in the CARS images.

A concern with loaded silica microparticles has been the potential presence of drug particles outside or on the surface of the silica, as such drug would be likely to crystallize during storage and decrease the dissolution of the drug in the patient. The analyses with CARS microscopy and CLEM in this study suggest that in all observed cases, the drug present was only present within the silica microparticle pores.

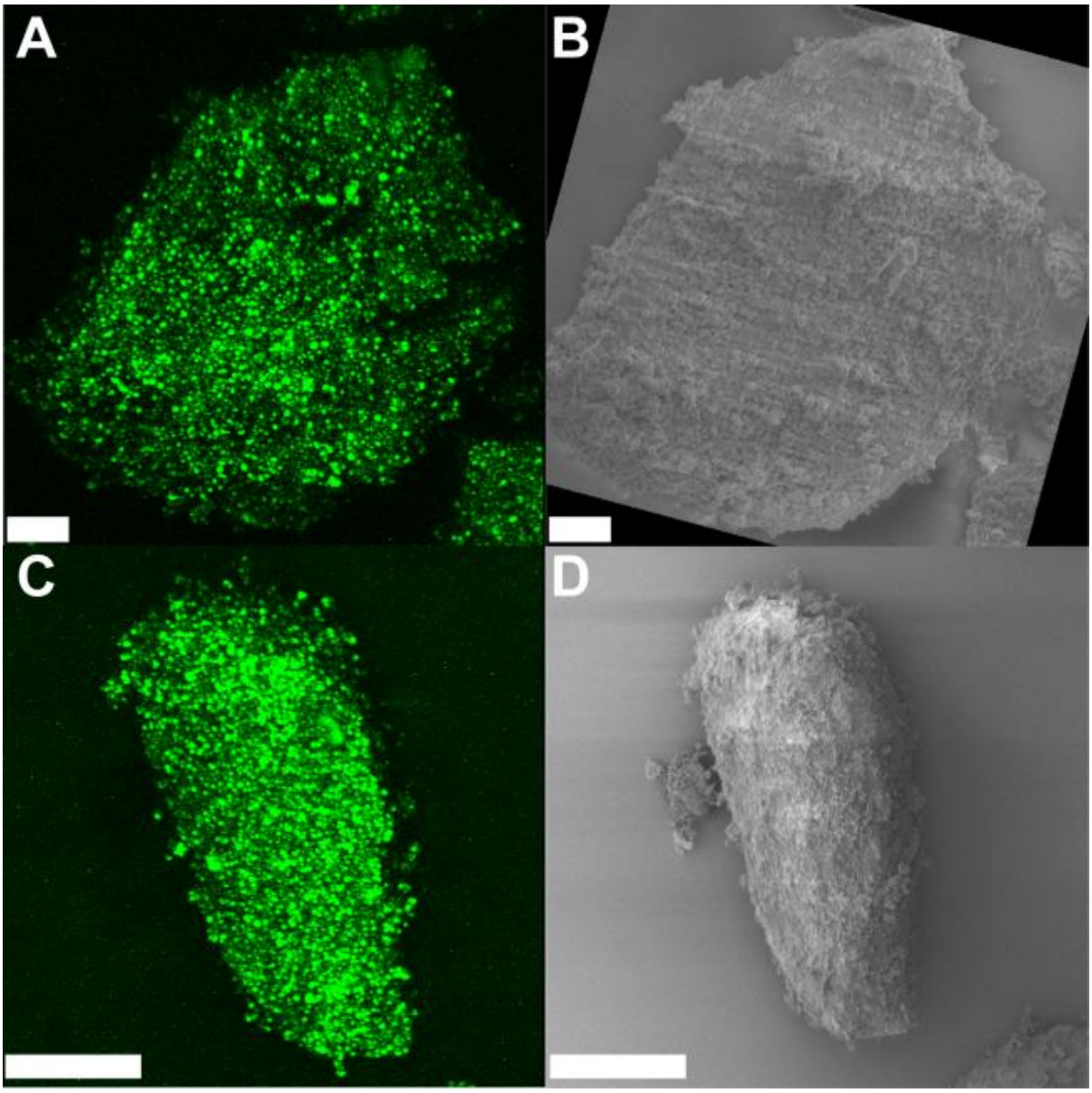

Figure 5. CLEM images for itraconazole (A and B), and griseofulvin (C and D) loaded MCM-41 (100–125 μm) using rotary evaporation: Z-stacked CARS images (A and C), with correlated SEM images (B and D). Scale bars are 20 μm (A and B) and 50 μm (C and D).

5.3.5 Hyperspectral imaging of drug loaded MCM-41 particles

Hyperspectral CARS imaging was used to obtain further structural information on the drug contained within the MCM-41 microparticles. Spectra from five regions of interest were averaged from the hyperspectral data and compared to those obtained from pure crystalline and amorphous drug to obtain information on the molecular

arrangement of the drug in the silica. Hyperspectral scans of pure crystalline and amorphous itraconazole and griseofulvin were recorded over the range of 2860–2960 cm^{-1} in 40 frames with each scan taking about 45 seconds. The hyperspectral images were then projected and regions of interest were selected from which the CARS spectra were extracted.

Itraconazole loaded MCM-41 particles

A hyperspectral image for itraconazole loaded MCM-41 using the immersion method, along with the extracted CARS spectra for the sample, and the reference amorphous and crystalline forms of pure itraconazole are shown in Figure 6. The colour in the hyperspectral image is consistent (only the intensity changes) over the whole sampled area. This reveals that there was no crystalline drug present and the physical structure of the drug was likely uniform within the sampled area.

As would be expected, the spectrum of the reference amorphous form contains broader and less distinct features than that of the crystalline form. The loaded MCM-41 sample spectrum closely resembles the amorphous itraconazole spectrum, and not the crystalline itraconazole spectrum. This similarity between the amorphous reference and loaded drug spectra suggested that the drug contained within the pores of the MCM-41 sample is also disordered.

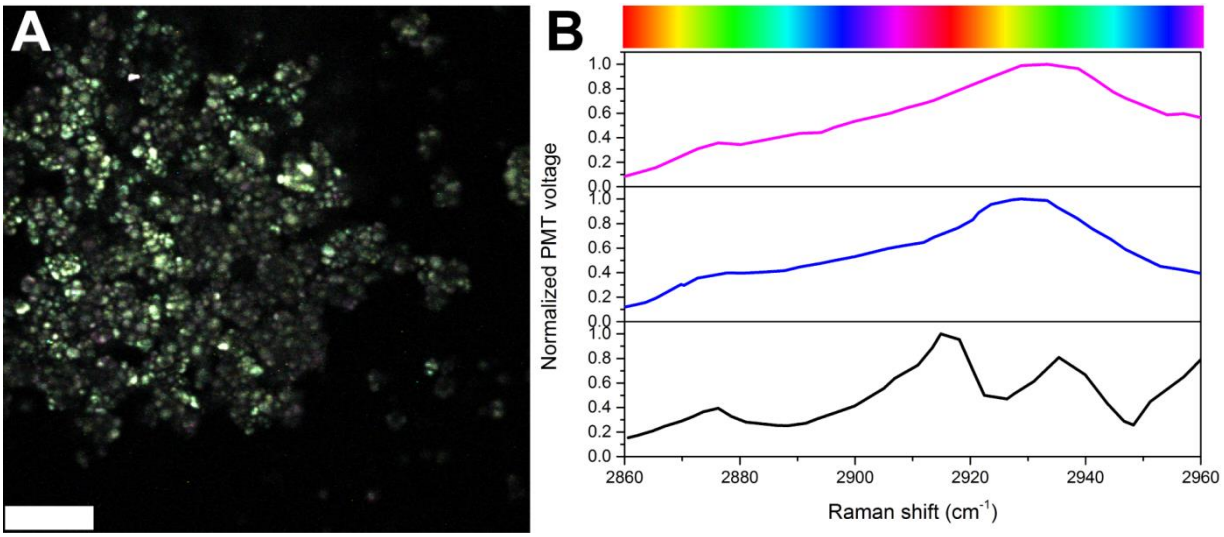

Figure 6. Hyperspectral image (A) and extracted CARS spectra averaged from five regions of interest (B) for itraconazole loaded MCM-41 using immersion method (magenta line), amorphous itraconazole (blue line) and crystalline itraconazole (black) plotted for comparison. Scale bar is 20 μm.

Griseofulvin loaded MCM-41 particles

The hyperspectral image for griseofulvin loaded using immersion method shown in Figure 7 is a very similar colour to that of the itraconazole samples except it appears more blue-green than the yellow-green colour seen in the itraconazole samples. The extracted spectrum shows a broad peak that has a peak maximum around 2940 cm^{-1} corresponding to the CH_3 stretching [39], which is in close agreement to that of the spectrum obtained for amorphous griseofulvin. There is no evidence of crystalline drug in the image.

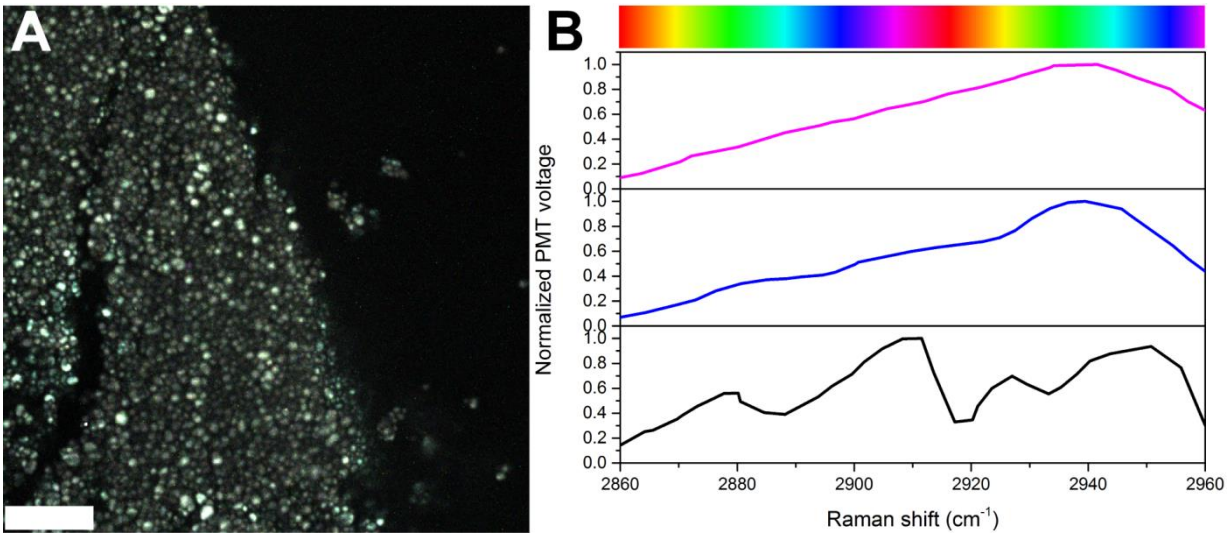

Figure 7. Hyperspectral image (A) and extracted CARS spectra averaged from five regions of interest (B) for griseofulvin loaded MCM-41 using immersion method (magenta line), amorphous griseofulvin (blue line) and crystalline griseofulvin (black line) plotted for comparison. Scale bar is 20 µm.

5.4 Conclusions and Outlook

In this work, CARS microscopy has been applied for the first time to probe drug distribution and physicochemical structure in ordered mesoporous silica particles. *Z*-stacked CARS microscopy was used as an analytical tool to selectively image the 3D distribution of drug loaded in MCM-41 microparticles. Using CARS microscopy to analyze the drug in MCM-41 samples prepared using two different loading methods (immersion and rotary evaporation) with two model drugs (itraconazole and griseofulvin), it was possible to visualize differences in drug loading distributions between the two different drugs, but not differences between the loading methods or particle size ranges. The analyses (including CLEM) did not reveal any evidence of drug particles outside the silica microparticles.

Hyperspectral CARS microscopy was used to further probe the physicochemical structure of the drug in the MCM-41 microparticles. Comparing CARS spectra extracted from the drug loaded MCM-41 samples and those extracted from the reference spectra obtained from pure amorphous and crystalline drug, it was

concluded that the drugs loaded within the pores of MCM-41 samples is in an amorphous form.

The combination of CARS microscopy with hyperspectral CARS analysis is a powerful tool for analyzing drugs loaded in mesoporous silica-based materials and has the potential to allow improved characterization and streamline the loading procedure for drug loaded mesoporous materials.

5.5 References

1. Fussell, A.L., et al., *Coherent anti-Stokes Raman scattering (CARS) microscopy driving the future of drug loaded ordered mesoporous silica imaging.* Analytical Chemistry, Submitted.
2. Ku, M., *Use of the Biopharmaceutical Classification System in Early Drug Development.* The AAPS Journal, 2008. **10**(1): p. 208-212.
3. Leuner, C. and J. Dressman, *Improving drug solubility for oral delivery using solid dispersions.* European Journal of Pharmaceutics and Biopharmaceutics, 2000. **50**(1): p. 47-60.
4. Ford, J.L., *The Current Status of Solid Dispersions.* Pharmaceutica Acta Helvetiae, 1986. **61**(3): p. 69-88.
5. Lu, Q. and G. Zografi, *Phase behavior of binary and ternary amorphous mixtures containing indomethacin, citric acid, and PVP.* Pharmaceutical Research, 1998. **15**(8): p. 1202-1206.
6. Kinnari, P., et al., *Comparison of mesoporous silicon and non-ordered mesoporous silica materials as drug carriers for itraconazole.* International Journal of Pharmaceutics, 2011. **414**(1–2): p. 148-156.
7. Wang, S., *Ordered mesoporous materials for drug delivery.* Microporous and Mesoporous Materials, 2009. **117**(1–2): p. 1-9.
8. Sarparanta, M., et al., *18F-Labeled Modified Porous Silicon Particles for Investigation of Drug Delivery Carrier Distribution in Vivo with Positron Emission Tomography.* Molecular Pharmaceutics, 2011. **8**(5): p. 1799-1806.
9. Prestidge, C.A., et al., *Mesoporous silicon: a platform for the delivery of therapeutics.* Expert Opinion on Drug Delivery, 2007. **4**(2): p. 101-110.
10. Yiu, H.H.P. and P.A. Wright, *Enzymes supported on ordered mesoporous solids: a special case of an inorganic-organic hybrid.* Journal of Materials Chemistry, 2005. **15**(35-36): p. 3690-3700.
11. Selvam, P., S.K. Bhatia, and C.G. Sonwane, *Recent Advances in Processing and Characterization of Periodic Mesoporous MCM-41 Silicate Molecular Sieves.* Industrial & Engineering Chemistry Research, 2001. **40**(15): p. 3237-3261.

12. Qian, K.K. and R.H. Bogner, *Application of mesoporous silicon dioxide and silicate in oral amorphous drug delivery systems.* Journal of Pharmaceutical Sciences, 2012. **101**(2): p. 444-463.
13. Ambrogi, V., et al., *Improvement of dissolution rate of piroxicam by inclusion into MCM-41 mesoporous silicate.* European Journal of Pharmaceutical Sciences, 2007. **32**(3): p. 216-222.
14. Watanabe, T., et al., *Solid state radical recombination and charge transfer across the boundary between indomethacin and silica under mechanical stress.* Journal of Solid State Chemistry, 2002. **164**(1): p. 27-33.
15. Hailu, S.A. and R.H. Bogner, *Complex effects of drug/silicate ratio, solid-state equivalent pH, and moisture on chemical stability of amorphous quinapril hydrochloride coground with silicates.* Journal of Pharmaceutical Sciences, 2011. **100**(4): p. 1503-1515.
16. Ambrogi, V., et al., *Role of mesoporous silicates on carbamazepine dissolution rate enhancement.* Microporous and Mesoporous Materials, 2008. **113**(1–3): p. 445-452.
17. Limnell, T., et al., *Delivery Formulations of Ordered and Nonordered Mesoporous Silica: Comparison of Three Drug Loading Methods.* Journal of Pharmaceutical Sciences, 2011. **100**(8): p. 3294-3306.
18. Kang, E., et al., *Paclitaxel distribution in poly(ethylene glycol)/poly(lactide-co-glycolic acid) blends and its release visualized by coherent anti-Stokes Raman scattering microscopy.* Journal of Controlled Release, 2007. **122**(3): p. 261-268.
19. Kang, E., et al., *In Situ Visualization of Paclitaxel Distribution and Release by Coherent Anti-Stokes Raman Scattering Microscopy.* Analytical Chemistry, 2006. **78**(23): p. 8036-8043.
20. Mellaerts, R., et al., *Increasing the oral bioavailability of the poorly water soluble drug itraconazole with ordered mesoporous silica.* European Journal of Pharmaceutics and Biopharmaceutics, 2008. **69**(1): p. 223-230.
21. Parekh, S.H., et al., *Label-Free Cellular Imaging by Broadband Coherent Anti-Stokes Raman Scattering Microscopy.* Biophysical Journal, 2010. **99**(8): p. 2695-2704.

22. Vanea, E. and V. Simon, *XPS and Raman study of zinc containing silica microparticles loaded with insulin.* Applied Surface Science, 2013. **280**(0): p. 144-150.
23. Prestidge, C.A., et al., *Loading and release of a model protein from porous silicon powders.* Physica Status Solidi a-Applications and Materials Science, 2007. **204**(10): p. 3361-3366.
24. Jarvis, K.L., T.J. Barnes, and C.A. Prestidge, *Thermal Oxidation for Controlling Protein Interactions with Porous Silicon.* Langmuir, 2010. **26**(17): p. 14316-14322.
25. Barnes, T.J., I.M. Kempson, and C.A. Prestidge, *Surface analysis for compositional, chemical and structural imaging in pharmaceutics with mass spectrometry: A ToF-SIMS perspective.* International Journal of Pharmaceutics, 2011. **417**(1–2): p. 61-69.
26. Hellsten, S., et al., *Raman spectroscopic imaging of indomethacin loaded in porous silica.* Crystengcomm, 2012. **14**(5): p. 1582-1587.
27. Evans, C.L. and X.S. Xie, *Coherent anti-stokes Raman scattering microscopy: chemical imaging for biology and medicine.* Annu Rev Anal Chem (Palo Alto Calif), 2008. **1**: p. 883-909.
28. Pautot, S., et al., *Spontaneous formation of lipid structures at oil/water lipid interfaces.* Langmuir, 2003. **19**(24): p. 10281-10287.
29. Windbergs, M., et al., *Chemical Imaging of Oral Solid Dosage Forms and Changes upon Dissolution Using Coherent Anti-Stokes Raman Scattering Microscopy.* Analytical Chemistry, 2009. **81**(6): p. 2085-2091.
30. Jurna, M., et al., *Coherent anti-Stokes Raman scattering microscopy to monitor drug dissolution in different oral pharmaceutical tablets.* Journal of Innovative Optical Health Sciences, 2009. **2**(1): p. 37-43.
31. Fussell, A., et al., *In situ dissolution analysis using coherent anti-Stokes Raman scattering (CARS) and hyperspectral CARS microscopy.* European Journal of Pharmaceutics and Biopharmaceutics, 2013. **85**(3, Part B): p. 1141-1147.
32. Slipchenko, M.N., et al., *Vibrational imaging of tablets by epi-detected stimulated Raman scattering microscopy.* Analyst, 2010. **135**(10): p. 2613-2619.

33. Hartshorn, C.M., et al., *Multicomponent Chemical Imaging of Pharmaceutical Solid Dosage Forms with Broadband CARS Microscopy.* Analytical Chemistry, 2013. **85**(17): p. 8102-8111.
34. Limnell, T., et al., *Physicochemical stability of high indomethacin payload ordered mesoporous silica MCM-41 and SBA-15 microparticles.* International Journal of Pharmaceutics, 2011. **416**(1): p. 242-251.
35. Heikkilä, T., et al., *Cytotoxicity study of ordered mesoporous silica MCM-41 and SBA-15 microparticles on Caco-2 cells.* European Journal of Pharmaceutics and Biopharmaceutics, 2010. **74**(3): p. 483-494.
36. Garbacik, E.T., et al., *Rapid identification of heterogeneous mixture components with hyperspectral coherent anti-Stokes Raman scattering imaging.* Journal of Raman Spectroscopy, 2012. **43**(5): p. 651-655.
37. Coats, A.W. and J.P. Redfern, *Thermogravimetric analysis. A review.* Analyst, 1963. **88**(1053): p. 906-924.
38. Salonen, J., et al., *Mesoporous silicon microparticles for oral drug delivery: Loading and release of five model drugs.* Journal of Controlled Release, 2005. **108**(2–3): p. 362-374.
39. Smith, E. and G. Dent, *Modern Raman Spectroscopy*2005: John Wiley and Sons. 210.

Executive summary and Outlook

This dissertation demonstrates coherent anti-Stokes Raman scattering (CARS) microscopy as a tool in pharmaceutical solid state development. CARS microscopy is a nonlinear optical imaging technique that uses inelastic scattering of light known as Raman scattering to provide chemically specific imaging. CARS microscopy is suitable for early stage pharmaceutical development, analyzing pure API powders as well as late stage analysis of more complex dosage forms. The strengths and weaknesses of CARS microscopy are explored in the context of pharmaceutical analysis over a wide range of samples covering a number of commonly used pharmaceutical formulation strategies.

The four experimental chapters utilize three of the main imaging techniques available for our custom built CARS microscope which are: single plane CARS imaging at a single Raman vibrational frequency, z-stacked CARS imaging at a single Raman vibrational frequency, and hyperspectral CARS imaging over a range of Raman vibrational frequencies. Each of these imaging techniques has their own strengths and weaknesses and can provide different information about the sample.

Firstly, single plane CARS imaging at a single Raman vibrational frequency has the main strength of being rapid, providing up to video rate collection of CARS images. Rapid imaging allows visualization of chemical changes over time as seen in chapter three while imaging the conversion of theophylline anhydrate to monohydrate during dissolution testing. The biggest weakness to this imaging technique is reduced chemical selectivity due to potentially overlapping vibrational spectra for two or more components that might be present in the sample. This weakness has led to the development of hyperspectral CARS imaging.

Secondly, hyperspectral CARS imaging (as discussed in chapter two) has the strength that it overcomes the issue of single Raman vibration frequency imaging by recording a stack of images with each image recorded at a different frequency. The stack of images is then processed and projected producing a single image where different chemicals and different solid state forms appear as different colors. The main weakness to this hyperspectral imaging technique is that the sample must remain stationary as any movement of the sample will affect the final color projection thus precluding analysis of dynamic processes such as dissolution analysis.

Finally, the third imaging technique known as z-stacked CARS imaging provides the capability of three dimensional imaging. This three dimensional imaging is possible because CARS microscopy is inherently confocal with CARS signal only generated in the focal volume of the microscope objective. Z-stacked imaging is performed by recording images while moving the objective in a step-wise manner towards the sample. The main strength of z-stacked CARS in terms of pharmaceutical analysis is the improved field of view improving the ability to image rough surfaces such as powders and granule samples. The main weaknesses of z-stacked CARS are the same as those for single Raman vibrational frequency imaging (reduced chemical selectivity) and hyperspectral CARS imaging (stationary sample requirement) effectively limiting the applications to stationary samples with a small number of constituents such as granules, adhesive mixtures (see chapter four), and drug loaded silica particles (see chapter five).

Two main areas of future development of narrowband CARS that would be beneficial for pharmaceutical analysis are Raman fingerprint imaging and quantitative image analysis. Currently most narrowband CARS microscopy is performed in the C-H vibrational stretch region (2800-3200 cm^{-1}) while there is a large region known as the fingerprint region (around 500-2000 cm^{-1}) that could be used to increase the chemical selectivity of the imaging technique. As CARS microscopy is a nonlinear optical technique, the signal intensity does not scale linearly with the concentration of the chemical making it difficult to quantitatively determine the content in the CARS image. Currently, it is possible using complex mathematics to calculate chemical

concentration in CARS images but further development to automate and validate these methods would enable their use in routine analysis.

Narrowband CARS microscopy has strong potential as a tool for routine analysis in a pharmaceutical environment. However, for this commercial potential to be realized the system will have to have a large number of imaging techniques available to the end user. In addition to the imaging techniques mentioned above Second Harmonic Generation, and Two Photon Fluorescence would also be very useful to be incorporated into such a system. There is a system currently available on the market (Leica TCS SP8 CARS) which has many of these features making it an interesting option for a pharmaceutical research environment. However, one drawback to this system is the large system footprint. This commercial CARS microscope is not a bench top system and requires an optical table for the laser system which is not ideal for pharmaceutical research labs which typically contain mostly bench top equipment with a small footprint.

Further improvements to make the system more attractive for a pharmaceutical lab could include, reducing system operation complexity, and increasing system stability. These improvements would allow minimally trained operators to use the system. The CARS microscope used for this work is a complex, homebuilt system which had stability issues making it difficult to perform robust reproducible experiments. In the pharmaceutical industry validation of analytical methods is required, making it necessary to have a robust imaging system. Most of the development in this area would be automation, allowing the system operator to control most aspects of the CARS microscope (i.e. wavelengths, optical parametric oscillator cavity size, temperature, and light filters) using a single software program.

Overall, this dissertation has shown that there is great potential for narrowband CARS microscopy as a tool for solid state pharmaceutical analysis with a wide range of applications including solid state form determination, drug distribution analysis, as well as dissolution analysis. There is also still a lot of development and refinement

required to both the CARS technique and the equipment to make it attractive and competitive for routine analysis in a pharmaceutical environment.

Samenvatting

Dit proefschrift beschrijft de ontwikkeling van coherente anti-Stokes Raman verstrooiing (CARS) microscopie als een techniek voor farmaceutische analyse. CARS microscopie is een niet-lineaire optische techniek die gebruik maakt van inelastische verstrooiing van licht. inelastische verstrooiing van licht gebeurt vanwege een interactie tussen de moleculen en het licht. De frequentie of kleuren van het verstrooide licht hangt af van de moleculen. Dit betekent dat CARS microscopie een chemisch specifieke techniek is: het geeft een manier om de verschillende chemicaliën van een mengsel te identificeren zonder labels te gebruiken. CARS is een indrukwekkende techniek met veel toepassingen in de natuurwetenschappen; onder andere biomedische technologie, scheikunde en nu ook farmaceutische technologie.

Hoofdstuk één is een introductie over de traditionele farmaceutische 'solid-state' analyse en over de achtergrond van CARS microscopie.

Hoofdstuk twee introduceert hyperspectrale CARS microscopie en geeft voorbeelden van metingen met verschillende farmaceutische tabletten en poeders.

Hoofdstuk drie beschrijft de ontwikkeling van CARS microscopie als een techniek voor farmaceutische dissolution analyse. Een CARS oplossings opstelling is gebouwd die het mogelijk maakt om tegelijkertijd naar de tablet te kijken en de concentratie van het medicijn in vloeistof te meten.

Hoofdstuk vier onderzoekt CARS microscopie voor de analyse van 'adhesive mixtures for inhalation'. Z-stacked (op de Z-as gestapeld) CARS microscopie wordt

gebruikt om medicijn distributie over het oppervlak van dragende deeltjes te bepalen. Ook is onderzocht wat de grootte is van de medicijn deeltjes.

Hoofdstuk vijf onderzoekt CARS microscopie voor analyse van mesoporeus MCM-41 silica microdeeltjes. Z-stacked CARS microscopie is gebruikt om medicijn distributie in de gaten van het mesoporeuse MCM-41 silica te bepalen. Hyperspectrale CARS is verder nog gebruikt om de vast vorm van het medicijn te bepalen.

Acknowledgments

Everyone who is reading this has undoubtedly contributed to the success of this work in one way or another and for this I am truly grateful. I am fortunate to be surrounded by a large number of colleagues, family, and friends without whom this project would not have been possible and there are not enough words to completely describe each person's individual contribution so please accept my apologies if you don't get a specific mention in the acknowledgments.

I would like to begin by thanking my supervisors Herman Offerhaus, Peter Kleinebudde and Clare Strachan who have functioned magnificently well as an international team leading and motivating me non-stop throughout the PhD. Herman, I cannot thank you enough for everything that you have done for me. Your open door policy and "go for it" attitude has really helped me get through troubled times when it really felt as though progress was only a series of sidesteps with nothing going forward. Peter, it really truly has been a pleasure working with you and learning from your enormous wisdom. I know I haven't exactly been a stereotypical PhD student, randomly appearing and then disappearing from your institute while occasionally breaking things. Clare, firstly thanks for introducing me to this line of research and getting me involved in this project. I am not sure where I would have been without you but I am fairly sure I wouldn't have been living in Enschede. Additionally, thanks for the everlasting enthusiasm and excitement about the latest results. This enthusiasm really motivated me to work harder and produce more results.

Beyond the direct supervision from my supervisors there has been endless support and advice from the Optical Sciences group lead by Jennifer Herek. I have to begin by thanking Jennifer for bringing together such a talented group of researchers and technical support staff. Jennifer, I am grateful for being warmly welcomed as a pharmacist into your optics group. I feel very much at home as a member of Optical Sciences (OS). Among the members of a special mention is deserved for the

technical staff, namely Frans Segerink and Jeroen Korterik who assisted me in the lab and did their best to keep me sane in body and in mind. It doesn't need to be said that the PhD students were also a massive influence and motivation behind the success of my work. An extra special mention is deserved for Erik Garbacik who taught me all of the practical aspects to CARS microscopy as well as troubleshooting every system malfunction that anyone could imagine.

The University workshop deserves a special mention for taming my imagination and bringing my ideas into reality during the CARS flow cell design and building, without their engineering expertise my drawings would still be unrealized. Their ideas and wisdom were necessary during every iteration of the design and build process.

Düsseldorf is a special place for me. It's not special because of the river, neither because of the Alt beer, it's special because of the awesome people whom I sat with by the river drinking Alt beer. I can't mention everyone who has helped me during my frequent visits to Düsseldorf but Julian Quodbach has done the most to ensure my experiments were successful and more importantly providing the coffee that kept me going during the long days. The collaboration with Raphael Krampe and his film samples also deserves mentioning not only because we had some successful results but also because I am still puzzled as to what is causing the problems with those samples. I wish Raphael luck finding solutions for the film samples and look forward to seeing further progress.

The University of Groningen has also been important in the success of my work with a particular thanks to Floris Grasmeijer and his adhesive mixtures. The day that the first samples arrived somewhat unexpectedly in my lab accompanied by an introduction letter was a big changing point in my research. Imaging the adhesive mixtures provided great relief when other aspects of my work were only causing frustration.

Many good times were had with Korbinian Löbmann both as a collaborator on the work with co-amorphous mixtures and as roommate during a number of conference trips. I doubt I will ever forget the music performance we gave at the Otago pharmacy school but I am hoping everyone else present has already forgotten it.

One person I cannot afford to forget is Kamilla Koichumanova. Her love and affection is off the scale, along with immeasurable support for everything I do. I don't think I can do justice to everything she has done for me. Beyond all of the personal aspects Kamilla also acted on a professional level providing knowledge and ideas as well as access to equipment in her lab.

Finally, I must thank my family, particularly my parents for their support throughout all aspects of my life and their hands off approach to allow me to pursue my PhD dreams on the other side of the world. I still remember the day I told my parents that I planned to travel half-way around the world to watch tablets dissolve using a special type of microscope. A lot of things have happened since then and I am extremely glad I have had their guidance throughout.

List of publications

Journal articles

Offerhaus, H. L., Garbacik E. T., van Rhijn A.C.W., Fussell A.L., Herek J.L. (2012). *Phase aspects of (broadband) stimulated Raman scattering.* **Reviews in Analytical Chemistry** 31(1): 1-6.

Fussell, A. L., Garbacik, E.T., Offerhaus, H.L., Kleinebudde, P., & Strachan, C.J. (2013). *In situ dissolution analysis using coherent anti-Stokes Raman scattering (CARS) and hyperspectral CARS microscopy*. **European journal of pharmaceutics and biopharmaceutics**. 85(3) Part B: 1141-1147.

Fonteyne, M., Fussell A.L., Vercruysse, J., Vervaet, C., Remon, J.P., Strachan, C., Rades, T., de Beer T. (2013). *Distribution of binder in granules produced by means of twin screw granulation.* **International Journal of Pharmaceutics.** 462(1-2): 8-10.

Fussell, A.L., Grasmeijer, F., Herek, J.L., Frijlink, H.W., de Boer, A.H., & Offerhaus, H.L. (2013). *Coherent anti-Stokes Raman scattering (CARS) microscopy as a tool for studying adhesive mixtures for inhalation.* **Journal of Raman spectroscopy. In press**

Fussell, A.L., Kleinebudde, P., Herek, J.L., Strachan, C.J., Offerhaus, H.L. (2014). *Coherent anti-Stokes Raman scattering (CARS) microscopy visualizes pharmaceutical tablets during dissolution.* **Journal of Visualized Experiments. In press**

Fussell, A. L., Mah, P.T., Offerhaus, H.L., Niemi, S.M., Salonen, J., Santos H.A., Strachan, C.J. (2014) *Coherent anti-Stokes Raman scattering (CARS) microscopy driving the future of drug loaded ordered mesoporous silica imaging.* **submitted**

Conference proceedings

Garbacik, E. T., Fussell, A. L., Gures, S., Korterik, J. P., Otto, C., Herek, J. L., Offerhaus, H. L. (2013). *Hyperspectral coherent anti-Stokes Raman scattering microscopy for in situ analysis of solid-state crystal polymorphs.* Multiphoton Microscopy in the Biomedical Sciences Xiii 8588

Fussell, A.L., Garbacik, E.T., Löbmann, K., Offerhaus, H.L., Kleinebudde, P., Strachan, C.J. (2014). *In situ dissolution analysis of pharmaceutical dosage forms using coherent anti-Stokes Raman scattering (CARS) microscopy*. Multiphoton Microscopy in the Biomedical Sciences XIV 8588. **Submitted**

Oral presentations

Fussell, A.L., Offerhaus, H.L., Kleinebudde, P., & Strachan, C.J. (2011, February). *In situ imaging of dosage forms during dissolution.* Dunedin, New Zealand, Pharmacy department seminar

Fussell, A.L., Garbacik, E.T., Güres, S., Offerhaus, H.L., Kleinebudde, P., & Strachan, C.J. (2011, September 26). *Hyperspectral CARS imaging for Pharmaceutics*. Helsinki, Finland, PSSRC Symposium 2011

Fussell, A.L., Offerhaus, H.L., Kleinebudde, P., & Strachan, C.J. (2012, February 10). *Coherent Raman microscopy for in-situ imaging of dosage forms during dissolution*. Basel, Switzerland, Invited talk

Fussell, A.L., Garbacik, E.T., Offerhaus, H.L., Kleinebudde, P., & Strachan, C.J. (2012, August). *In situ dissolution analysis using CARS microscopy*. Lisbon, Portugal, PSSRC Symposium 2012

Fussell, A.L., Garbacik, E.T., Offerhaus, H.L., Kleinebudde, P., & Strachan, C.J. (2012, October). *In situ dissolution analysis using CARS microscopy*. Utrecht, the Netherlands, Biopharmacy day 2012

Fussell, A.L., Grasmeijer, F., de Boer, A.H., Frijlink H.W., Offerhaus, H.L. (2013, April). *CARS microscopy to analyse adhesive mixtures for inhalation*. Exeter, England, ECONOS 2013

Fussell, A.L., Offerhaus, H.L. (2013, May). Pharmaceutical applications of CARS microscopy. Helsinki, Finland, invited talk Pharmacy department

Fussell, A.L., Loebmann, K., Offerhaus, H.L., Kleinebudde, P., Strachan, C.J. (2013, June). *In situ analysis of co-amorphous tablet dissolution using coherent anti-Stokes Raman scattering (CARS) microscopy*. Lille, France, PSSRC symposium 2013

Fussell, A.L., Offerhaus, H.L. (2014, March). Rapid stimulated Raman scattering for pharmaceutics. Darmstadt, Germany, invited talk Merck Millipore

Fussell, A.L., Mah, M., Offerhaus, H.L., Niemi, S.M., Salonen, J., Santos, H.A., Strachan, C.J. (2014, April). *Coherent anti-Stokes Raman scattering (CARS) microscopy providing in depth imaging of drug loaded mesoporous MCM-41 silica*. Lisbon, Portugal, 9th World meeting on Pharmaceutics, Biopharmaceutics and Pharmaceutical technology 2014

Poster presentations

Fussell, A. L., Garbacik, E.T., Güres, S., Offerhaus, H.L., Kleinebudde, P., & Strachan, C.J. (2012, January 18). *Pharmaceutical imaging using hyperspectral coherent anti-Stokes Raman scattering (CARS)*. Veldhoven, Netherlands, Physics @ FOM conference 2012

Fussell, A. L., Garbacik, E.T., Güres, S., Offerhaus, H.L., Kleinebudde, P., & Strachan, C.J. (2012, January 22). *Pharmaceutical imaging using hyperspectral coherent anti-Stokes Raman scattering (CARS)*. San Francisco, USA, SPIE photonics west 2012

Fussell, A. L., Garbacik, E.T., Güres, S., Offerhaus, H.L., Kleinebudde, P., & Strachan, C.J. (2012, March 22). *Hyperspectral coherent anti-Stokes Raman scattering (CARS) imaging for pharmaceutics*. Istanbul, Turkey, 8th World meeting on Pharmaceutics, Biopharmaceutics and Pharmaceutical technology 2012

Van Rijn, A.C.W., Garbacik, E.T., Fussell, A.L., Jafarpour, A., Jurna, M., Timmermans, F., Korai, R.P., Korterik, J.P., Otto, C., Offerhaus, H.L., Herek, J.L. (2012, September). *Chemically selective imaging using CARS.* Enschede, the Netherlands, MESA+ symposium 2012

Fussell, A. L., Garbacik, E.T., Offerhaus, H.L., Kleinebudde, P., & Strachan, C.J. (2012, October). *In situ dissolution analysis using CARS microscopy*. Chicago, USA, AAPS annual meeting and exposition 2012

Fussell, A. L., Grasmeijer, F., de Boer, A.H., Frijlink H.W., Offerhaus, H.L. (2012, November). *CARS microscopy to analyse adhesive mixtures for inhalation*. Utrecht, the Netherlands, Biopharmacy day 2012

Fussell, A. L., Grasmeijer, F., de Boer, A.H., Frijlink H.W., Offerhaus, H.L. (2013, March). *CARS microscopy to analyse adhesive mixtures for inhalation*. Maastricht, the Netherlands, Focus on microscopy conference 2013

Krampe, R., Fussell, A.L., Sieber, D., Pein. M., Kleinebudde, P., Breitkreutz, J. (2013, September). *Influence of different solvents on the properties of orodispersible films.* Barcelona, Spain, European paediatric formulation initiative conference 2013

Krabbendam, R., Fussell, A.L., Garbacik, E.T., Otto, C., Offerhaus, H.L., Herek, J.L. (2013, September). *Coherent anti-Stokes Raman scattering (CARS) imaging for pharmaceutics.* Enschede, the Netherlands, MESA+ symposium 2013

Fussell, A. L., Garbacik, E.T., Offerhaus, H.L., Kleinebudde, P., & Strachan, C.J. (2013, September). *In situ dissolution analysis using CARS microscopy*. Murten, Switzerland, Frontiers in Optical Imaging 2013

Fussell, A. L., Grasmeijer, F., de Boer, A.H., Frijlink H.W., Offerhaus, H.L. (2013, November). *CARS microscopy to analyse adhesive mixtures for inhalation*. San Antonio, United States of America, AAPS annual meeting and exhibition 2013

Fussell, A.L., Offerhaus, H.L., Kucera, S., Lubda D. (2013, November). *Coherent anti-Stokes Raman scattering (CARS) microscopy to analyse drug loaded silica microparticles.* San Antonio, United States of America, AAPS annual meeting and exhibition 2013

Fussell, A.L., Fonteyne, M., Vercruysse, J., Vervaet, C., Remon J.P., Rades, T., Offerhaus H.L., Strachan, C., de Beer, T. (2013, December). *Chemical distribution imaging of granules using coherent anti-Stokes Raman scattering microscopy.* Gent, Belgium, Biopharmacy day 2013

Fussell, A.L., Garbacik, E.T., Löbmann, K., Offerhaus, H.L., Kleinebudde, P., Strachan, C.J. (2014, February). *In situ dissolution analysis of pharmaceutical dosage forms using coherent anti-Stokes Raman scattering (CARS) microscopy*. San Francisco, United States of America, SPIE photonics west 2014

Fussell, A.L., Fonteyne, M., Sprunk, A., Offerhaus H.L., Kleinebudde P., Strachan, C. (2014, April). *Drug distribution analysis using coherent anti-Stokes Raman scattering microscopy.* Lisbon, Portugal, 9th World meeting on Pharmaceutics, Biopharmaceutics and Pharmaceutical technology 2014

Magazine / Website articles

Offerhaus, H.L., Garbacik, E.T., Fussell, A.L., Korterik, J.P., Mukamel, S., Herek, J.L. (2013). *Microscopie bekeken vanuit het molecuul.* Nederlands Tijdschrift voor Natuurkunde.

Fussell, A.L., Mah, M., Priemel, P., Strachan, C.J. (2013). *Non-linear optical imaging of solid drugs and dosage forms.* Pharmaceutical Solid State Research Cluster. http://www.pssrc.org/component/k2/91/non-linear-optical-imaging-of-solid-drugs-and-dosage-forms

Fussell, A.L., Isomäki, A., Strachan, C.J. (2013). *Non-linear optical imaging – Introduction and pharmaceutical applications.* American Pharmaceutical Review. Vol. 16, Issue 6 p54-63 October 2013.

Awards

Pharmaceutical Solid State Research Cluster (PSSRC) travel grant to attend PSSRC symposium Helsinki 2011

EUCOST MicroCOR travel grant to attend Focus on Microscopy conference 2013

Poster presentation award at Frontiers in Optical Imaging Murten 2013

Merck sponsored travel grant to attend AAPS annual meeting San Antonio 2013

This dissertation is the culmination of work performed investigating coherent anti-Stokes Raman scattering (CARS) microscopy as a tool for pharmaceutical development. *In situ* dissolution imaging using CARS was performed and variants of CARS microscopy were employed to provide rapid chemically selective images of a number of solid dosage forms.

Andrew L. Fussell did his PhD research at the Optical Sciences group of the University of Twente in the Netherlands, as part of a collaboration with the Heinrich-Heine University in Germany, and the University of Helsinki in Finland. He investigated applications of CARS microscopy in the area of solid state pharmaceutics.